CHAPTER

3

Spectroscopy and Photochemistry

Fundamentals

The chemistry of the atmosphere is driven to a very large measure by light, i.e., by photochemical processes. For example, the generation of the OH free radical in remote areas occurs primarily via the photolysis of O_3 in the presence of water vapor. Thus, the fundamental spectroscopy and photochemistry of atmospheric species is central to understanding the chemistry. In addition, as discussed in Chapter 11, the interaction of molecules with light is used extensively for detecting and measuring both trace species and urban air pollutants. As we shall see in Chapter 14, the interaction of gases and particles with infrared radiation plays a central role in the earth's climate.

In this chapter, we give a brief overview of the fundamentals of spectroscopy and photochemistry needed in atmospheric chemistry; for detailed treatments, see Calvert and Pitts (1966), Okabe (1978), Turro (1978), Wayne (1988), and Gilbert and Baggott (1991). Specifics for individual molecules are found in Chapter 4. Excellent treatments of atmospheric radiation are given by Liou (1980), Goody and Yung (1989), and Lenoble (1993).

A. BASIC PRINCIPLES

1. Molecular Energy Levels and Absorption and Emission Spectroscopy

We shall deal first with the simplest system, that of diatomic molecules, and then extrapolate to polyatomic systems.

Atoms in molecules undergo a variety of motions relative to each other. As illustrated in Fig. 3.1 for the water molecule, these can be separated into vibrational motions involving the various chemical bonds in the molecule, rotation of the molecule as a whole, and translational motion of the molecule, i.e., movement in the three coordinates x, y, and z. However, since the interaction of light with the molecule only directly changes the vibrational and rotational motions, we shall not consider translation further here. Of course, once the molecule has absorbed the light initially, the energy may also be converted into translational energy, at least in part, leading to an increase in temperature.

In addition to inducing changes in the positions of atoms within the molecule, the absorption of light can lead to changes in electron distribution. In contrast to vibrational and rotational changes, such electronic transitions typically require sufficient energy (in the ultraviolet and visible regions) that they can lead to breaking of chemical bonds; i.e., photochemistry can occur. It is this latter process that, in general, is of most interest in atmospheric chemistry.

a. Diatomic Molecules

(1) Vibrational energy and transitions As seen in Fig. 3.2a, the bond between the two atoms in a diatomic molecule can be viewed as a vibrating spring in which, as the internuclear distance changes from the equilibrium value r_e, the atoms experience a force that tends to restore them to the equilibrium position. The *ideal*, or harmonic, oscillator is defined as one that obeys Hooke's law; that is, the restoring force F on the atoms in a diatomic molecule is proportional to their displacement from the equilibrium position.

Substitution of the potential energy for this harmonic oscillator into the Schrödinger wave equation gives the allowed vibrational energy levels, which are quantified and have energies E_v given by

$$E_v = h\nu_{vib}(v + 1/2), \qquad \text{(A)}$$

where ν_{vib} is a constant characteristic of the molecule and is related to the strength of the bond and the

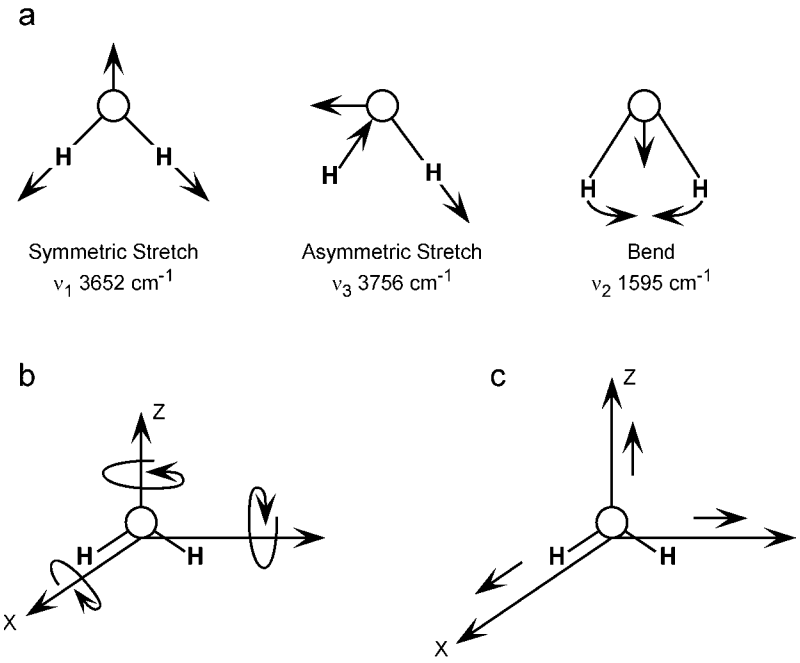

FIGURE 3.1 (a) Internal vibrations of the bonds in the water molecule, (b) rotational motion of water, and (c) translation of the water molecule.

reduced mass of the molecule. The *vibrational quantum number* v can have the integral values 0, 1, 2, ... Thus the vibrational energy levels of this ideal oscillator are equally spaced.

However, as seen in Fig. 3.2, this idealized harmonic oscillator (Fig. 3.2b) is satisfactory only for low vibrational energy levels. For real molecules, the potential energy rises sharply at small values of r, when the atoms approach each other closely and experience significant charge repulsion; furthermore, as the atoms move apart to large values of r, the bond stretches until it ultimately breaks and dissociation occurs (Fig. 3.2c).

To obtain the allowed energy levels, E_v, for a real diatomic molecule, known as an *anharmonic* oscillator, one substitutes the potential energy function describing the curve in Fig. 3.2c into the Schrödinger equation; the allowed energy levels are

$$E_v = h\nu_{vib}(v + 1/2) - h\nu_{vib}x_e(v + 1/2)^2 + h\nu_{vib}y_e(v + 1/2)^3 + \cdots . \quad \text{(B)}$$

Once again v is the vibrational quantum number with allowed values of 0, 1, 2, . . . , and x_e and y_e are anharmonicity constants characteristic of the molecule.

Equation (B) is often expressed in wavenumbers, ω_{vib}; the allowed energy states, $\overline{E}_v$, in units of wavenumbers (cm^{-1}) become

$$\overline{E}_v = \omega_e(v + 1/2) - \omega_e x_e(v + 1/2)^2 + \omega_e y_e(v + 1/2)^3 + \cdots . \quad \text{(C)}$$

Note that throughout this book we use a bar over a parameter (e.g., $\overline{E}$) if it is expressed in units of wavenumbers. Values for ω_e, x_e, and y_e for a number of diatomic molecules are found in Herzberg's classic *Molecular Spectra and Molecular Structure. I. Spectra of Diatomic Molecules* (1950) and in Huber and Herzberg (1979).

An important consequence of using the potential energy for a real molecule in the Schrödinger equation is that the vibrational energy levels become more closely spaced with increasing quantum number v (Fig. 3.2c versus 3.2b).

When exposed to electromagnetic radiation of the appropriate energy, typically in the infrared, a molecule can interact with the radiation and absorb it, exciting the molecule into the next higher vibrational energy level. For the ideal harmonic oscillator, the selection rules are $\Delta v = \pm 1$; that is, the vibrational energy can only change by one quantum at a time. However, for anharmonic oscillators, weaker overtone transitions due to $\Delta v = \pm 2, \pm 3$, etc. may also be observed because of their nonideal behavior. For polyatomic molecules with more than one fundamental vibration, e.g., as seen in Fig. 3.1a for the water molecule, both overtones and

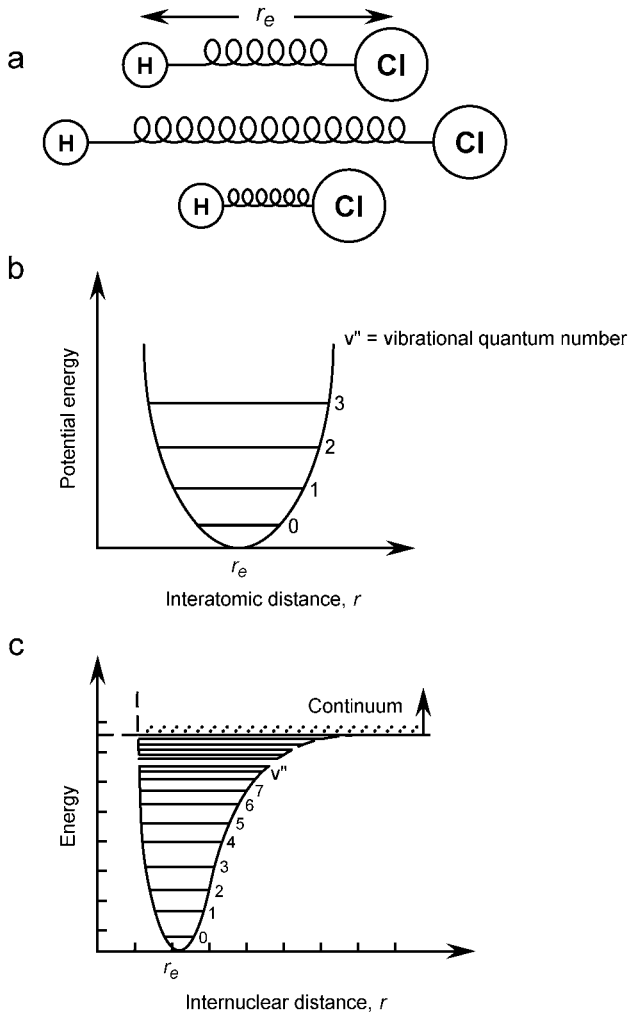

FIGURE 3.2 (a) Vibration of diatomic molecule, HCl, (b) potential energy of an ideal harmonic oscillator, and (c) an anharmonic oscillator described by the Morse function.

combination bands (i.e., those that are the sum of two or more fundamental vibrations) occur.

Because the vibrational energy level spacing is relatively large (typically of the order of 10^3 cm^{-1}) compared to their thermal energy, most molecules at room temperature are in their lowest vibrational energy level and light absorption normally occurs from $v = 0$.

For a purely vibrational transition, the selection rule for absorption of light requires that there be a changing dipole moment during the vibration. This oscillating dipole moment produces an electric field that can interact with the oscillating electric and magnetic fields of the electromagnetic radiation. Thus heteronuclear diatomic molecules such as NO, HCl, and CO absorb infrared radiation and undergo vibrational transitions, whereas homonuclear diatomic molecules such as O_2 and H_2, whose dipole moments remain constant during vibration, do not.

Since at room temperature most molecules are in the $v'' = 0$ state, and $\Delta v = \pm 1$ is by far the strongest transition, most molecules go from $v'' = 0$ to $v' = 1$. (We follow the Herzberg convention that the quantum number of the upper state is designated by a prime, and the lower state by a double prime; e.g., in this example, $v'' = 0 \rightarrow v' = 1$.) As a result, a single vibrational absorption band (with associated rotational structure) is normally observed in the infrared, the region corresponding to the energy level differences given by Eq. (C).

(2) Rotational energy and transitions If a molecule has a permanent dipole moment, its rotation in space produces an oscillating electric field; this can also interact with electromagnetic radiation, resulting in light absorption.

In the idealized case for rotation of a diatomic molecule, one assumes the molecule is analogous to a dumbbell with the atoms held at a fixed distance r from each other; that is, it is a *rigid rotor*. The simultaneous vibration of the molecule is ignored, as is the increase of internuclear distance at high rotational energies arising from the centrifugal force on the two atoms.

For this idealized case, the rotational energy levels (in cm^{-1}) are given by

$$\overline{E}_r = \overline{B}(J)(J + 1)\ cm^{-1}, \qquad (D)$$

where $\overline{B}$, the rotational constant characteristic of the molecule, is given by

$$\overline{B} = h/8\pi^2 Ic. \qquad (E)$$

I is the moment of inertia of the molecule, given by $I = \mu r^2$, where μ is the reduced mass defined by $\mu^{-1} = [(M_A^{-1}) + (M_B^{-1})]$, M_A and M_B are the atomic masses, and r is the fixed, internuclear distance. J is the rotational quantum number; its allowed values are $0, 1, 2, \ldots$.

For a real rotating diatomic molecule, known as a nonrigid rotor, Eq. (D) becomes

$$\overline{E}_r = \overline{B}(J)(J + 1) - \overline{D}(J)^2(J + 1)^2. \qquad (F)$$

The constant $\overline{D}$ is characteristic of the diatomic molecule and is much smaller than $\overline{B}$; generally, $\overline{D} \approx 10^{-4}\overline{B}$. The second term in Eq. (F) generally becomes important at large values of J when centrifugal force increases the separation between atoms.

Because of the requirement of a permanent dipole moment, only heteronuclear molecules can absorb radiation and change their rotational energy. For the

idealized case of a rigid rotor, the selection rule is $\Delta J = \pm 1$. For the energy levels given by Eq. (D), the energy level splitting between consecutive rotational energy levels is given by

$$\Delta \bar{E}_r = 2\bar{B}J', \tag{G}$$

where J' is the quantum number of the *upper* rotational state involved in the transition. Thus the spacing between rotational energy levels increases with increasing rotational quantum number. Splittings are small compared to those between vibrational energy levels, typically of the order of 10 cm^{-1} in the lower levels; this corresponds to absorption in the microwave region. Indeed, these spacings are sufficiently small that the population of the rotational energy levels above $J = 0$ is significant at room temperature because the thermal energy available is sufficient to populate the higher rotational levels.

The Boltzmann expression can be used to calculate the relative populations of molecules in any rotational state J compared to the lowest rotational state $J = 0$ at temperature T (K):

$$N_J/N_0 = (2J + 1)e^{-E_J/kT}. \tag{H}$$

In Eq. (H), k is the Boltzmann constant (1.381×10^{-23} J K^{-1}) and E_J is the energy of the Jth rotational level given by Eq. (D) for the ideal rigid rotor, or Eq. (F) for the nonideal case.

The exponential energy factor in Eq. (H) gives decreasing populations with increasing J, but the degeneracy factor $(2J + 1)$ works in the opposite direction. As a result, rotational populations increase initially with increasing J, reach a peak, and subsequently decrease.

The combination of increased spacing between energy levels as J increases and the significant population of molecules in higher rotational energy levels means that the absorption of microwave radiation occurs from a number of different initial states, resulting in a series of absorption lines, rather than a single line as seen in the pure vibrational infrared spectra of diatomic molecules. From the spacing of these lines, the rotational constant $\bar{B}$, and hence the moment of inertia and the internuclear spacing, can be obtained using Eq. (G).

(3) Vibration–rotation Molecules, of course, vibrate and rotate simultaneously. It is a good approximation that the total energy of the molecule (excluding translation) is the sum of the vibrational (V), rotational (R), and electronic (E) energy of a molecule; that is, $E_{total} = E_V + E_R + E_E$. For the case where there is no electronic energy change for an ideal harmonic oscillator–rigid rotor, the selection rules $\Delta v = \pm 1$ and $\Delta J = \pm 1$ apply. At room temperature, $v'' = 0 \rightarrow v' = 1$ is the only significant vibrational transition in absorption, but, as discussed earlier, a variety of rotational transitions can occur.

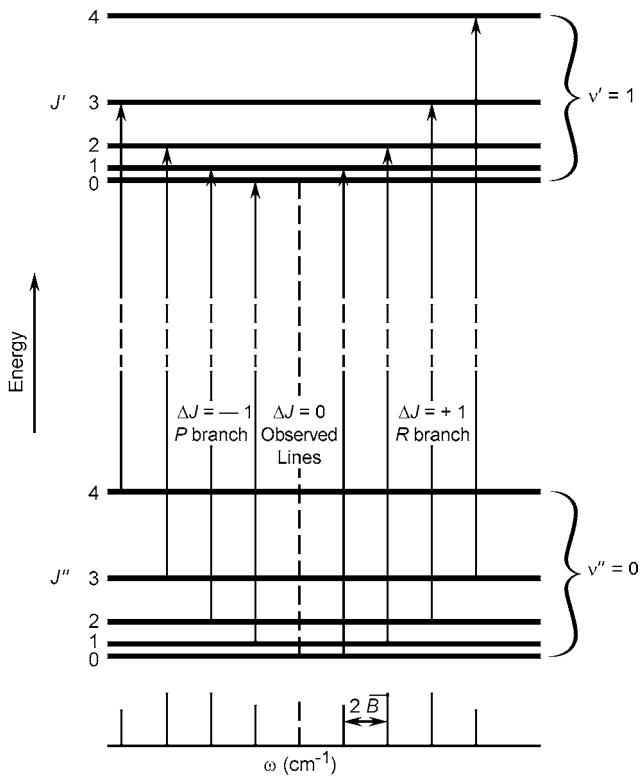

FIGURE 3.3 Schematic diagram of energy levels involved in HCl vibration–rotation transitions at room temperature (from Herzberg, 1950).

Figure 3.3 shows some of these possible transitions for HCl. Those with $\Delta J = +1$ are known as the R branch and occur at the high-energy side of the hypothetical transition $\Delta v = 1$, $\Delta J = 0$ (this is not allowed because of the selection rule, $\Delta J = \pm 1$). Those with $\Delta J = -1$ on the low-frequency side of the hypothetical transition form the P branch. Figure 3.4 shows the absorption spectrum of HCl at room temperature, with the rotational transitions responsible for each line. The relative intensities of the lines reflect the relative populations of the absorbing rotational levels; the peaks are doublets due to the separate absorptions of the two chlorine isotopes, that is, $H^{35}Cl$ and $H^{37}Cl$, which have different reduced masses and hence values of the rotational constant $\bar{B}$.

(4) Electronic energy and transitions The electronic states of a diatomic molecule are described by several

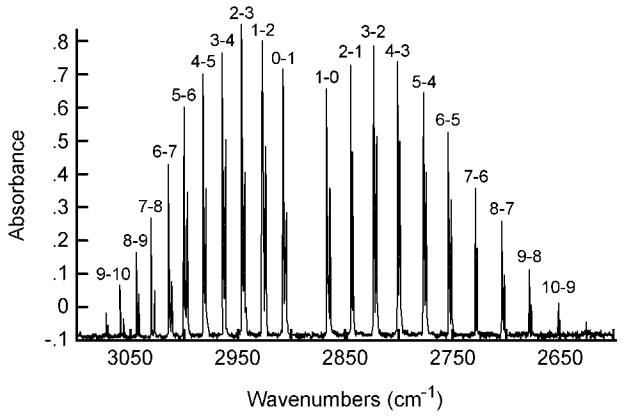

FIGURE 3.4 Vibration–rotation spectrum of 0.18 Torr HCl at room temperature using a path length of 19.2 m. Resolution is 0.25 cm^{-1}. The rotational transitions are shown as (initial J, final J) (from B. J. Finlayson-Pitts and S. N. Johnson, unpublished data).

molecular quantum numbers, Λ, S, and Ω. Λ is the component of the total electronic orbital angular momentum L along the internuclear axis and can be determined from the electronic spectrum of the molecule (see Herzberg, 1950). Allowed values of Λ of 0, 1, 2, and 3 correspond to electronic states designated as Σ, Π, Δ, and Φ, respectively.

The spin quantum number S represents the net spin of the electrons. It has an integral value or zero for even numbers of electrons and half-integral value for odd numbers. The *multiplicity* of a molecular state is defined as $(2S + 1)$ and is written as a superscript to the left of the symbol corresponding to Λ. Values of S of 0, 1/2, and 1, corresponding to multiplicities of 1, 2, and 3, are referred to as singlet, doublet, and triplet states, respectively. While most stable molecules have ground singlet states, one important exception is O_2, where the ground state is a triplet. As discussed in Chapter 4, this has important implications for its spectroscopy and photochemistry.

For many molecules the quantum number Ω is defined and is given by the vector sum of Λ and Σ,

$$\Omega = |\Lambda + \Sigma|,$$

where Σ is the vector component of S in the direction of the internuclear axis. Σ can have the values $+S$, $S - 1, \ldots, -S$ and can be positive, negative, or zero.

Two other symbols are used in designating electronic states according to their symmetry. For homonuclear diatomic molecules, states are designated "g" or "u" as a subscript to the right of the Λ symbol, depending on whether or not the wavefunction describing the molecular state changes sign when reflected through the center of symmetry of the molecule. If it does change sign, it is designated "u" (for ungerade = uneven); if it does not, it is designated "g" (for gerade = even).

Finally, the symbols + and −, written as superscripts to the Λ symbol, refer to two types of sigma states, Σ^+ and Σ^-. If the wavefunction is unaltered by reflection through a plane passing through the two nuclei, the state is positive (+); if it changes sign, it is negative (−).

The selection rules for electronic transitions are not as clear-cut as in the case of vibration and rotation. In the case of molecules consisting of relatively light nuclei, which is the case for many molecules of tropospheric interest, the selection rules

$$\Delta\Lambda = 0, \pm 1 \quad \text{and} \quad \Delta S = 0$$

apply. Thus transitions between states of unlike multiplicity (e.g., singlet → triplet) are "forbidden" but in some cases may occur with a relatively small probability, most notably with the oxygen molecule, which has a triplet ground state. In terms of the symmetry of the wavefunctions, u ↔ g transitions are allowed but u ↔ u and g ↔ g are forbidden. In addition, Σ^+ states cannot combine with Σ^- states; that is, $\Sigma^+ \leftrightarrow \Sigma^+$ and $\Sigma^- \leftrightarrow \Sigma^-$ transitions are allowed but $\Sigma^+ \leftrightarrow \Sigma^-$ are forbidden. Table 3.1 summarizes these selection rules for molecules with light nuclei.

Upon absorption of light of an appropriate wavelength, a diatomic molecule can undergo an *electronic* transition, along with simultaneous vibrational and rotational transitions. In this case, there is no restriction on Δv. That is, the selection rule $\Delta v = \pm 1$ valid for purely vibrational and vibrational–rotational transitions no longer applies; thus numerous vibrational transitions can occur. If the molecule is at room temperature, it will normally be in its lower state, $v'' = 0$; hence transitions corresponding to $v'' = 0$ to $v' = 0$,

TABLE 3.1 Allowed[a] Electronic Transitions of Diatomic Molecules Having Light Nuclei[b]

Homonuclear diatomic (equal nuclear charge)	Heteronuclear diatomic (unequal nuclear charge)
$\Sigma_g^+ \leftrightarrow \Sigma_u^+$	$\Sigma^+ \leftrightarrow \Sigma^+$
$\Sigma_g^- \leftrightarrow \Sigma_u^-$	$\Sigma^- \leftrightarrow \Sigma^-$
$\Pi_g \leftrightarrow \Sigma_u^+$, $\Pi_u \leftrightarrow \Sigma_g^+$	$\Pi \leftrightarrow \Sigma^+$
$\Pi_g \leftrightarrow \Sigma_u^-$, $\Pi_u \leftrightarrow \Sigma_g^-$	$\Pi \leftrightarrow \Sigma^-$
$\Pi_g \leftrightarrow \Pi_u$	$\Pi \leftrightarrow \Pi$
$\Pi_g \leftrightarrow \Delta_u$, $\Pi_u \leftrightarrow \Delta_g$	$\Pi \leftrightarrow \Delta$
$\Delta_g \leftrightarrow \Delta_u$	$\Delta \leftrightarrow \Delta$

[a] Presuming that the rule $\Delta S = 0$ is obeyed.
[b] Source: Herzberg (1950), p. 243.

1, 2, 3,... in the upper electronic state are usually observed.

The rotational selection rule is $\Delta J = 0, \pm 1$, except for the case of a transition involving $\Omega = 0$ for both the upper and lower states. Thus three sets of lines (known as the P, Q, and R branches) corresponding to $\Delta J = -1$, 0, and $+1$, respectively, are observed for each band arising from a particular vibrational transition. Figure 3.5 illustrates these transitions schematically. However, if $\Omega = 0$ for both upper and lower states ($^1\Sigma \rightarrow {}^1\Sigma$ transition), the rotational selection rule is $\Delta J = \pm 1$, and the Q branch does not appear. For further details, see Herzberg (1945, 1950, 1967).

As a general rule, the most probable, that is, most intense, vibrational transitions within a given electronic transition will be those in which the vibrational probabilities are maximum in both the initial and final states. An important restriction is that only *vertical* transitions are allowed. This is a consequence of the Franck–Condon principle, which states that the time for an electronic transition to occur (typically 10^{-15} s) is so short relative to the time it takes for one vibration ($\sim 10^{-13}$ s) that the internuclear distance remains essentially constant during the electronic transition.

Figure 3.6 shows the Morse potential energy curves for two hypothetical electronic states of a diatomic molecule, the vibrational energy levels for each, and the shape of the vibrational wavefunctions (ψ) within each vibrational energy level. At room temperature, most molecules will originate in $v'' = 0$; the vertical line is at the midpoint of $v'' = 0$ since the probability of finding the molecule at $r = r_e$ is a maximum here.

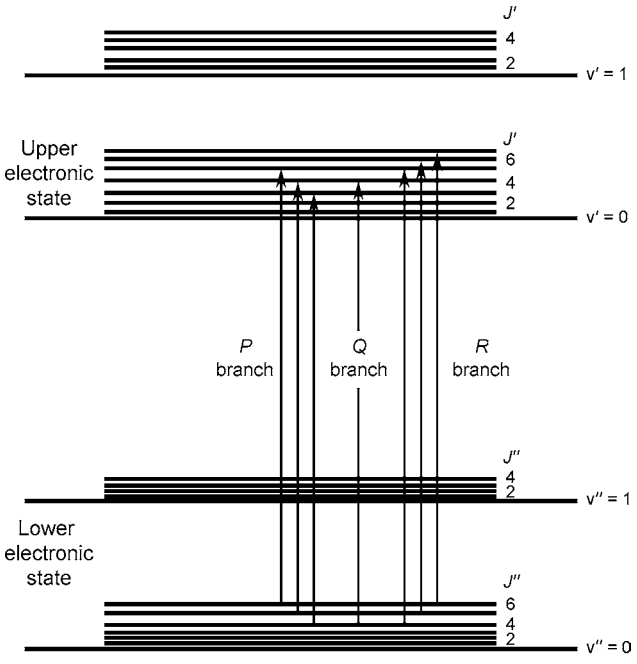

FIGURE 3.5 Schematic of some possible rotational and vibrational transitions involved during an electronic transition of a diatomic molecule from the ground electronic state.

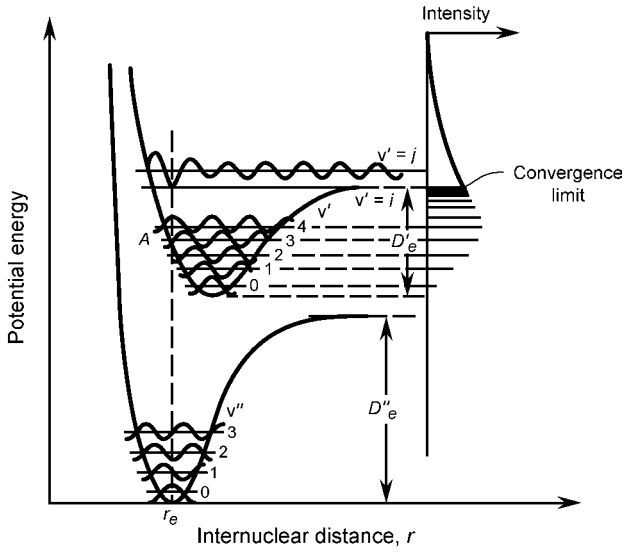

FIGURE 3.6 Potential energy curves for the ground state and an electronically excited state of a hypothetical diatomic molecule. Right-hand side shows relative intensities expected for absorption bands (from Calvert and Pitts, 1966).

The probability of a particular transition from $v'' = 0$ to an upper vibrational level v' is determined largely by the product of the wavefunctions for the two states, $\psi_{v'}\psi_{v''}$. A qualitative examination of the wavefunctions in the upper state, $\psi_{v'}$, in Fig. 3.6 shows that $\psi_{v'}$, and hence the product $\psi_{v'}\psi_{v''}$, is a maximum around $v' = 4$; thus the vibrational transition corresponding to $v'' = 0 \rightarrow v' = 4$ is expected to be the most intense. On the other hand, the wavefunction at $v' = 0$ is very small; hence the $v'' = 0 \rightarrow v' = 0$ transition should be weak. The right side of Fig. 3.6 shows the corresponding intensities expected for the various absorption lines in this electronic transition.

The potential energy curves of excited electronic states need not have potential energy minima, such as those shown in Fig. 3.6. Thus Fig. 3.7 shows two hypothetical cases of *repulsive states* where no minima are present. Dissociation occurs immediately following light absorption, giving rise to a spectrum with a structureless continuum. Transition *a* represents the case where dissociation of the molecule AB produces the atoms A and B in their ground states, and transition *b* the situation where dissociation produces one of the atoms in an electronically excited state, designated A*.

Some molecules may have a number of excited electronic states, some of which have potential minima, as

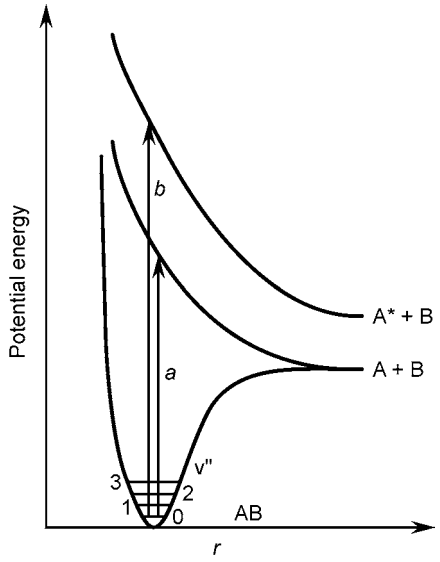

FIGURE 3.7 Potential energy curves for a hypothetical diatomic molecule showing electronic transitions to two repulsive excited states having no minima. A* is an electronically excited atom.

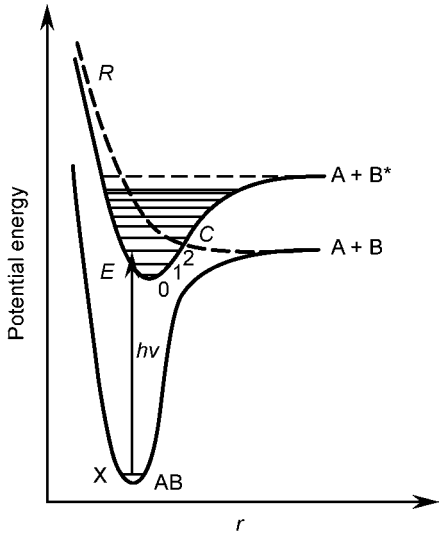

FIGURE 3.8 Potential energy curves for the ground state and two electronically excited states in a hypothetical diatomic molecule. Predissociation may occur when the molecule is excited into higher vibrational levels of the state E and crosses over to repulsive state R at the point C (from Okabe, 1978).

in Fig. 3.6, and some of which are wholly repulsive, as in Fig. 3.7. In this case, depending on the wavelength absorbed (i.e., the electronically excited state reached), the molecule may dissociate or undergo one of the photophysical processes described below.

A simplified, hypothetical example of this situation is shown in Fig. 3.8. If the molecule absorbs light corresponding to energies insufficient to produce vibrational energy levels above $v' = 2$ in the excited state E, a structured absorption (and emission) spectrum is observed. However, if the photon energy is greater than that required to produce A + B, that is, greater than the bond dissociation energy, then the molecule may be excited either into the repulsive state R, from which it immediately dissociates into ground-state atoms A + B, or alternatively into vibrational levels $v' > 2$ of excited state E. In the latter case, the excited molecule may undergo one of the photophysical processes discussed below (fluorescence, deactivation, etc.) or it may cross over from state E into the repulsive state R (point C in Fig. 3.8) and dissociate. This phenomenon is known as *predissociation.* In a case such as that in Fig. 3.8, the absorption spectrum would be expected to show well-defined rotational and vibrational structure up to a certain energy corresponding to the transition $v'' = 0 \rightarrow v' = 2$. For transitions to higher vibrational levels, the rotational structure becomes blurred, and a *predissociation spectrum* is observed. I_2 is an example of a molecule with both a low-lying repulsive electronically excited state and bound excited states; excitation from the ground $^1\Sigma$ state into the repulsive $^1\Pi$ state results in dissociation into the ground state iodine atoms. On the other hand, excitation into the $B^3\Pi$ state below the dissociation limit gives electronically excited I_2, which returns to the ground state via light emission or crosses into the repulsive $^1\Pi$ state and predissociates (Okabe, 1978).

Finally, if the incident photon is sufficiently energetic and the appropriate selection rules are obeyed, the excited molecule may be produced in vibrational levels of state E that are sufficiently high that the molecule immediately dissociates into A + B*, where B* is an electronically excited state.

b. Polyatomic Molecules

The principles discussed for diatomic molecules generally apply to polyatomic molecules, but their spectra are much more complex. For example, instead of considering rotation only about an axis perpendicular to the internuclear axis and passing through the center of mass, for nonlinear molecules, one must think of rotation about three mutually perpendicular axes as shown in Fig. 3.1b. Hence we have three rotational constants $\bar{A}$, $\bar{B}$, and $\bar{C}$ with respect to these three principal axes.

Furthermore, polyatomic molecules consisting of n atoms have $3n - 6$ vibrational degrees of freedom (or $3n - 5$ in the special case of a linear polyatomic molecule), instead of just one as in the case of a diatomic molecule. Some or all of these may absorb infrared radiation, leading to more than one infrared absorption band. In addition, overtone bands ($\Delta v > 1$)

and combination bands (absorptions corresponding to the sum of two or more of the fundamental vibrations) are much more common.

An atmospherically relevant example of just how complex infrared spectra of polyatomic molecules can be is water vapor. A multitude of observed transitions occurs in the regions $\sim 1300-2000$ cm^{-1} and $3000-4000$ cm^{-1}. This, combined with the relatively high, and often rapidly changing, concentrations of water vapor, makes long-path-length infrared spectroscopic determination of trace atmospheric species in ambient air very difficult in these wavelength regions. Similarly, absorption of CO_2 renders the region from ~ 2230 to ~ 2390 cm^{-1} unusable for ambient air studies.

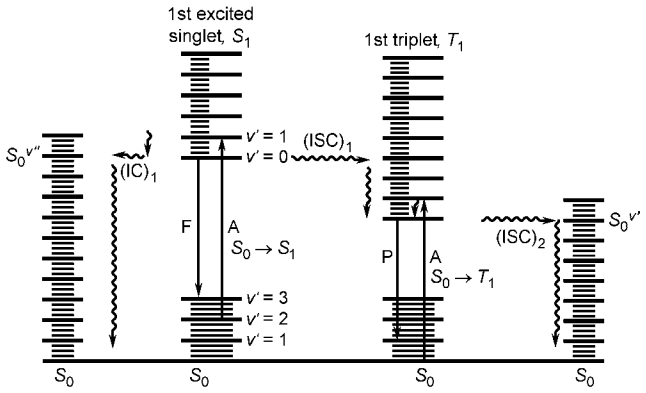

FIGURE 3.9 Jablonski diagram illustrating photophysical radiative and nonradiative transitions. S_0 = ground singlet state, S_1 = first excited singlet state, T_1 = first triplet state, A = absorption of light, F = fluorescence, P = phosphorescence, IC = internal conversion, ISC = intersystem crossing. Radiative transitions are shown by solid lines, and nonradiative transitions by wavy lines. Photochemical processes are not indicated.

2. Fates of Electronically Excited Molecules

Once a molecule is excited into an electronically excited state by absorption of a photon, it can undergo a number of different primary processes. *Photochemical* processes are those in which the excited species dissociates, isomerizes, rearranges, or reacts with another molecule. *Photophysical* processes include *radiative* transitions in which the excited molecule emits light in the form of fluorescence or phosphorescence and returns to the ground state and *nonradiative* transitions in which some or all of the energy of the absorbed photon is ultimately converted to heat.

a. Photophysical Processes

Photophysical processes are often displayed in the form of the Jablonski-type energy level diagram shown in Fig. 3.9. The common convention is that singlet states are labeled S_0, S_1, S_2, and so on and the triplets are labeled T_1, T_2, T_3, and so on, in order of increasing energy. Vibrational and rotational states are shown as being approximately equally spaced only for clarity of presentation. Radiative transitions, for example, fluorescence (F) and phosphorescence (P), are shown as solid lines, and nonradiative transitions as wavy lines. Vertical distances between the vibrational–rotational levels of the singlet ground state, S_0, and the two electronically excited states, the first excited singlet, S_1, and its triplet, T_1, correspond to their energy gaps.

Fluorescence is defined as the emission of light due to a transition between states of like multiplicity, for example, $S_1 \rightarrow S_0 + h\nu$. This is an allowed transition, and hence the lifetime of the upper state with respect to fluorescence is usually short, typically $10^{-6}-10^{-9}$ s. For example, the fluorescence lifetime of OH in the electronically excited $A^2\Sigma^+$ state is ~ 0.7 μs (McDermid and Laudenslager, 1982; Crosley, 1989). Chemiluminescence is similar to fluorescence except that the excited state is generated in a chemical reaction.

Phosphorescence is defined as the emission of light due to a transition between states of different spin multiplicities. Because this is theoretically not an allowed transition for an ideal unperturbed molecule, phosphorescence lifetimes tend to be relatively long, typically $10^{-3}-10^{-2}$ s.

Intersystem crossing (ISC) is the intramolecular crossing from one state to another of different multiplicity without the emission of radiation. In Fig. 3.9 $(ISC)_1$ shows the transfer from the first excited singlet state S_1 to the first excited triplet state T_1. Since the process is horizontal, the total energy remains the same and the molecule initially is produced in upper vibrational and rotational levels of T_1, from which it is deactivated as shown by the vertical wavy line. Similarly, $(ISC)_2$ shows the intersystem crossing from T_1 to upper vibrational and rotational states of the ground state S_0, from which vibrational deactivation to $v'' = 0$ then occurs.

Internal conversion (IC) is the intramolecular crossing of an excited molecule from one state to another of the same multiplicity without the emission of radiation. As seen in Fig. 3.9, the horizontal wavy line $(IC)_1$ represents internal conversion from the lowest excited singlet state S_1 to high vibrational levels of the ground state S_0; this is generally followed by vibrational deactivation to $v'' = 0$.

Intramolecular photophysical processes available to an excited molecule shown in Fig. 3.9 predominate at

low pressures where collisions with other molecules are relatively infrequent. However, at 1 atm pressure, or in the liquid state, the excited molecule can undergo many collisions with ground-state molecules; this can lead to collisional deactivation of the excited species by several paths. For example, an electronically excited molecule, A*, in the $S_1^{v'>0}$ state could undergo a series of collisions, be vibrationally (and rotationally) deactivated, and fall into the $S_1^{v'=0}$ state. The energy lost by A* is carried off as translational energy of the ground-state collision partner, B. From here, A ($S_1^{v'=0}$) can undergo photophysical or photochemical processes. Alternatively, *energy transfer* from A* to the collision partner can occur in which the excitation energy appears as excess vibrational, rotational, and/or electronic energy of molecule B.

Collisional deactivation and energy transfer play important roles in tropospheric chemistry. For example, electronically excited SO_2 in the $^3B_1$ state can be deactivated by O_2 (as well as by N_2 and H_2O) to the ground ($^1A_1$) state, with part of this process occurring via triplet–triplet energy transfer to generate singlet electronically excited states of O_2:

$$SO_2(^3B_1) + O_2(^3\Sigma_g^-) \rightarrow SO_2(^1A_1) + O_2(^1\Sigma_g^+, {}^1\Delta_g). \quad (1)$$

Note that in the transfer of electronic energy between an excited atom or molecule and a second atom or molecule, the Wigner spin conservation rule generally applies. This states that the overall spin angular momentum of the system should not change during the energy transfer (see Herzberg for details). Because O_2 has the unusual property of having a ground triplet state, energy transfer from triplet collision partners can produce the reactive singlet states of molecular oxygen. Indeed this is the mode of action in some photodynamic therapies in medicine.

Similarly, collisional deactivation is an important factor in trying to detect and measure various gaseous species in the troposphere using the technique of induced fluorescence. For example, as discussed in Chapter 11, induced fluorescence is one of the techniques applied to determine the concentration of OH free radicals in the troposphere. The OH is excited to the $A^2\Sigma^+$ state, from which it fluoresces as it returns to the ground state. However, collisional deactivation of excited OH by O_2 and N_2 is significant at 1 atm pressure; this reduces the emitted light relative to interfering signals. Expansion of the air sample to lower pressures reduces this quenching and increases the overall sensitivity (see Chapter 11).

b. Photochemical Processes

In contrast to the photo*physical* processes just described, photochemical processes produce new chemical species. Such processes can be characterized by the type of chemistry induced by light absorption: photodissociation, intramolecular rearrangements, photoisomerization, photodimerization, hydrogen atom abstraction, and photosensitized reactions.

Of these, photodissociation is by far the most pervasive and important in atmospheric chemistry. For example, the photodissociation of NO_2 into ground-state oxygen atoms,

$$NO_2(X^2A_1) + h\nu \ (290 < \lambda < 430 \text{ nm}) \rightarrow NO(X^2\Pi) + O(^3P), \quad (2)$$

followed by the reaction of $O(^3P)$ with O_2, is the sole known source of anthropogenically produced O_3 in the troposphere.

The reader will encounter numerous other examples of photodissociation throughout this text, so it will not be treated further here. However, as will become obvious in examining the chemistry of both the troposphere and stratosphere in later chapters, it is photochemistry that indeed drives the chemistry of the atmosphere.

c. Quantum Yields

The relative efficiencies of the various photophysical and photochemical primary processes are described in terms of quantum yields, ϕ. The primary quantum yield, ϕ, for the ith process, either photophysical or photochemical, is given by Eq. (I):

$$\phi_i = \frac{\text{Number of excited molecules proceeding by process } i}{\text{Total number of photons absorbed}} \quad (I)$$

For example, the nitrate radical, which plays an important role in nighttime chemistry (see Chapter 6), absorbs light in the red region of the visible (600–700 nm). The electronically excited state formed on light absorption can dissociate into either $NO_2 + O$ or into $NO + O_2$, or it can fluoresce:

$$NO_3 + h\nu \rightarrow NO_3^*, \quad (3)$$

$$NO_3^* \rightarrow NO_2 + O, \quad (4a)$$

$$\rightarrow NO + O_2, \quad (4b)$$

$$\rightarrow NO_3 + h\nu. \quad (4c)$$

The primary quantum yields for each process are defined as follows:

$$\phi_{4a} = \frac{\text{Number of } NO_2 \text{ or } O(^3P) \text{ formed in the primary process}}{\text{Number of photons absorbed by } NO_3},$$

$$\phi_{4b} = \frac{\text{Number of NO or } O_2 \text{ formed in the primary process}}{\text{Number of photons absorbed by } NO_3},$$

$$\phi_{4c} = \frac{\text{Number of photons emitted by } NO_3}{\text{Number of photons absorbed by } NO_3}.$$

ϕ_{4c} is also known as the fluorescence quantum yield, ϕ_f.

By definition, the sum of the primary quantum yields for all photochemical and photophysical processes taken together must add up to unity, i.e.,

$$\Sigma(\phi_f + \phi_p + \phi_{deact} + \ldots \phi_a + \phi_b + \ldots) = 1.0,$$

where ϕ_f, ϕ_p, and ϕ_{deact} are the primary quantum yields for the photophysical processes of fluorescence, phosphorescence, and collisional deactivation, respectively, and ϕ_a, ϕ_b, and so on are the primary quantum yields for the various possible photochemically reactive decomposition paths of the excited molecule.

For example, in the case of NO_3, ϕ_{4a} is, within experimental error, 1.0 up to 585 nm and then decreases to zero at 635 nm. As path (4a) falls off above 585 nm, path (4b), ϕ_{4b} increases to a peak of 0.36 at approximately 595 nm and then also decreases at longer wavelengths (Orlando *et al*., 1993; Davis *et al*., 1993; Johnston *et al*., 1996). As the quantum yields for both (4a) and (4b) decline, fluorescence, (4c) is observed (Nelson *et al*., 1983; Ishiwata *et al*., 1983), increasing toward unity at $\sim$ 640 nm. In short, at different wavelengths the contribution of the various processes, (4a), (4b), and (4c), varies, but always consistent with their sum being unity.

While the aim of photochemical studies is generally to measure primary quantum yields, this is not always experimentally feasible. For example, NO reacts rapidly with NO_3 to form NO_2. Thus determination of ϕ_{4a} or ϕ_{4b} by measuring the NO and NO_2 formed can be complicated by this secondary reaction of NO with NO_3, and the measured yields of NO and NO_2 may not reflect the efficiency of the primary photochemical processes.

In some cases, then, the *overall* quantum yield, rather than the *primary* quantum yield, is reported. The overall quantum yield for a particular product A, usually denoted by Φ_A, is defined as the number of molecules of the product A formed per photon absorbed. Because of the potential contribution of secondary chemistry to the formation of stable products, the overall quantum yield of a particular product may exceed unity. Indeed, in chain reactions, overall quantum yields for some products may be of the order of 10^6 or more.

B. ABSORPTION OF LIGHT

1. Basic Relationships

Light has both wave-like and particle-like properties. As a wave, it is a combination of oscillating electric and magnetic fields perpendicular to each other and to the direction of propagation (Fig. 3.10). The distance between consecutive peaks is the wavelength, λ, and the number of complete cycles passing a fixed point in 1 s is the frequency, ν. They are inversely proportional through the relationship

$$\lambda = c/\nu, \qquad \text{(J)}$$

where c is the speed of light in a vacuum, 2.9979×10^8 m s^{-1}.

Considered as a particle, the energy of a quantum of light E is

$$E = h\nu = hc/\lambda, \qquad \text{(K)}$$

where h is Planck's constant, 6.6262×10^{-34} J s per quantum, and the frequency ν is in s^{-1}. In the visible and ultraviolet regions of the spectrum, wavelength is commonly expressed in nanometer units, 1 nm = 10^{-9} m. In the older literature, units of angstroms, 1 Å = 10^{-10} m, are also found.

In the infrared region both microns [1 micron = 1 micrometer (μm) = 10^{-6} m] and wavenumbers ω (in cm^{-1}) are employed; ω is the reciprocal of the wave-

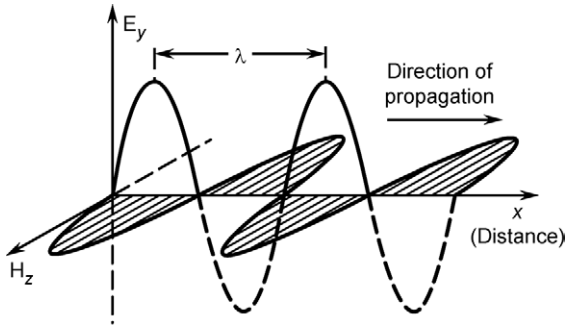

FIGURE 3.10 The instantaneous electric (E_y) and magnetic (H_z) field strength vectors of a plane-polarized light wave as a function of position along the axis of propagation (x) (from Calvert and Pitts, 1966).

length λ expressed in centimeters. It is directly related to energy through the Planck relationship,

$$E = hc\omega, \tag{L}$$

and today is generally the unit of choice in infrared spectroscopy.

Since chemists often deal experimentally with moles rather than molecules, a convenient unit is a mole of quanta, defined as 1 einstein. The energy of 1 einstein of light of wavelength λ in nm is

$$\begin{aligned} E &= (6.02 \times 10^{23})h\nu = 6.02 \times 10^{23} hc/\lambda, \\ &= 1.196 \times 10^5/\lambda \text{ kJ einstein}^{-1}, \\ &= 2.859 \times 10^4/\lambda \text{ kcal einstein}^{-1}. \end{aligned} \tag{M}$$

Another unit used in photochemistry to express the energy of a quantum of radiation is the electron volt; 1 eV = 96.49 kJ mol^{-1} = 23.06 kcal mol^{-1}. Thus for λ in nm

$$E = hc/\lambda = 1.240 \times 10^3/\lambda \text{ eV}. \tag{N}$$

To put these energies and wavelengths in perspective, Table 3.2 gives some typical wavelengths, frequencies, wavenumbers, and energies of various regions of the electromagnetic spectrum. The region of most direct interest in tropospheric photochemistry ranges from the visible at $\sim$ 700 nm to the near-ultraviolet at $\sim$ 290 nm, the short-wavelength cutoff of the stratospheric ozone layer. The corresponding energies [Eq. (M)], 170.9 and 412.4 kJ $einstein^{-1}$ (or 40.8 and 98.6 kcal $einstein^{-1}$), are sufficient to break chemical bonds ranging from, for example, the weak O_2—O bond in ozone, $\sim$ 100 kJ mol^{-1} ($\sim$ 25 kcal mol^{-1}), to the moderately strong C—H bond in formaldehyde, $\sim$ 368 kJ mol^{-1} ($\sim$ 88 kcal mol^{-1}).

Other spectral regions are also important because the detection and quantification of small concentrations of labile molecular, free radical, and atomic species of tropospheric interest both in laboratory studies and in ambient air are based on a variety of spectroscopic techniques that cover a wide range of the electromagnetic spectrum. For example, the relevant region for infrared spectroscopy of stable molecules is generally from $\sim$ 500 to 4000 cm^{-1} (20–2.5 μm), whereas the detection of atoms and free radicals by resonance fluorescence employs radiation down to 121.6 nm, the Lyman α line of the H atom.

Table 3.3 gives some relationships between commonly used energy units. Today the SI system of units is in general use, although much of the data in the literature is in the older units. Thus we use both types of units for energy, that is calories or kilocalories and joules or kilojoules, where 1 cal = 4.184 J.

2. The Beer–Lambert Law

The basis for the measurement of the strength of light absorption by a molecule at various wavelengths is shown in Fig. 3.11. A parallel monochromatic light beam of wavelength λ and power P_0 or intensity I_0, defined as the energy per second striking a unit area,

TABLE 3.2 Typical Wavelengths, Frequencies, Wavenumbers, and Energies of Various Regions of the Electromagnetic Spectrum

Name	Typical wavelength or range of wavelengths (nm)	Typical range of frequencies ν (s^{-1})	Typical range of wavenumbers ω (cm^{-1})	Typical range of energies (kJ $einstein^{-1}$)[a]
Radiowave	$\sim 10^8$–10^{13}	$\sim 3 \times 10^4$–3×10^9	10^{-6}–0.1	$\sim 10^{-3}$–10^{-8}
Microwave	$\sim 10^7$–10^8	$\sim 3 \times 10^9$–3×10^{10}	0.1–1	$\sim 10^{-2}$–10^{-3}
Far-infrared	$\sim 10^5$–10^7	$\sim 3 \times 10^{10}$–3×10^{12}	1–100	$\sim 10^{-2}$–1
Near-infrared	$\sim 10^3$–10^5	$\sim 3 \times 10^{12}$–3×10^{14}	10^2–10^4	$\sim$ 1–10^2
Visible				
Red	700	4.3×10^{14}	1.4×10^4	1.7×10^2
Orange	620	4.8×10^{14}	1.6×10^4	1.9×10^2
Yellow	580	5.2×10^{14}	1.7×10^4	2.1×10^2
Green	530	5.7×10^{14}	1.9×10^4	2.3×10^2
Blue	470	6.4×10^{14}	2.1×10^4	2.5×10^2
Violet	420	7.1×10^{14}	2.4×10^4	2.8×10^2
Near-ultraviolet	400–200	$(7.5–15.0) \times 10^{14}$	$(2.5–5) \times 10^4$	$(3.0–6.0) \times 10^2$
Vacuum ultraviolet	$\sim$ 200–50	$(1.5–6.0) \times 10^{15}$	$(5–20) \times 10^4$	$\sim (6.0–24) \times 10^2$
X-Ray	$\sim$ 50–0.1	$\sim (0.6–300) \times 10^{16}$	$(0.2–100) \times 10^6$	$\sim 10^3$–10^6
γ-Ray	$\leq$ 0.1	$\sim 3 \times 10^{18}$	$\geq 10^8$	$> 10^6$

[a] For kcal $einstein^{-1}$, divide by 4.184 (1 cal = 4.184 J).

TABLE 3.3 Some Relationships between Commonly Used Energy Units

(kJ mol^{-1})
$\times 0.2390$ = kcal mol^{-1}
$\times 0.0104$ = eV
$\times 83.59$ = cm^{-1}
(kcal mol^{-1})
$\times 4.184$ = kJ mol^{-1}
$\times 0.04336$ = eV
$\times 349.8$ = cm^{-1}
(cm^{-1})
$\times 1.196 \times 10^{-2}$ = kJ mol^{-1}
$\times 2.859 \times 10^{-3}$ = kcal mol^{-1}
$\times 1.240 \times 10^{-4}$ = eV
(eV)
$\times 96.49$ = kJ mol^{-1}
$\times 23.06$ = kcal mol^{-1}
$\times 8.064 \times 10^{3}$ = cm^{-1}

passes through a sample of length l (cm) and concentration C (mol L^{-1}). If this wavelength is absorbed by the sample, the power of the beam exiting the sample is reduced to P (or I). The transmittance (T) is defined as I/I_0 (or P/P_0).

As the light passes through a thickness of sample dl, it undergoes a fractional reduction in intensity proportional to the absorbing path length, i.e.,

$$(dI/I \propto) - (dl), \tag{O}$$

where the negative sign reflects the reduction in intensity with an increase in path length. Since the constant of proportionality must involve the concentration (C) of the absorbing substance, this integrates to

$$\ln(I/I_0) = -kCl. \tag{P}$$

The most commonly used form of this Beer–Lambert law involves logarithms to the base 10:

$$\log(I_0/I) = \varepsilon Cl. \tag{Q}$$

C is in units of mol L^{-1}, l is in cm, and the constant of proportionality ε (L mol^{-1} cm^{-1}) is known as the molar absorptivity or molar extinction coefficient. The dimensionless quantity $\log(I_0/I)$ is known as the absorbance, A, which is related to the transmittance by $A = \log(I_0/I) = -\log T$.

Most commercial spectrometers report absorbance, as defined in Eq. (Q), versus wavelength. This is very important to recognize, since as we will see later, calculations of the rate of light absorption in the atmosphere require the use of absorption coefficients to the base e rather than to the base 10. While the recent atmospheric chemistry literature reports absorption cross sections to the base e, most measurements of absorption coefficients reported in the general chemical literature are to the base 10. If these are to be used in calculating photolysis rates in the atmosphere, the factor of 2.303 must be taken into account.

In gas-phase tropospheric chemistry, the most common units for concentration, N, are molecules cm^{-3} and for path length, l, units of cm. The form of the Beer–Lambert law is then

$$\ln(I_0/I) = \sigma Nl \tag{R}$$

or

$$I/I_0 = \exp(-\sigma Nl), \tag{S}$$

where it must again be emphasized that σ, known as the absorption cross section, must have been measured with the appropriate form of the Beer–Lambert law to the base e. The dimensionless exponent σNl is often referred to as the "optical depth."

In the past, some absorption coefficients for gases have been reported with concentrations in units of atmospheres, so that the absorption coefficient is in units of atm^{-1} cm^{-1}. Since the pressure depends on temperature, the latter (usually 273 or 298 K) were also reported.

For most tropospheric situations involving gaseous species, the Beer–Lambert law is an accurate method for treating light absorption; similar considerations apply to nonassociated molecules in dilute solution. However, under laboratory conditions with relatively high concentrations of the absorbing species, deviations may arise from a variety of factors, including concentration- and temperature-dependent association or dissociation reactions, deviations from the ideal gas law, and saturation of very narrow lines with increasing

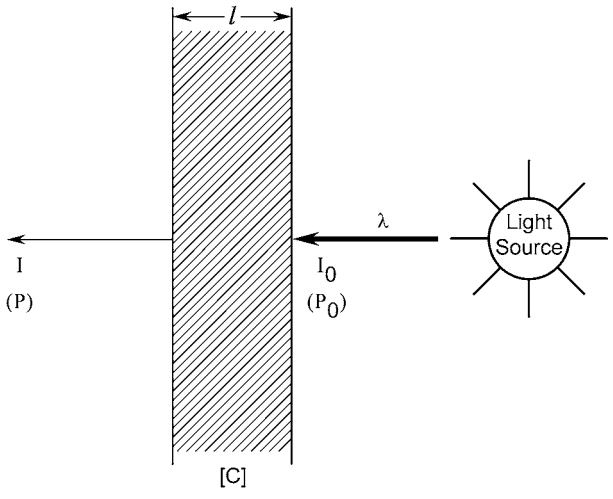

FIGURE 3.11 Schematic diagram of experimental approach to the Beer–Lambert law.

TABLE 3.4 Conversion Factors for Changing Absorption Coefficients from One Set of Units to Another

Both units in either logarithmic base e or base 10	
(cm^2 molecule^{-1})	$\times 2.69 \times 10^{19} = (\text{atm at } 273\text{ K})^{-1}\ (cm^{-1})$
	$\times 2.46 \times 10^{19} = (\text{atm at } 298\text{ K})^{-1}\ (cm^{-1})$
	$\times 3.24 \times 10^{16} = (\text{Torr at } 298\text{ K})^{-1}\ (cm^{-1})$
	$\times 6.02 \times 10^{20} = \text{L mol}^{-1}\ cm^{-1}$
(atm at 298 K)$^{-1}$ (cm^{-1})	$\times 4.06 \times 10^{-20} = cm^2$ molecule^{-1}
	$\times 1.09 = (\text{atm at } 273\text{ K})^{-1}\ (cm^{-1})$
(L mol^{-1} cm^{-1})	$\times 4.46 \times 10^{-2} = (\text{atm at } 273\text{ K})^{-1}\ (cm^{-1})$
	$\times 4.09 \times 10^{-2} = (\text{atm at } 298\text{ K})^{-1}\ (cm^{-1})$
	$\times 5.38 \times 10^{-5} = (\text{Torr at } 298\text{ K})^{-1}\ (cm^{-1})$
	$\times 1.66 \times 10^{-21} = cm^2$ molecule^{-1}
Change of both logarithmic base and units	
(cm^2 molecule^{-1}), base e	$\times 1.17 \times 10^{19} = (\text{atm at } 273\text{ K})^{-1}\ (cm^{-1})$, base 10
	$\times 1.07 \times 10^{19} = (\text{atm at } 298\text{ K})^{-1}\ (cm^{-1})$, base 10
	$\times 1.41 \times 10^{16} = (\text{Torr at } 298\text{ K})^{-1}\ (cm^{-1})$, base 10
	$\times 2.62 \times 10^{20} = \text{L mol}^{-1}\ cm^{-1}$, base 10
(L mol^{-1} cm^{-1}), base 10	$\times 3.82 \times 10^{-21} = cm^2$ molecule^{-1}, base e
	$\times 0.103 = (\text{atm at } 273\text{ K})^{-1}\ (cm^{-1})$, base e
	$\times 9.42 \times 10^{-2} = (\text{atm at } 298\text{ K})^{-1}\ (cm^{-1})$, base e
(atm at 273 K)$^{-1}$ (cm^{-1}), base 10	$\times 8.57 \times 10^{-20} = cm^2$ molecule^{-1}, base e
	$\times 51.6 = \text{L mol}^{-1}\ cm^{-1}$, base e
(Torr at 298 K)$^{-1}$ (cm^{-1}), base 10	$\times 7.11 \times 10^{-17} = cm^2$ molecule^{-1}, base e
	$\times 4.28 \times 10^{4} = \text{L mol}^{-1}\ cm^{-1}$, base e
(atm at 298 K)$^{-1}$ (cm^{-1}), base 10	$\times 9.35 \times 10^{-20} = cm^2$ molecule^{-1}, base e
	$\times 2.51 = (\text{atm at } 273\text{ K})^{-1}\ (cm^{-1})$, base e

concentrations, i.e., increasing pressures. Particularly important is the situation in which a "monochromatic" analyzer beam actually has a bandwidth that is broad relative to very narrow lines of an absorbing species. In this case, which is often encountered in the infrared, for example, the Beer–Lambert law is nonlinear. Clearly, to be on the safe side, it is good practice to verify the linearity of $\ln(I_0/I)$ plots as a function of absorber concentration when experimentally determining absorption coefficients.

Table 3.4 gives conversion factors for converting absorption coefficients from one set of units to another and for changing between logarithms to the base 10 and base e.

C. ATMOSPHERIC PHOTOCHEMISTRY

1. Solar Radiation and Its Transmission through the Atmosphere

a. The Sun and Its Relationship to the Earth: Some Important Definitions for Atmospheric Chemistry

The sun can be considered a spherical light source of diameter 1.4×10^6 km located 1.5×10^8 km from the earth's surface. Incoming direct sunlight at the earth's surface is treated as a beam with an angle of collimation of $\sim 0.5°$ and thus is essentially parallel to $\pm 0.25°$.

The total intensity of sunlight outside the earth's atmosphere is characterized by the solar constant, defined as the total amount of light received per unit area normal to the direction of propagation of the light; the mean value is 1368 W m^{-2}, although variations from this mean are common (Lean, 1991).

Of more direct interest for atmospheric photochemistry is the solar flux per unit interval of wavelength. Values up to approximately 400 nm are provided by Atlas 3 (see Web site in Appendix IV) and from 400 nm on by Neckel and Labs (1984). Figure 3.12 shows the solar flux as a function of wavelength outside the atmosphere and at sea level for a solar zenith angle of 0° (Howard *et al*., 1960).

Outside the atmosphere, the solar flux approximates blackbody emission at ~ 5770 K. However, light absorption or scattering by atmospheric constituents modifies the spectral distribution. The attenuation due to the presence of various naturally occurring atmospheric constituents is shown by the hatched areas in Fig. 3.12.

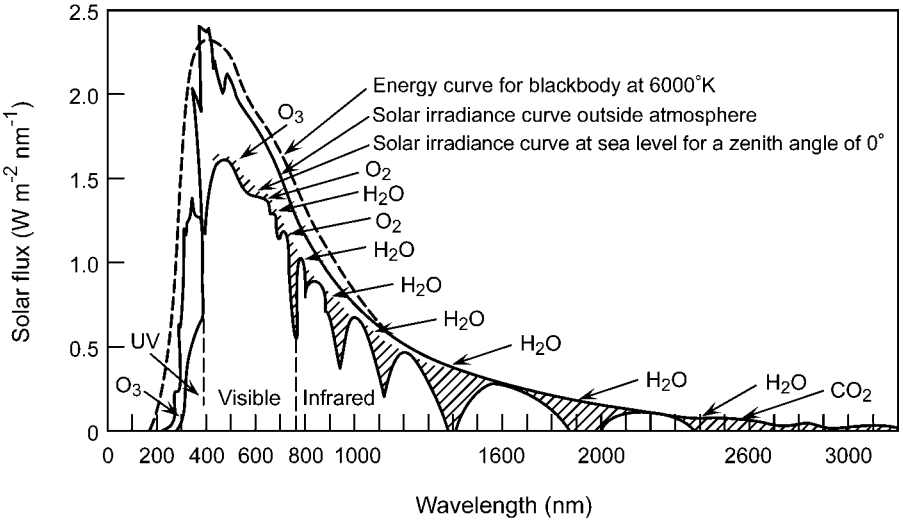

FIGURE 3.12 Solar flux outside the atmosphere and at sea level, respectively. The emission of a blackbody at 6000 K is also shown for comparison. The species responsible for light absorption in the various regions (O_3, H_2O, etc.) are also shown (from Howard *et al*., 1960).

Figure 3.13 shows the altitude corresponding to maximum light absorption by atomic and molecular oxygen and nitrogen and by O_3 as a function of wavelength up to $\lambda = 300$ nm with the sun directly overhead (Friedman, 1960).

Because of the presence of these absorbing species in the upper atmosphere, only light of $\lambda > 290$ nm is available for photochemical reactions in the troposphere. It is often expressed as the integrated radiation coming from all directions to a sphere and is referred to as *actinic radiation*, although in the strictest sense, "actinic" means "capable of causing photochemical reactions."

The ultraviolet region, $\lambda < 400$ nm, is often divided into what is known as the UV-A region from 315 to 400 nm, the UV-B region from 280 to 315 nm, and the UV-C region from 200 to 280 nm.

The effect of light scattering and absorption by atmospheric constituents on the intensity and wavelength distribution of sunlight at the earth's surface depends on both the nature and concentration of the gases and particles as well as the path length through

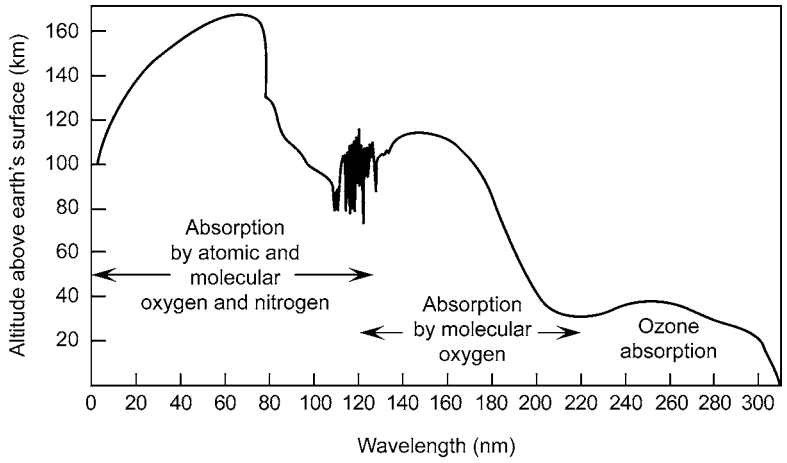

FIGURE 3.13 Approximate regions of maximum light absorption of solar radiation in the atmosphere by various atomic and molecular species as a function of altitude and wavelength with the sun overhead (from Friedman, 1960).

which the light passes, as expected from the Beer–Lambert law. The path length, that is, the distance from the outer reaches of the atmosphere to an observer on the earth's surface, is a function of the angle of the sun and hence time of day, latitude, and season. In addition, reflection of light from the earth's surface alters the light intensity at any given point in the atmosphere, as does the presence of clouds.

The angle of the sun relative to a fixed point on the surface of the earth is characterized by the solar zenith angle θ, defined, as shown in Fig. 3.14, as the angle between the direction of the sun and the vertical. Thus a zenith angle of zero corresponds to an overhead, noonday sun, and a zenith angle of $\sim 90°$ approximates sunrise and sunset. The greater the zenith angle, the longer is the path length through the atmosphere and hence the greater the reduction in solar intensity by absorption and scattering processes.

The path length L for direct solar radiation traveling through the earth's atmosphere to a fixed point on the earth's surface can be estimated geometrically using Fig. 3.14. This "flat earth" approximation is accurate for zenith angles $< 60°$. One can approximate L using

$$\cos\theta \cong h/L \tag{T}$$

or

$$L \cong h/\cos\theta \cong h \sec\theta. \tag{U}$$

A common term used to express the path length traversed by solar radiation to reach the earth's surface is the air mass, m, defined as

$$m = \frac{\text{Length of path of direct solar radiation through the atmosphere}}{\text{Length of vertical path through the atmosphere}}. \tag{V}$$

With reference to Fig. 3.14, for zenith angles less than 60°,

$$m \cong L/h \cong \sec\theta. \tag{W}$$

At larger angles, corrections for curvature of the atmosphere and refraction must be made to L and m.

Table 3.5 shows values of the air mass at various zenith angles θ, either estimated using $m = \sec\theta$ or corrected for curvature of the atmosphere and for refraction; it is seen that only for $\theta > 60°$ does this correction become significant.

b. Solar Spectral Distribution and Intensity in the Troposphere

When the radiation from the sun passes through the earth's atmosphere, it is modified both in intensity and in spectral distribution by absorption and scattering by gases as well as by particulate matter. As a result, the actual actinic flux to which a given volume of air is exposed is affected by the zenith angle (i.e., time of day, latitude, and season), by the extent of surface reflections, and by the presence of clouds. Madronich (1993) discusses these variables, with particular emphasis on the effects on the UV reaching the earth's surface.

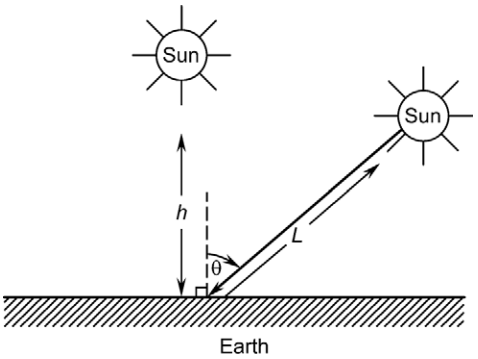

FIGURE 3.14 Definition of solar zenith angle θ at a point on the earth's surface.

To estimate the solar flux available for photochemistry in the troposphere then, one needs to know not only the flux outside the atmosphere but also the extent of light absorption and scattering within the atmosphere. We discuss here the actinic flux $F(\lambda)$ at the earth's surface; the effects of elevation and of height above the surface are discussed in Sections C.2.d and C.2.e.

The reduction in solar intensity due to scattering and absorption can be estimated using a form of the Beer–Lambert law:

$$I/I_0 = e^{-tm}. \tag{X}$$

In Eq. (X), I_0 is the light intensity at a given wavelength incident at the top of the atmosphere and I is the intensity of the light transmitted to the earth's surface; t is the total attenuation coefficient described below and m is the air mass as defined earlier. For the sun directly overhead (i.e., zenith angle $\theta = 0$) the air mass is unity ($m = 1.0$); the attenuation coefficient then reflects the minimum possible attenuation by the atmosphere. As θ increases until the sun is on the horizon (i.e., sunset or sunrise), m also increases (Table 3.5); thus the attenuation of the sunlight increases due to the increased path length in the atmosphere through which the light must travel to reach the earth's surface.

The attenuation coefficient, t, represents a combination of light scattering and absorption by gases and

BOX 3.1
CALCULATION OF SOLAR ZENITH ANGLE

The solar zenith angle can be calculated in the following manner for any particular location (i.e., latitude and longitude), day of the year (d_n), and time of day as described by Spencer (1971) and Madronich (1993). First, one needs to calculate what is known as the local hour angle (t_h), which is defined as the angle (in radians) between the meridian of the observer and that of the sun:

$$t_h \text{ (in radians)} = \pi[(\text{GMT}/12) - 1 + (\text{longitude}/180)] + \text{EQT},$$

where GMT is Greenwich mean time converted from the local time, longitudes (in degrees) west of the Greenwich meridian are negative, and EQT is the "equation of time," given by

$$\text{EQT} = 7.5 \times 10^{-5} + 1.868 \times 10^{-3} \cos N - 3.2077 \times 10^{-2} \sin N - 1.4615 \times 10^{-2} \cos 2N - 4.0849 \times 10^{-2} \sin 2N.$$

where N is defined as

$$N \text{ (in radians)} = 2\pi d_n/365.$$

The day of the year, d_n, is defined as the day number (0–364), with 0 corresponding to January 1 and 364 to December 31.

The second derived parameter that is needed for calculating the solar zenith angle at a particular time and place is the solar declination, δ, defined as the angle between the direction of the sun and the equatorial plane of the earth. The value of δ, which is 0° at the spring and fall equinoxes and falls between +23.45° (June 21) and −23.45° (December 21), can be calculated from the following:

$$\delta \text{ (in radians)} = 6.918 \times 10^{-3} - 0.399912 \cos N + 0.070257 \sin N - 6.758 \times 10^{-3} \times \cos 2N + 9.07 \times 10^{-4} \times \sin 2N - 2.697 \times 10^{-3} \cos 3N + 1.480 \times 10^{-3} \sin 3N.$$

The solar zenith angle (θ) for that particular time and place is then determined from:

$$\cos\theta = \sin\delta \sin(\text{latitude}) + \cos\delta \cos(\text{latitude}) \cos t_h,$$

where δ and t_h are calculated as already described and latitudes north of the equator (expressed in radians) are positive and south are negative. If all of the input parameters are in radians, θ is also obtained in radians and can be converted to degrees using 1 rad = 57.296°. For example, at Los Angeles, California (latitude = 34.03°N, longitude = 118.14°W) on September 21 at noon PST, GMT = 20.0, $N = 4.53$, EQT = 0.0301, $t_h = 0.0626$, $\delta =$ 0.0179 rad, and $\cos\theta = 0.837$, giving a solar zenith angle of 0.579 rad, or 33°.

particles and is actually a sum of four terms,

$$t = t_{sg} + t_{ag} + t_{sp} + t_{ap}, \qquad \text{(Y)}$$

where sg = light scattering by gases, ag = light absorption by gases, sp = light scattering by particles, and ap = light absorption by particles.

Gases scatter light by molecular, or Rayleigh, scattering. The intensity, $I(\lambda, \Theta)$ of light of wavelength λ scattered at an angle θ to the direction of incident light is determined by a number of factors. These include the incident light intensity, the angle Θ, the distance from the scattering molecule, and the index of refraction and size of the scattering molecule. In addition, and most importantly, Rayleigh scattering varies inversely with the fourth power of the wavelength.

Making the simplifying assumptions of a homogeneous atmosphere of fixed height of 7.996×10^5 cm and of uniform temperature and pressure throughout, Rayleigh scattering can be simplified for application to the atmosphere; as discussed in detail by Leighton (1961), the attenuation coefficient for scattering by gases, t_{sg}, becomes

$$t_{sg} = 1.044 \times 10^5 (n_{0\lambda} - 1)^2/\lambda^4, \qquad \text{(Z)}$$

where $n_{0\lambda}$ is the index of refraction of air at wavelength λ and the pressure and temperature of interest.

TABLE 3.5 Values of the Air Mass m at the Earth's Surface for Various Zenith Angles: (a) Calculated from $m = \sec\theta$ and (b) Corrected for Atmospheric Curvature and for Refraction

Zenith angle θ (deg)	$m = \sec\theta$	Air mass (m)
0	1.00	1.00
10	1.02	1.02
20	1.06	1.06
30	1.15	1.15
40	1.31	1.31
50	1.56	1.56
60	2.00	2.00
70	2.92	2.90
78	4.81	4.72
86	14.3	12.4

Source: Demerjian *et al*. (1980).

The dependence of Rayleigh scattering on λ^{-4} is evident in Fig. 3.15, which shows the attenuation coefficient for Rayleigh scattering as a function of wavelength from 290 to 700 nm; shorter wavelengths (i.e., in the blue ultraviolet region) are scattered much more strongly than the longer wavelengths.

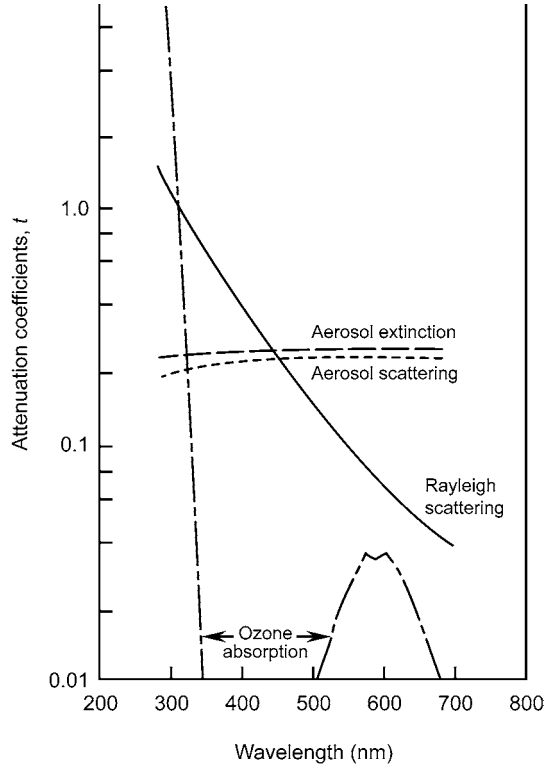

FIGURE 3.15 Attenuation coefficients (t) for light scattering (Rayleigh scattering) and absorption (ozone absorption) by gases and for scattering and scattering plus absorption (aerosol extinction) by particles [from Peterson (1976) and Demerjian *et al*. (1980)].

In the atmosphere, light absorption in the ultraviolet region is predominantly due to O_3 and this is predominantly in the stratosphere (Figs. 3.12 and 3.13). Since the absorption coefficients (σ) of O_3 are reasonably well established, a variant of the Beer–Lambert law can be applied to determine how much of the incident light is absorbed by O_3:

$$\frac{I}{I_0} = e^{-\sigma A m}. \qquad \text{(AA)}$$

A is the effective column O_3 (molecules cm^{-2}), σ its absorption cross section at that wavelength, and m the air mass. One needs to know, in addition to σ, the O_3 concentration as a function of altitude (z), that is,

$$A = \int_{z=0}^{\infty} O_3(z)\, dz.$$

Using the published absorption coefficients (σ) as a function of wavelength, one can then apply the Beer–Lambert law to calculate the intensity of light transmitted through such a vertical column to the earth's surface or to an altitude z. The resulting attenuation coefficients for O_3 are shown in Fig. 3.15 for an overhead sun. Clearly, O_3 is responsible for most of the attenuation of light directly from the sun of $\lambda < 310$ nm reaching the earth's surface.

This region of the spectrum around 300 nm is a crucial one for tropospheric photochemistry in both clean and polluted atmospheres. As we have indicated earlier, it is here that species such as ozone and aldehydes photolyze to produce atoms and free radicals critical to the chemistry of the troposphere.

Scattering and absorption of light by particulate matter are much more complex and will not be treated in detail here. Clearly, the size distribution and chemical composition, as well as the concentration of the particles, are very important in determining the extent of light scattering and absorption. Since these parameters will vary significantly geographically, seasonally, and diurnally, accurately estimating their impact on light intensities at a particular location at the earth's surface is difficult. Simplifications for the attenuation coefficient for scattering by particles such as

$$t_{sp} = b/\lambda^n \qquad \text{(BB)}$$

are often made, where b depends on the concentration of particles and n on their size; for example, n decreases from ~ 4 to 0 as the particle size increases (Leighton, 1961).

One estimate of the attenuation coefficients for light scattering by particles, t_{sp}, is also given in Fig. 3.15

(Demerjian *et al*., 1980). Also shown are these researchers' estimates of total scattering plus absorption due to particulate matter, known as the *aerosol extinction*:

$$t_{sp} + t_{ap} = \text{Aerosol extinction}.$$

In this case, the radii of the particles were assumed to fall between 0.01 and 2.0 μm; the peak in the number versus size distribution was at 0.07 μm.

Given estimated values for the attenuation coefficients for scattering and absorption of light by gases and particles (i.e., t_{sg}, t_{ag}, t_{sp}, and t_{ap}), one can calculate from Eq. (X) the fraction of the direct solar intensity incident on the top of the atmosphere that is transmitted to the earth's surface at any given wavelength. However, when one considers the *actual* light intensity that reaches a given volume of gas in the troposphere, one must take into account not only this direct solar radiation but also two other sources of indirect light: (1) light, either from the sun or reflected from the earth's surface, that is scattered to the volume by gases or particles, known as diffuse solar radiation or sky radiation, and (2) light that is reflected from the earth's surface. These are illustrated in Fig. 3.16.

Estimating the intensity of the scattered light at a given point in the atmosphere is difficult because of the substantial uncertainties and variability involved in the factors that contribute to light scattering; for example, the size distribution, concentration, and composition of particles, which to a large extent cause this scattering, are highly variable geographically and temporally and are not always well known for a particular point in space and time.

The amount of light reflected from the earth's surface to a volume of air clearly depends on the type of surface, as well as the wavelength of light; thus snow is highly reflecting, whereas black lava rock reflects very little of the incident radiation. The term used to describe the extent of this reflection is the *surface albedo*, which is the fraction of light incident on the surface that is reflected. Reflection can be specular, in which the angles of incidence and reflection are equal (e.g., a water surface at large zenith angles), or diffuse, in which light is reflected equally in all directions regardless of the angle of incidence (e.g., white rocks or buildings); the latter is known as "Lambertian" reflection. Table 3.6 gives some reported values of surface albedos for different types of surfaces. It should be noted that, as expected, albedos are wavelength dependent (e.g., see McLinden *et al*. (1997) for wavelength dependence of ocean albedos and Herman and Celarier (1997) for albedos in the UV from 340 to 380 nm).

One can thus estimate the total light intensity incident on a given volume of air in the troposphere due to direct solar radiation, scattering, and reflection. The light absorbed in that volume can then be calculated

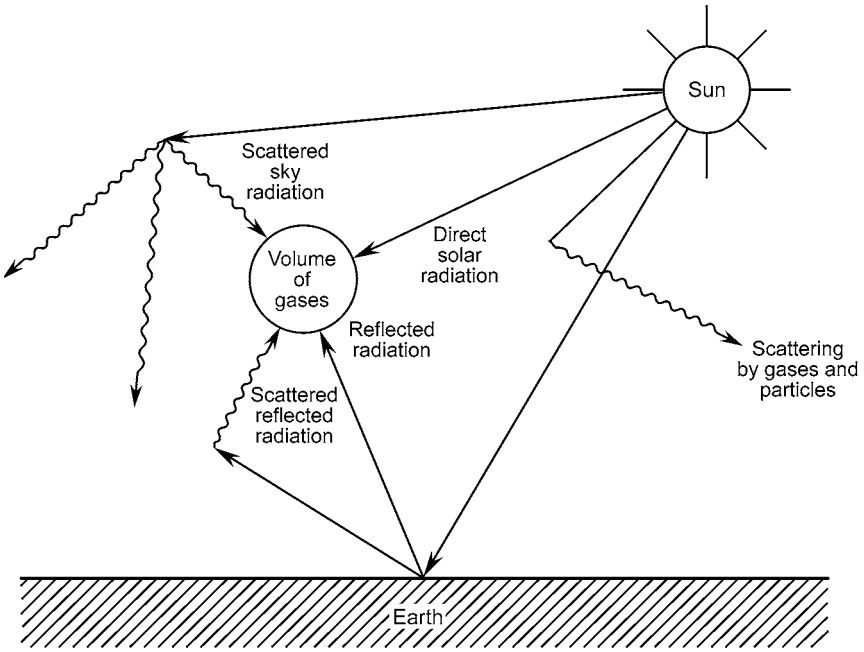

FIGURE 3.16 Different sources of radiation striking a volume of gas in the atmosphere. These sources are direction radiation from the sun, radiation scattered by gases and particles, and radiation reflected from the earth's surface.

TABLE 3.6 Some Typical Albedos for Various Types of Surfaces

Type of surface	Albedo	Reference
Snow	0.69	Angle *et al*., 1992
	0.93[b]	Dickerson *et al*., 1982
	0.9–1.0	Junkermann, 1994
Ocean	0.07[b]	Dickerson *et al*., 1982
	0.06–0.08[a]	Eck *et al*., 1987
Forests	0.06–0.18[b]	Dickerson *et al*., 1982
	0.02[a]	Eck *et al*., 1987
	0.17	Angle *et al*., 1992
Fields and meadows	0.03–0.04[a]	Eck *et al*., 1987
Desert	0.06–0.09[a]	Eck *et al*., 1987
Salt flats	0.57–0.65[a]	Eck *et al*., 1987

[a] Minimum reflectivities at 370 nm.
[b] Measured with respect to NO_2 photolysis.

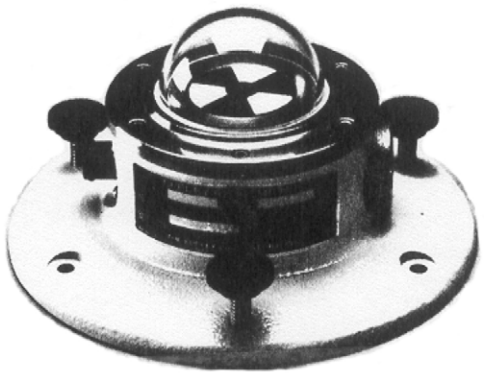

FIGURE 3.17 Typical device (Eppley Laboratories Model 8-48) used to measure solar irradiance. The detector consists of a differential thermopile with the hot junction receivers blackened with flat black coating and the cold junction receivers whitened with $BaSO_4$ (photo supplied courtesy of G. L. Kirk, Eppley Laboratories).

using the Beer–Lambert law, if the concentrations and absorption coefficients of all absorbing species are known.

2. Calculating Photolysis Rates in the Atmosphere

a. Photolysis Rate Constant [k_p], *Radiance* [$L(\lambda)$], *Actinic Flux* [$F(\lambda)$], *and Irradiance* [$E(\lambda)$]

The rate of photodissociation of a molecule, A, upon light absorption,

$$A + h\nu \rightarrow B + C, \tag{5}$$

can be described as a first-order process (see Chapter 5) with a rate constant, k_p, known as the photolysis rate constant:

$$d[A]/dt = -k_p[A]. \tag{CC}$$

In effect, k_p takes into account the intensity of available light that the molecule can absorb, the intrinsic strength of light absorption in that region by A, i.e., the absorption cross section σ, and the quantum yield for photodissociation, ϕ.

The light available to a molecule in air for absorption and photodissociation includes both direct and scattered and reflected radiation coming from all directions as described earlier and depicted in Fig. 3.16. The term *actinic flux* or *spherically integrated actinic flux,* denoted by $F(\lambda)$, is used to describe the total intensity of this light and is the quantity of interest in calculating k_p.

However, in practice, available light intensity is often measured using flat-plate devices such as the one shown in Fig. 3.17. Here light of a given wavelength that comes from all directions in a hemisphere and crosses the surface is measured. The net flux crossing the surface per unit area and time is known as the *irradiance*, $E(\lambda)$, and represents the flow of light across a flat plane rather than the total light coming from all directions that a molecule actually encounters in the atmosphere. Although actinic flux and irradiance are clearly related, they are not identical; for a detailed treatment of the actinic flux, irradiance, and radiance (defined next), see Madronich (1987).

An expression for the number of A molecules dissociating per unit volume per unit time is developed in Box 3.2. Comparing Eq. (NN) in Box 3.2 to Eq. (CC), the photolysis rate constant k_p must be given by

$$k_p = \int_\lambda \phi(\lambda)\sigma(\lambda)\int_\omega L(\lambda, \Theta, \phi)\, d\omega\, d\lambda$$
$$= \int_\lambda \phi(\lambda)\sigma(\lambda)F(\lambda)\, d\lambda, \tag{OO}$$

where $F(\lambda)$ is the spherically integrated actinic flux, Eq. (FF). We again stress that $\sigma(\lambda)$ is the absorption cross section to the base e, arising from the use of the differential form of the Beer–Lambert law to obtain Eq. (KK).

There are several approaches to measuring actinic fluxes and photolysis rate constants. One approach is to measure the rate of decay of a species such as NO_2 directly, so-called "chemical actinometry" (e.g. see Madronich *et al*., 1983). Another approach is to measure the light intensity and convert this to an actinic flux.

BOX 3.2
RELATIONSHIPS BETWEEN RADIANCE, IRRADIANCE, ACTINIC FLUX, AND PHOTOLYSIS RATE CONSTANTS

To calculate k_p, let us take the case shown in Fig. 3.18a of light striking the top of a very thin layer of air of thickness dz. The light originates in a solid angle $d\omega$ and strikes the top surface of the thin layer at an angle θ to the vertical. The intensity of the incoming light at angle θ shown in Fig. 3.18a is known as the *radiance*, $L(\lambda, \theta, \phi)$. By definition, radiance is the number of photons (or energy) in the wavelength interval $d\lambda$ originating from a small solid angle $d\omega$ and striking a small surface area da in time dt at an angle θ to the vertical.

However, the net flux across the surface is, in effect, determined by the portion of the surface that is perpendicular to the incoming light beam. As seen in Fig. 3.18b, from simple geometric considerations the portion of the surface perpendicular to the incoming beam is $2x = (da)\cos\theta$. Thus the net photons (or energy), dP in a wavelength interval $d\lambda$ that originates in a solid angle $d\omega$ and at an angle θ to the normal and crosses a small surface area, da, in time dt is given by

$$dP = L(\lambda, \theta, \phi)\cos\theta\, da\, d\omega\, dt\, d\lambda. \qquad \text{(DD)}$$

The *irradiance* $E(\lambda)$, which is directly measured by flat-plate devices, is by definition the total number of photons per unit surface area, time, and wavelength. Thus

$$E(\lambda) = \int (dP/da\, d\lambda\, dt) = \int L(\lambda, \theta, \phi)\cos\theta\, d\omega. \qquad \text{(EE)}$$

The actinic flux $F(\lambda)$ is the total incident light intensity integrated over all solid angles, given by

$$F(\lambda) = \int_{\omega} L(\lambda, \theta, \phi)\, d\omega. \qquad \text{(FF)}$$

Thus the irradiance, $E(\lambda)$, and the actinic flux, $F(\lambda)$, differ by the factor $\cos\theta$. Only for $\theta = 0°$, i.e., for a parallel beam of light perpendicular to the surface, are the irradiance and flux equal.

We now need to convert $d\omega$ into terms involving the spherical coordinates θ and ϕ. As shown in Fig. 3.19a, a given solid angle ω traces an area a on the surface of a sphere of radius r. When $a = r^2$, the solid angle ω is by definition 1 sr (sr = steradian). For the more general case of a surface area a subtended by the solid angle ω,

$$\omega \text{ (steradians)} = a/r^2$$

or

$$d\omega = da/r^2. \qquad \text{(GG)}$$

As shown in Fig. 3.19b, for small changes in the angles θ and ϕ, there is a change in the surface area, da, on a sphere of radius r given by

$$da = (r\sin\theta\, d\phi)(r\, d\theta) = r^2 \sin\theta\, d\theta\, d\phi,$$

i.e.,

$$d\omega = da/r^2 = \sin\theta\, d\theta\, d\phi. \qquad \text{(HH)}$$

Combining Eqs. (FF) and (HH), the actinic flux becomes

$$F(\lambda) = \int_{\phi}\int_{\theta} L(\lambda, \theta, \phi)\sin\theta\, d\theta\, d\phi. \qquad \text{(II)}$$

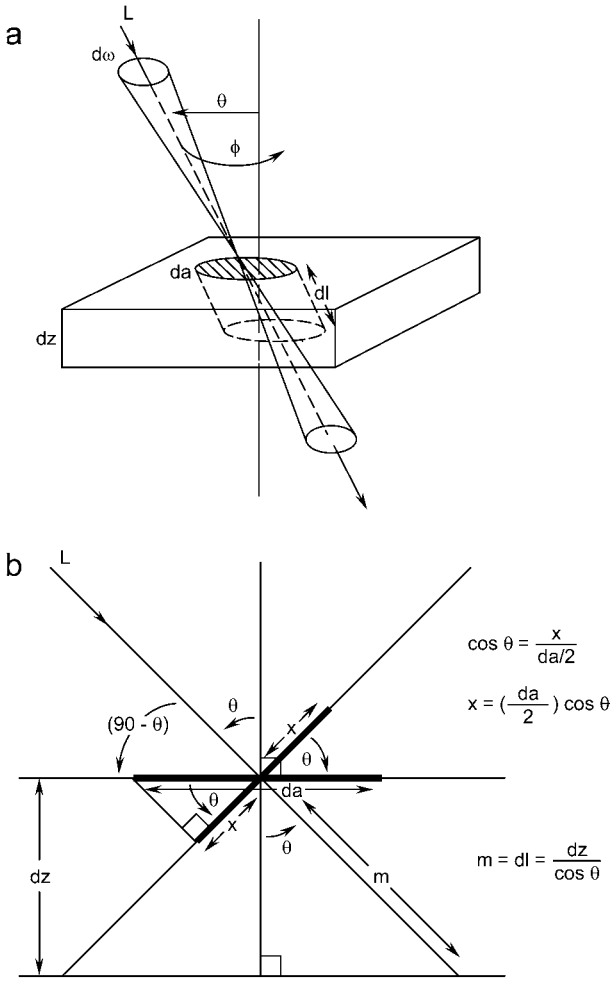

FIGURE 3.18 Typical light ray striking a thin layer of air in the atmosphere (adapted from Madronich, 1987).

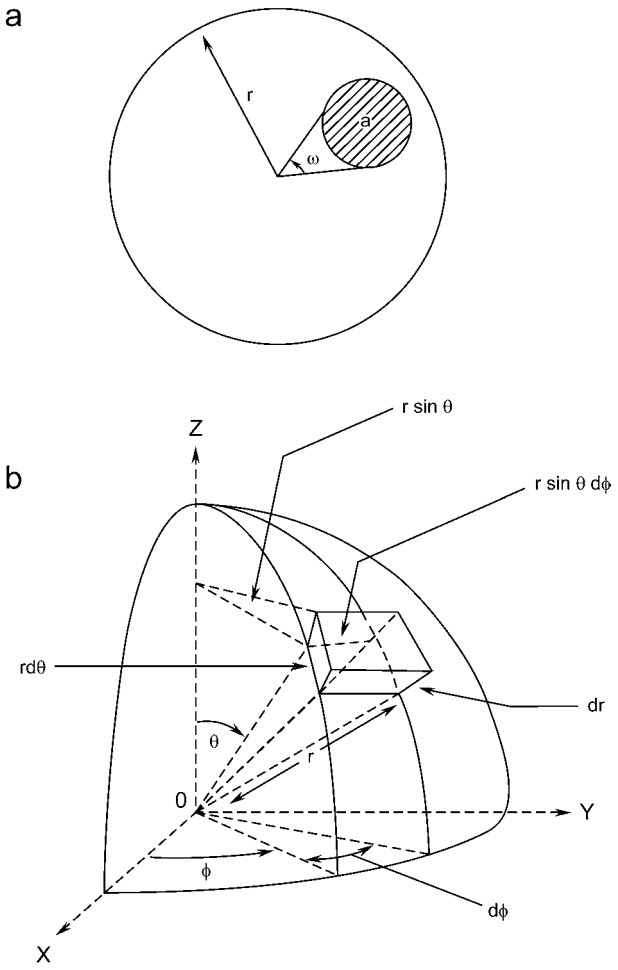

FIGURE 3.19 Conversion of solid angle ω to spherical coordinates.

Similarly, the irradiance $E(\lambda)$ is given by

$$E(\lambda) = \int_{\omega} L(\lambda, \theta, \phi)\cos\theta \, d\omega$$
$$= \int_{\phi}\int_{\theta} L(\lambda, \theta, \phi)\sin\theta\cos\theta \, d\theta \, d\phi. \quad \text{(JJ)}$$

Returning to Fig. 3.18a, as light passes through this thin layer of air, it can be absorbed by the molecules of A. From the differential form of the Beer–Lambert law, Eq. (O), the change in light intensity, dI, on passing through this small volume of air containing the absorber A is given by

$$dI/I \propto -(dl) = -k\,dl = -\sigma[\mathrm{A}]\,dl,$$

where the negative sign indicates that the intensity decreases as the light passes through the sample.

It is important to note that the application of this form of the Beer–Lambert law, inherent in which are natural logarithms, means that the absorption cross section, σ, must be that to the base e.

The absolute change in intensity at a particular wavelength is thus given by $dI = \sigma(\lambda)[\mathrm{A}]I\,dl$. This is just the number of photons absorbed as the light passes through the thin layer. I is the incident light, i.e., dP from Eq. (DD). If the quantum yield at this wavelength is $\phi(\lambda)$, then using $I = dP$ and substituting in for dP from Eq. (DD), the total number of molecules of A that photodissociate is given by

$$\text{Number of A dissociating}$$
$$= \phi(\lambda)\,dI = \phi(\lambda)\sigma(\lambda)[\mathrm{A}]\,dP\,dl$$
$$= \phi(\lambda)\sigma(\lambda)[\mathrm{A}]\,dl$$
$$\times\{L(\lambda, \theta, \phi)\cos\theta\,da\,d\omega\,dt\,d\lambda\}. \quad \text{(KK)}$$

Since the total path length for light absorption is given by $dl = dz/\cos\theta$ (Fig. 3.18b), this becomes

$$\text{Number of A dissociating}$$
$$= \phi(\lambda)\sigma(\lambda)[\mathrm{A}]\,dz \times \{L(\lambda, \theta, \phi)\,da\,d\omega\,dt\,d\lambda\}. \quad \text{(LL)}$$

However, this represents the number of A molecules dissociating only due to light absorption in the wavelength interval $d\lambda$ and only for incident light over the solid angle $d\omega$ and surface area da. To obtain the total number of A dissociating, Eq. (LL) must be integrated over all wavelengths, solid angles, and surface areas

$$\text{Total number of A dissociating}$$
$$= \int_{\lambda}\int_{\omega}\int_{a} \phi(\lambda)\sigma(\lambda)[\mathrm{A}]L(\lambda, \theta, \phi)dz\,da\,d\omega\,dt\,d\lambda$$
$$= [\mathrm{A}]\,dt\left(\int_{a} dz\,da\right)$$
$$\times\left\{\int_{\lambda}\int_{\omega} \phi(\lambda)\sigma(\lambda)L(\lambda, \theta, \phi)\,d\omega\,d\lambda\right\}. \quad \text{(MM)}$$

The first integration over the surface area a is just the volume. Rearranging, Eq. (MM) becomes

$$\frac{\text{Total number of A dissociating/volume}}{dt}$$
$$= -\frac{d[\mathrm{A}]}{dt}$$
$$= [\mathrm{A}]\int_{\lambda}\int_{\omega} \phi(\lambda)\sigma(\lambda)L(\lambda, \theta, \phi)\,d\omega\,d\lambda$$
$$= [\mathrm{A}]\int_{\lambda} \phi(\lambda)\sigma(\lambda)\int_{\omega} L(\lambda, \theta, \phi)\,d\omega\,d\lambda. \quad \text{(NN)}$$

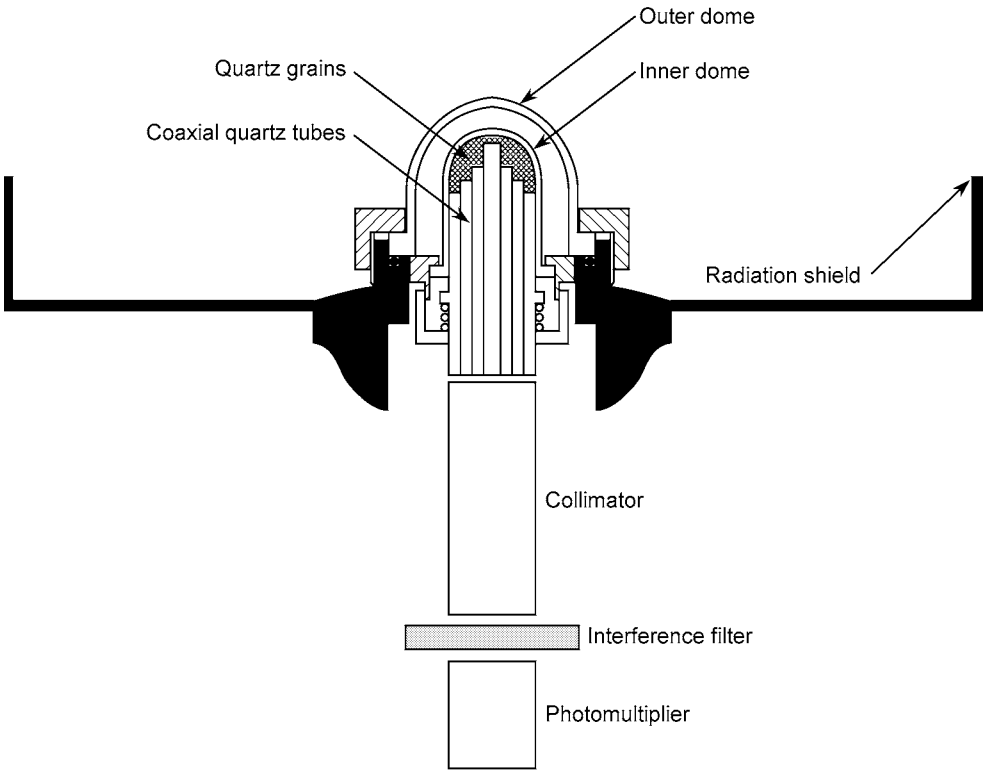

FIGURE 3.20 Schematic diagram of a 2π radiometer used to measure actinic fluxes (adapted from Junkermann *et al*., 1989).

Light intensities can be measured using flat-plate radiometers such as that in Fig. 3.17. As discussed earlier, this measures the flux through a horizontal plane, and as a result there is a difference of $\cos\theta$ between this measured *irradiance* and the actinic flux (Box 3.2). Another approach is to use what is sometimes referred to as a 2π radiometer, which measures the light intensity striking half of a sphere. A typical example is shown in Fig. 3.20 (Junkermann *et al*., 1989). The light collector consists of coaxial quartz tubes located inside a quartz dome, such that light is collected from all directions in a hemisphere equally well (hence the "2π" designation). Because light is collected from all directions within 2π sr, the $\cos\theta$ factor does not apply. The space between the quartz tubes and the dome is filled with quartz grains to scatter the light. The scattered light is transmitted by the quartz tubes through a set of interference filters to a detector. The filter–detector combination is chosen for the particular measurement of interest, e.g., O_3 or NO_2 photolysis. The shield is used to limit the field of view to exactly 2π sr. Two such detectors, one pointing up and one pointing down, can be used to cover the entire 4π sphere. A similar detector for aircraft use is described by Volz-Thomas *et al*. (1996).

b. Estimates of the Actinic Flux, F(λ), at the Earth's Surface

There are a number of estimates of the actinic flux at various wavelengths and solar zenith angles in the literature (e.g., see references in Madronich, 1987, 1993). Clearly, these all involve certain assumptions about the amounts and distribution of O_3 and the concentration and nature (e.g., size distribution and composition) of particles which determine their light scattering and absorption properties. Historically, one of the most widely used data sets for actinic fluxes at the earth's surface is that of Peterson (1976), who recalculated these solar fluxes from 290 to 700 nm using a radiative transfer model developed by Dave (1972). Demerjian *et al*. (1980) then applied them to the photolysis of some important atmospheric species. In this model, molecular scattering, absorption due to O_3, H_2O, O_2, and CO_2, and scattering and absorption by particles are taken into account.

Madronich (1998) has calculated actinic fluxes using updated values of the extraterrestrial flux. In the 150- to 400-nm region, values from *Atlas* are used (see Web site in Appendix IV) whereas from 400 to 700 nm those of Neckel and Labs (1984) are used. In addition, the

ozone absorption cross sections of Molina and Molina (1986) and the radiation scheme of Stamnes *et al.* (1988) were used. Other assumptions, e.g., the particle concentration and distribution, are the same as those of Demerjian *et al.* (1980).

In the "average" case for which the model calculations were carried out, absorption and scattering as the light traveled from the top of the atmosphere to the earth's surface were assumed to be due to O_3 (UV light absorption with column O_3 of 300 Dobson units), air molecules (scattering), and particles (scattering and absorption). The "best estimate" surface albedo varied from 0.05 in the 290- to 400-nm region to 0.15 in the 660- to 700-nm region. The surface was assumed to be what is known as an ideal "Lambert surface," meaning that it diffuses the incident light sufficiently well that it is reradiated equally in all upward directions, i.e., isotropically.

Table 3.7 gives the calculated actinic fluxes at the earth's surface as a function of zenith angle assuming the "best estimate" surface albedo. These data are plotted for six wavelength intervals as a function of zenith angle in Fig. 3.21. The initially small change in actinic flux with zenith angle as it increases from 0 to $\sim 50°$ at a given wavelength followed by the rapid drop of intensity from 50 to 90° is due to the fact that the air mass m changes only gradually to $\sim 50°$ but then increases much more rapidly to $\theta = 90°$ [see Table 3.5 and Eq. (X)]. At the shorter wavelengths at a fixed zenith angle, the rapid increase in actinic flux with wavelength is primarily due to the strongly decreasing O_3 absorption in this region.

The actinic fluxes calculated by Madronich (1998) for altitudes of 15, 25, and 40 km are collected in Tables 3.15 to 3.17.

c. Effects of Latitude, Season, and Time of Day on $F(\lambda)$

To estimate photolysis rates for a given geographical location, one must take into account the latitude and season, as well as the time of day.

The data in Table 3.7 are representative for the average earth–sun distance characteristic of early April and October. The orbit of the earth is slightly elliptical, so that there is a small change in the earth–sun distance, which causes a small change ($< 3\%$) in the solar flux with season. Correction factors for this seasonal variation for some dates from Demerjian *et al.* (1980) are given in Table 3.8. As discussed by Madronich (1993), the correction factors for solar intensity can be calculated for any other date using the following

$$(R_0/R_n)^2 = 1.000110 + 0.034221\cos N + 1.280 \times 10^{-3}\sin N + 7.19 \times 10^{-4}\cos 2N + 7.7 \times 10^{-5}\sin 2N,$$

where R_0 is the average earth–sun distance, R_n is the earth–sun distance on day d_n as defined earlier, $N = 2\pi d_n/365$ radians, and $(R_0/R_n)^2$ represents the correction factor.

Table 3.9 summarizes the solar zenith angles at latitudes of 20, 30, 40, and 50°N as a function of month and true solar time. True solar time, also known as apparent solar time or apparent local solar time, is defined as the time scale referenced to the sun crossing the meridian at noon. For example, at a latitude of 50°N at the beginning of January, two hours before the sun crosses the meridian corresponds to a true solar time of 10 a.m.; from Table 3.9, the solar zenith angle at this time is 77.7°.

To obtain the actinic flux at this time at any wavelength, one takes the fluxes in Table 3.7 listed under 78°; thus the flux in the 400- to 405-nm wavelength interval at 10 a.m. at 50°N latitude is 0.48×10^{15} photons cm^{-2} s^{-1}.

For other latitudes, dates, and times, the solar zenith angle can be calculated as described by Madronich (1993) and summarized earlier.

Afternoon values of θ are not given in Table 3.9 as the data are symmetrical about noon. Thus at a time of 2 p.m. at 50°N latitude, the flux would be the same as calculated for 10 a.m.

Figure 3.22 shows the solar angle θ as a function of true solar time for several latitudes and different times of the year. As expected, only for the lower latitudes at the summer solstice does the solar zenith angle approach 0° at noon. For a latitude of 50°N even at the summer solstice, θ is 27°.

Figure 3.23 shows the diurnal variation of the solar zenith angle as a function of season for Los Angeles, which is located at a latitude of 34.1°N. Clearly, the peak solar zenith angle varies dramatically with season.

These differences in light intensity, and in its diurnal variation at different latitudes and seasons, are critical because they alter the atmospheric chemistry at various geographical locations due to the fact that photochemistry is the major source of the free radicals such as OH that drive the chemistry.

d. Effect of Surface Elevation on $F(\lambda)$

The variation in the actinic flux with *surface* elevation is important because some of the world's major cities are located substantially above sea level. For example, Mexico City and Denver, Colorado, are at elevations of 2.2 and 1.6 km, respectively.

Table 3.10 shows the calculated percentage increase in the actinic flux at the earth's surface for an elevation of 1.5 km and atmospheric pressure of 0.84 atm (corresponding approximately to Denver) as a function of zenith angle for four wavelength intervals. In this calculation, it was assumed that the vertical O_3 and particle

TABLE 3.7 Actinic Flux Values $F(\lambda)$ at the Earth's Surface as a Function of Wavelength Interval and Solar Zenith Angle within Specific Wavelength Intervals for Best Estimate Surface Albedo Calculated by Madronich (1998)[a]

Wavelength interval (nm)	Exponent[b]	Solar zenith angle (deg)									
		0	10	20	30	40	50	60	70	78	86
		Actinic fluxes (photons cm^{-2} s^{-1})									
290–292	14	0.00	0.00	0.00	0.00	0.00	0.00	0.00	0.00	0.00	0.00
292–294	14	0.00	0.00	0.00	0.00	0.00	0.00	0.00	0.00	0.00	0.00
294–296	14	0.00	0.00	0.00	0.00	0.00	0.00	0.00	0.00	0.00	0.00
296–298	14	0.01	0.01	0.01	0.01	0.00	0.00	0.00	0.00	0.00	0.00
298–300	14	0.03	0.03	0.02	0.02	0.01	0.00	0.00	0.00	0.00	0.00
300–302	14	0.07	0.07	0.06	0.04	0.03	0.01	0.00	0.00	0.00	0.00
302–304	14	0.18	0.18	0.15	0.12	0.08	0.04	0.01	0.00	0.00	0.00
304–306	14	0.33	0.32	0.29	0.23	0.16	0.09	0.04	0.01	0.00	0.00
306–308	14	0.51	0.49	0.45	0.37	0.28	0.17	0.08	0.02	0.00	0.00
308–310	14	0.66	0.65	0.60	0.51	0.40	0.27	0.14	0.04	0.01	0.00
310–312	14	0.99	0.97	0.90	0.79	0.64	0.45	0.25	0.09	0.02	0.00
312–314	14	1.22	1.19	1.12	1.00	0.82	0.61	0.36	0.14	0.04	0.00
314–316	14	1.37	1.34	1.27	1.14	0.96	0.73	0.46	0.20	0.06	0.01
316–318	14	1.67	1.64	1.56	1.42	1.22	0.95	0.62	0.29	0.10	0.01
318–320	14	1.70	1.68	1.60	1.47	1.27	1.01	0.69	0.34	0.13	0.02
320–325	14	5.30	5.24	5.03	4.66	4.10	3.34	2.36	1.27	0.52	0.10
325–330	14	7.72	7.63	7.36	6.88	6.15	5.12	3.75	2.15	0.96	0.22
330–335	14	8.26	8.17	7.91	7.44	6.70	5.65	4.23	2.50	1.16	0.29
335–340	14	7.98	7.91	7.67	7.24	6.56	5.59	4.25	2.58	1.23	0.33
340–345	14	8.64	8.57	8.32	7.88	7.17	6.15	4.73	2.91	1.40	0.38
345–350	14	8.73	8.65	8.42	7.99	7.30	6.30	4.88	3.04	1.47	0.40
350–355	14	10.00	9.92	9.67	9.20	8.43	7.31	5.71	3.60	1.76	0.47
355–360	14	8.98	8.91	8.69	8.28	7.62	6.64	5.22	3.33	1.64	0.43
360–365	14	9.97	9.90	9.67	9.23	8.52	7.46	5.91	3.80	1.88	0.49
365–370	15	1.24	1.23	1.20	1.15	1.07	0.94	0.75	0.48	0.24	0.06
370–375	15	1.10	1.09	1.07	1.02	0.95	0.84	0.67	0.44	0.22	0.06
375–380	15	1.26	1.25	1.22	1.17	1.09	0.97	0.78	0.52	0.26	0.07
380–385	15	1.06	1.06	1.04	1.00	0.93	0.82	0.67	0.45	0.23	0.06
385–390	15	1.17	1.16	1.14	1.10	1.03	0.92	0.75	0.50	0.26	0.06
390–395	15	1.17	1.17	1.14	1.10	1.03	0.92	0.76	0.51	0.27	0.07
395–400	15	1.43	1.42	1.40	1.35	1.26	1.13	0.93	0.64	0.33	0.08
400–405	15	2.02	2.01	1.98	1.91	1.79	1.61	1.33	0.91	0.48	0.12
405–410	15	1.97	1.96	1.92	1.86	1.75	1.57	1.30	0.90	0.48	0.12
410–415	15	2.06	2.04	2.01	1.94	1.83	1.65	1.37	0.96	0.51	0.12
415–420	15	2.09	2.08	2.05	1.98	1.87	1.69	1.41	0.99	0.54	0.13
420–430	15	4.13	4.11	4.04	3.92	3.70	3.36	2.82	2.00	1.09	0.26
430–440	15	4.26	4.24	4.18	4.05	3.84	3.50	2.96	2.12	1.17	0.28
440–450	15	5.05	5.03	4.96	4.82	4.57	4.18	3.56	2.58	1.45	0.34
450–460	15	5.66	5.64	5.56	5.39	5.12	4.67	3.98	2.90	1.65	0.38
460–470	15	5.75	5.72	5.64	5.48	5.21	4.77	4.08	3.00	1.72	0.39
470–480	15	5.86	5.83	5.75	5.60	5.32	4.89	4.19	3.10	1.80	0.41
480–490	15	5.74	5.72	5.64	5.49	5.23	4.81	4.14	3.08	1.80	0.40
490–500	15	5.94	5.91	5.83	5.68	5.42	5.00	4.31	3.22	1.90	0.42
500–510	15	6.10	6.07	5.99	5.82	5.54	5.09	4.38	3.27	1.92	0.42
510–520	15	5.98	5.95	5.87	5.71	5.44	5.00	4.32	3.24	1.92	0.41
520–530	15	6.20	6.17	6.09	5.92	5.64	5.20	4.49	3.37	2.00	0.42
530–540	15	6.38	6.38	6.27	6.10	5.81	5.35	4.63	3.48	2.07	0.42
540–550	15	6.37	6.34	6.26	6.10	5.81	5.35	4.63	3.49	2.08	0.42
550–560	15	6.55	6.52	6.43	6.26	5.96	5.49	4.74	3.57	2.13	0.43
560–570	15	6.61	6.58	6.49	6.31	6.01	5.53	4.78	3.59	2.13	0.41
570–580	15	6.69	6.66	6.57	6.39	6.09	5.60	4.84	3.64	2.17	0.41
580–600	16	1.35	1.34	1.32	1.29	1.23	1.13	0.98	0.74	0.45	0.09
600–620	16	1.36	1.35	1.34	1.30	1.24	1.14	0.99	0.75	0.46	0.09
620–640	16	1.37	1.37	1.35	1.31	1.26	1.16	1.01	0.78	0.48	0.10
640–660	16	1.38	1.37	1.35	1.32	1.26	1.17	1.02	0.79	0.50	0.11
660–680	16	1.43	1.42	1.40	1.37	1.31	1.21	1.06	0.83	0.53	0.12
680–700	16	1.40	1.40	1.38	1.34	1.28	1.19	1.05	0.82	0.54	0.12

[a] The authors are grateful to Dr. Sasha Madronich for generously providing these calculations.

[b] This column lists the power of 10 by which all entries should be multiplied. For example, at $\theta = 0°$ the total actinic flux in the wavelength interval from 306 to 308 nm is 0.51×10^{14} photons cm^{-2} s^{-1}.

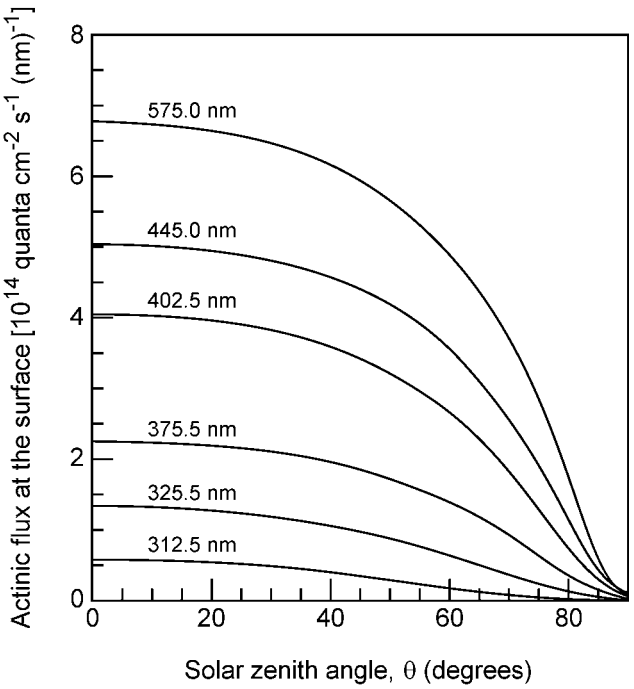

FIGURE 3.21 Calculated actinic flux centered on the indicated wavelengths at the earth's surface using best estimate albedos as a function of solar zenith angle (from Madronich, 1998).

concentrations were the same but that the Rayleigh scattering was reduced due to the lowered pressure, i.e., lower gas concentrations. The increase in actinic flux in the UV is relatively small ($< 5\%$) for zenith angles less than $\sim 45°$; at larger zenith angles, the change is less than 13%. For the longer wavelengths, it is small at all zenith angles. (Although these data are those of Peterson (1976) and Demerjian *et al*. (1980), since they are relative values, they are not expected to differ significantly from those that would be derived with the Madronich (1998) actinic flux values.)

TABLE 3.8 Correction Factors for Extraterrestrial Solar Flux Values Depending on Earth – Sun Distance at Various Times of the Year

Date	Correction factor	Date	Correction factor
Jan 1	1.033	Jul 1	0.966
Jan 15	1.032	Jul 15	0.967
Feb 1	1.029	Aug 1	0.970
Feb 15	1.024	Aug 15	0.974
Mar 1	1.018	Sep 1	0.982
Mar 15	1.011	Sep 15	0.989
Apr 1	1.001	Oct 1	0.998
Apr 15	0.993	Oct 15	1.006
May 1	0.984	Nov 1	1.015
May 15	0.978	Nov 15	1.022
Jun 1	0.971	Dec 1	1.027
Jun 15	0.968	Dec 15	1.031

Source: Demerjian *et al*. (1980).

e. Effect of Height above Earth's Surface on $F(\lambda)$

Figure 3.24 shows the *relative* changes in the total actinic flux as a function of altitude from 0 to 15 km at solar zenith angles of 20, 50, and 78° and at wavelengths of 332.5 (part a), 412.5 (part b), and 575 nm (part c), respectively. Again, since these are relative changes, these results of Peterson (1976) and Demerjian *et al*. (1980) are not expected to be significantly different from those that would be obtained with the Madronich (1998) actinic flux estimates.

At the largest solar zenith angle shown, 78°, all of the curves show a decrease in the actinic flux from 15 km to lower altitudes. This occurs because at these large values of θ and hence long path lengths through the atmosphere, backscattering of the light increases as it passes through the atmosphere.

The calculated actinic flux typically increases significantly in the first few kilometers. This is partly due to scattering of light by particulate matter and to light absorption by tropospheric O_3 close to the surface. The effect of O_3 can be seen by comparing the total fluxes at 332.5 nm (Fig. 3.24a), where O_3 absorbs, to those at 575 nm (Fig. 3.24b), where it does not.

Peterson and co-workers have examined the percentage increase in total actinic flux, going from the surface to ~ 1 km; they estimate that at short wavelengths ($\lambda \leq 310$ nm), the increase is $> 37.5\%$ for all zenith angles. This increase in flux with altitude at short wavelengths could be particularly significant in photochemical smog formation. Thus pollutants trapped in an inversion layer aloft may be exposed to higher actinic fluxes than at ground level and photolyze more rapidly, hastening the formation of various secondary pollutants. The increased actinic flux with altitude close to the earth's surface is the basis for their suggestion that the presence of increased O_3 in, or close to, the inversion layer may be at least partially the result of the height dependence of $F(\lambda)$.

These predictions have been borne out experimentally in studies in which the rate of photolysis of NO_2 was measured from the surface to ~ 7.6-km altitude and found to increase with height by more than 50% (Kelley *et al*., 1995; Volz-Thomas *et al*., 1996).

f. Sensitivity of Calculated Actinic Fluxes to Input Values for Surface Albedo and Ozone and Particle Concentrations

As discussed earlier, the net actinic flux incident on a volume of air is sensitive to a number of parameters,

TABLE 3.9 Tabulation of Solar Zenith Angles (deg) as a Function of True Solar Time and Month

	0400	0430	0500	0530	0600	0630	0700	0730	0800	0830	0900	0930	1000	1030	1100	1130	1200
								Latitude 20°N									
Jan 1							84.9	78.7	72.7	66.1	61.5	56.5	52.1	48.3	45.5	43.6	43.0
Feb 1						88.9	82.5	75.8	69.6	63.3	57.7	52.2	47.4	43.1	40.0	37.8	37.2
Mar 1						85.7	78.8	72.0	65.2	58.6	52.3	46.2	40.5	35.5	31.4	28.6	27.7
Apr 1					88.5	81.5	74.4	67.4	60.3	53.4	46.5	39.7	33.2	26.9	21.3	17.2	15.5
May 1					85.0	78.2	71.2	64.3	57.2	50.2	43.2	36.1	29.1	26.1	15.2	8.8	5.0
Jun 1				89.2	82.7	76.0	69.3	62.5	55.7	48.8	41.9	35.0	28.1	21.1	14.2	7.3	2.0
Jul 1				88.8	82.3	75.7	69.1	62.3	55.5	48.7	41.8	35.0	28.1	21.2	14.3	7.7	3.1
Aug 1					83.8	77.1	70.2	63.3	56.4	49.4	42.4	35.4	28.3	21.3	14.3	7.3	1.9
Sep 1					87.2	80.2	73.2	66.1	59.1	52.1	45.1	38.1	31.3	24.7	18.6	13.7	11.6
Oct 1						84.1	77.1	70.2	63.3	56.5	49.9	43.5	37.5	32.0	27.4	24.3	23.1
Nov 1						87.8	81.3	74.5	68.3	61.8	56.0	50.2	45.3	40.7	37.4	35.1	34.4
Dec 1							84.3	78.0	71.8	66.1	60.5	55.6	50.9	47.2	44.2	42.4	41.8
								Latitude 30°N									
Jan 1							89.4	83.7	78.3	73.2	68.4	64.1	60.4	57.3	55.0	53.5	53.0
Feb 1							86.2	80.3	74.6	69.1	64.1	59.4	55.3	51.9	49.3	47.7	47.2
Mar 1						87.5	81.1	74.9	68.8	62.9	57.4	52.2	47.5	43.5	40.3	38.4	37.7
Apr 1					87.2	81.4	74.9	68.5	62.1	55.8	49.6	43.8	38.2	33.3	29.3	26.5	25.5
May 1				88.9	82.7	76.3	69.9	63.4	56.9	50.4	44.0	37.6	31.4	25.6	20.4	16.5	15.0
Jun 1				85.3	79.2	73.1	66.8	60.4	54.0	47.5	41.0	34.5	28.1	21.7	15.7	10.5	8.0
Jul 1				84.7	78.7	72.5	66.3	60.0	53.5	47.1	40.6	34.1	27.7	21.2	15.1	9.6	6.9
Aug 1				87.2	81.0	74.7	68.3	61.9	55.4	48.9	42.4	36.0	29.7	23.6	18.1	13.7	11.9
Sep 1					85.9	79.4	72.9	66.4	60.0	53.6	47.3	41.2	35.5	30.2	25.8	22.8	21.6
Oct 1						85.1	78.7	72.4	66.2	60.1	54.4	48.8	43.8	39.5	36.1	33.9	33.1
Nov 1							84.6	78.4	72.8	67.1	62.0	57.0	53.0	49.3	46.7	44.9	44.4
Dec 1							88.7	82.8	77.3	72.2	67.3	63.0	59.2	56.0	53.7	52.2	51.8
								Latitude 40°N									
Jan 1								89.0	84.2	79.8	75.7	72.1	69.0	66.4	64.6	63.4	63.0
Feb 1								84.8	79.8	75.2	70.7	67.0	63.5	60.9	58.8	57.6	57.2
Mar 1						89.1	83.7	78.1	72.8	67.8	63.1	58.8	55.1	51.9	49.6	48.1	47.7
Apr 1					87.1	81.4	75.6	70.0	64.4	59.0	53.8	49.0	44.6	40.9	38.0	36.2	35.5
May 1				85.9	80.5	74.7	68.9	63.2	57.5	51.8	46.3	41.0	36.1	31.7	28.2	25.8	25.0
Jun 1			86.8	81.5	76.1	70.5	64.9	59.2	53.4	47.7	42.0	36.5	31.2	26.2	22.1	19.1	18.0
Jul 1			86.0	80.8	75.4	69.9	64.3	58.6	52.8	47.1	41.4	35.8	30.4	25.4	21.1	18.0	16.9
Aug 1			89.3	83.9	78.4	72.8	67.1	61.4	55.6	49.9	44.4	39.0	33.8	29.2	25.4	22.8	21.9
Sep 1					84.6	78.9	73.2	67.5	61.8	56.3	51.0	46.0	41.4	37.5	34.4	32.3	31.6
Oct 1						86.3	80.6	75.1	69.7	64.5	59.6	55.1	51.2	47.8	45.3	43.6	43.1
Nov 1							88.1	82.6	77.8	72.8	68.6	64.4	61.1	58.2	56.1	54.7	54.4
Dec 1								88.1	83.3	78.8	74.7	71.0	67.8	65.3	63.3	62.2	61.8
								Latitude 50°N									
Jan 1										86.5	83.2	80.2	77.7	75.7	74.2	73.3	73.0
Feb 1								89.5	85.3	81.5	78.0	74.9	72.2	70.0	68.5	67.5	67.2
Mar 1							86.3	81.8	77.4	73.3	69.6	66.2	63.2	60.9	59.1	58.0	57.7
Apr 1					86.6	81.8	76.9	72.2	67.6	63.2	59.1	55.4	52.0	49.3	47.2	45.9	45.5
May 1			87.8	83.2	78.5	73.7	68.9	64.1	59.4	54.7	50.3	46.2	42.5	39.4	37.0	35.5	35.0
Jun 1		86.7	82.4	78.0	73.3	68.6	63.8	59.0	54.2	49.5	44.9	40.6	36.6	33.1	30.4	28.6	28.0
Jul 1	89.7	85.7	81.5	77.1	72.5	67.8	63.0	58.2	53.4	48.7	44.1	39.7	35.6	32.1	29.3	27.5	26.9
Aug 1		89.7	85.4	80.8	76.2	71.4	66.6	61.8	57.0	52.4	47.9	43.7	39.9	36.6	34.1	32.5	31.9
Sep 1				88.3	83.6	78.8	74.0	69.2	64.6	60.1	55.9	52.0	48.5	45.7	43.5	42.1	41.6
Oct 1						87.6	82.8	78.2	73.8	69.6	65.7	62.1	59.1	56.5	54.7	53.5	53.1
Nov 1								87.1	83.0	79.0	75.5	72.3	69.5	67.3	65.7	64.7	64.4
Dec 1									89.2	85.5	82.1	79.1	76.5	74.5	73.0	72.1	71.8

Source: Peterson (1976) and Demerjian *et al*. (1980).

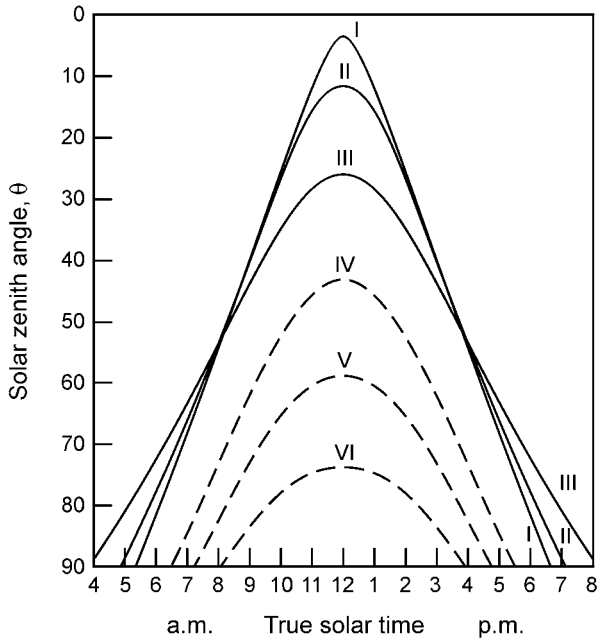

FIGURE 3.22 Effect of latitude on solar zenith angle. On the scale of true solar time, also called apparent solar time and apparent local solar time, the sun crosses the meridian at noon. The latitudes and seasons represented are as follows: I, 20°N latitude, summer solstice; II, 35°N latitude, summer solstice; III, 50°N latitude, summer solstice; IV, 20°N latitude, winter solstice; V, 35°N latitude, winter solstice; VI, 50°N latitude, winter solstice (from Leighton, 1961).

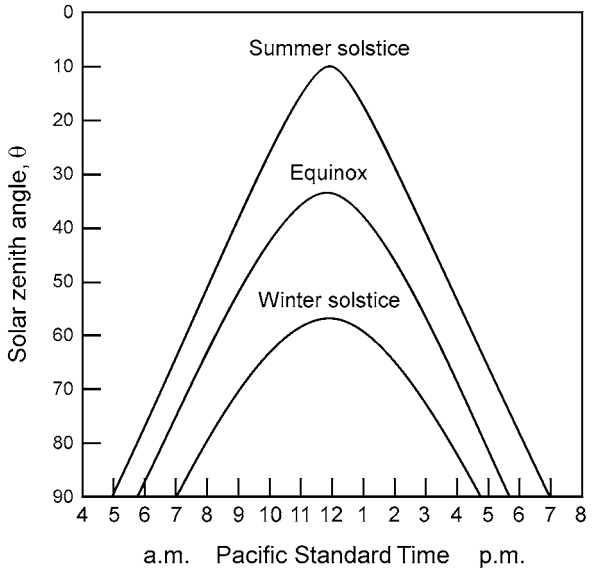

FIGURE 3.23 Relation between solar zenith angle and time of day at Los Angeles, California (from Leighton, 1961).

including surface reflection (i.e., albedo) and the concentrations of ozone and particulate matter, which scatter and/or absorb light.

(1) Surface albedo In Table 3.11 the calculated actinic fluxes are given for a surface albedo of 80%, which might correspond to the situation over snow, for example. As expected, the higher surface reflectivity leads to substantially higher actinic fluxes and hence enhanced photochemistry (see Problem 11).

(2) Total column ozone Since O_3 absorbs light primarily in the near-ultraviolet, a change in its concentration will have the greatest effect in this wavelength region. Table 3.12 shows the calculated percentage increase in actinic flux at the earth's surface for a 5% decrease in total column ozone (Madronich, 1998). Clearly, the UV flux is quite sensitive to changes in the O_3 concentration, with the greatest changes occurring at shorter wavelengths where the O_3 absorption cross sections are increasing sharply (see Chapter 4.B). This is particularly important since the total column abundance of O_3 can change by 10% or more within a season or latitude belt. In addition, decreases in stratospheric ozone due to chlorofluorocarbons (see Chapters 12 and 13) will impact the actinic flux and hence the photochemistry at the earth's surface.

TABLE 3.10 Percentage Increase in the Calculated Actinic Flux at a Surface Elevation of 1.5 km Using Best Estimate Albedos as a Function of Solar Zenith Angle and Selected Wavelengths[a] (Relative to Sea Level)[b]

Wavelength (nm)	Actinic flux increase (%)									
	0°[a]	10°	20°	30°	40°	50	60°	70°	78°	86°
340–345	2.1	2.3	2.6	3.2	4.2	5.7	8.1	11.4	12.4	7.5
400–405	0.9	0.9	1.1	1.5	2.1	3.0	4.6	7.6	10.9	6.7
540–550	0.2	0.2	0.2	0.4	0.5	0.9	1.4	2.4	4.3	4.7
680–700	0.02	0.02	0.05	0.1	0.2	0.3	0.5	1.0	1.7	2.8

[a] Zenith angles.
[b] Source: Peterson (1976) and Demerjian *et al*. (1980).

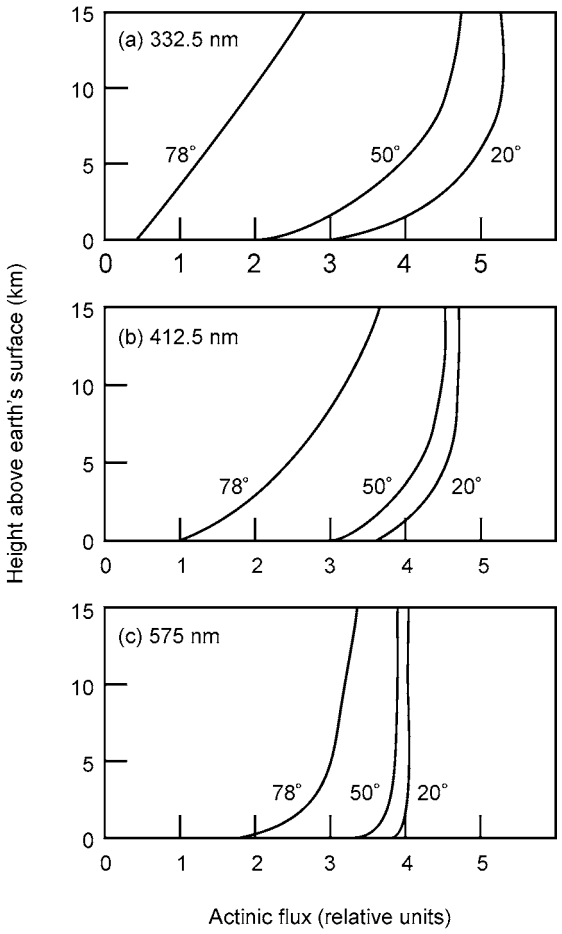

FIGURE 3.24 Calculated relative actinic flux using best estimate albedos as a function of height above the earth's surface for solar zenith angles θ of 20, 50, and 78°, respectively, at (a) 332.5, (b) 412.5, and (c) 575 nm [from Peterson (1976) and Demerjian *et al.* (1980)].

However, tropospheric ozone formed as an air pollutant by VOC–NO_x chemistry discussed throughout this book can also impact solar radiation reaching the earth's surface. For example, Frederick *et al.* (1993) reported that measurements of broadband UV in Chicago had a marginally significant negative correlation to surface O_3 concentrations under clear-sky conditions.

(3) Aerosol particles Table 3.13 shows the percentage change in the actinic flux calculated by Peterson (1976) and Demerjian *et al.* (1980) for two cases: (1) a particle concentration of zero, corresponding to a very clean atmosphere, and (2) a total particle concentration doubled compared to the base case. The actinic flux is predicted to increase if the total particle concentration is zero and decrease if it doubles (note, however, as discussed later, the sensitivity to the vertical distribution of particles and the relative importance of light scattering compared to absorption).

Figure 3.25 shows the results of one set of calculations of the effects of aerosol particles whose properties were judged to be characteristic of continental or urban situations, respectively, on the transmission of UV and visible radiation to the earth's surface (Erlick and Frederick, 1998). The ratio of the transmission with particles to that without is plotted in two wavelength regions, one in the UV and one in the visible. Two different relative humidity scenarios are shown. The "average summer relative humidity" was 70% RH in the boundary layer and 20% RH in the free troposphere. The high relative humidity case assumes 90% RH in the boundary layer and 30% in the free troposphere. (The RH in the stratosphere was taken to be 0% in both cases; see Chapter 12.)

The transmission of UV below $\sim$ 320 nm is particularly impacted by aerosol particles. This is primarily due to multiple scattering caused by the aerosol particles, which enhances the light absorption by O_3 in this region, since the effective absorption path length is increased (Erlick and Frederick, 1998). There is also a small contribution from assumed light absorption by aerosols (which, however, is highly uncertain; see Chapter 9). The increase in transmission with wavelength above 320 nm is due to decreased Mie light scattering by the particles, which depends on λ (see Chapter 9). It is evident that aerosol particles, particularly at high RH (which affects particle size by water uptake), can have significant impacts on the actinic flux at the earth's surface.

Model studies that incorporate both scattering and absorption of light by particles have shown that the vertical distribution and the relative importance of scattering versus absorption are critical in determining not only the magnitude but also the sign of the effect of particles on the actinic flux in the boundary layer and the associated photolysis rates for gases. For example, Dickerson *et al.* (1997) have shown that particles in the boundary layer which primarily scatter UV light lead to decreased actinic fluxes at the earth's surface but increased fluxes a few hundred meters above the surface. This leads to increased rates of photolysis of such species as NO_2 in the boundary layer. On the other hand, for aerosols that absorb strongly, the opposite effect occurs, reducing the actinic flux and photolysis rates of gases such as NO_2 (e.g., see Jacobson (1998) and Krotkov *et al.* (1998)).

It is these contrasting effects of aerosol particles, combined with uncertainties in the contribution of absorption due to O_3, that provide the largest uncertainties in calculations of actinic fluxes and photolysis rates in the boundary layer (e.g., Schwander *et al.*, 1997). As a result, it is important to use the appropriate input

TABLE 3.11 Actinic Flux Values $F(\lambda)$ at the Earth's Surface as a Function of Wavelength Interval and Solar Zenith Angle within Specified Wavelength Intervals for a Surface Albedo of 80% Calculated by Madronich (1998)[a]

Wavelength interval (nm)	Exponent[b]	Solar zenith angle (degrees)									
		0	10	20	30	40	50	60	70	78	86
		Actinic fluxes (photons cm^{-2} s^{-1})									
290–292	14	0.00	0.00	0.00	0.00	0.00	0.00	0.00	0.00	0.00	0.00
292–294	14	0.00	0.00	0.00	0.00	0.00	0.00	0.00	0.00	0.00	0.00
294–296	14	0.01	0.01	0.00	0.00	0.00	0.00	0.00	0.00	0.00	0.00
296–298	14	0.03	0.03	0.02	0.01	0.01	0.00	0.00	0.00	0.00	0.00
298–300	14	0.08	0.08	0.06	0.04	0.02	0.01	0.00	0.00	0.00	0.00
300–302	14	0.19	0.18	0.15	0.11	0.06	0.03	0.01	0.00	0.00	0.00
302–304	14	0.49	0.47	0.40	0.30	0.19	0.09	0.03	0.00	0.00	0.00
304–306	14	0.91	0.88	0.77	0.60	0.41	0.23	0.09	0.02	0.00	0.00
306–308	14	1.42	1.37	1.22	0.99	0.71	0.43	0.19	0.05	0.01	0.00
308–310	14	1.90	1.84	1.66	1.38	1.04	0.67	0.33	0.10	0.02	0.00
310–312	14	2.87	2.79	2.55	2.16	1.67	1.13	0.61	0.21	0.05	0.01
312–314	14	3.57	3.47	3.20	2.76	2.19	1.54	0.88	0.35	0.10	0.01
314–316	14	4.04	3.94	3.65	3.19	2.58	1.87	1.13	0.49	0.16	0.02
316–318	14	4.97	4.85	4.52	3.99	3.27	2.43	1.53	0.71	0.25	0.04
318–320	14	5.10	4.99	4.67	4.15	3.44	2.60	1.70	0.84	0.32	0.05
320–325	14	15.96	15.65	14.72	13.19	11.11	8.61	5.82	3.09	1.32	0.26
325–330	14	23.28	22.85	21.58	19.50	16.64	13.16	9.19	5.15	2.39	0.58
330–335	14	24.81	24.38	23.08	20.95	18.00	14.39	10.22	5.89	2.84	0.75
335–340	14	23.85	23.45	22.24	20.25	17.50	14.10	10.14	5.96	2.94	0.83
340–345	14	25.65	25.23	23.96	21.86	18.95	15.34	11.12	6.60	3.28	0.94
345–350	14	25.75	25.33	24.08	22.01	19.13	15.55	11.33	6.77	3.37	0.96
350–355	14	29.31	28.85	27.45	25.13	21.90	17.87	13.09	7.88	3.93	1.13
355–360	14	26.16	25.75	24.52	22.48	19.64	16.08	11.84	7.17	3.59	1.03
360–365	14	28.87	28.43	27.09	24.88	21.78	17.89	13.23	8.06	4.05	1.15
365–370	15	3.57	3.52	3.35	3.08	2.70	2.23	1.65	1.01	0.51	0.14
370–375	15	3.15	3.10	2.96	2.72	2.39	1.98	1.48	0.91	0.46	0.13
375–380	15	3.57	3.52	3.36	3.10	2.73	2.26	1.69	1.05	0.53	0.15
380–385	15	3.01	2.97	2.84	2.62	2.31	1.92	1.44	0.90	0.46	0.13
385–390	15	3.30	3.25	3.11	2.87	2.54	2.11	1.59	1.00	0.51	0.14
390–395	15	3.29	3.24	3.10	2.87	2.54	2.12	1.60	1.01	0.52	0.14
395–400	15	4.00	3.94	3.77	3.49	3.09	2.59	1.97	1.25	0.64	0.17
400–405	15	5.52	5.44	5.21	4.82	4.28	3.59	2.74	1.74	0.90	0.24
405–410	15	5.35	5.28	5.06	4.69	4.17	3.50	2.68	1.71	0.89	0.24
410–415	15	5.56	5.49	5.26	4.88	4.34	3.65	2.80	1.80	0.94	0.25
415–420	15	5.64	5.56	5.33	4.95	4.41	3.72	2.86	1.85	0.97	0.26
420–430	15	11.07	10.93	10.48	9.74	8.70	7.35	5.68	3.70	1.95	0.51
430–440	15	11.35	11.20	10.76	10.01	8.95	7.59	5.89	3.87	2.05	0.53
440–450	15	13.38	13.21	12.69	11.83	10.60	9.01	7.03	4.65	2.49	0.64
450–460	15	14.40	14.21	13.67	12.75	11.44	9.75	7.64	5.09	2.75	0.70
460–470	15	14.53	14.35	13.81	12.89	11.58	9.89	7.78	5.22	2.84	0.71
470–480	15	14.73	14.55	14.00	13.08	11.77	10.07	7.95	5.35	2.93	0.72
480–490	15	14.39	14.21	13.68	12.79	11.52	9.88	7.81	5.28	2.90	0.70
490–500	15	14.82	14.63	14.09	13.18	11.88	10.20	8.09	5.49	3.03	0.72
500–510	15	14.63	14.45	13.92	13.03	11.75	10.09	8.01	5.44	3.00	0.70
510–520	15	14.29	14.12	13.60	12.73	11.49	9.88	7.86	5.36	2.97	0.68
520–530	15	14.77	14.59	14.06	13.17	11.89	10.23	8.14	5.56	3.09	0.69
530–540	15	15.17	15.04	14.44	13.52	12.21	10.51	8.36	5.71	3.16	0.69
540–550	15	15.10	14.92	14.38	13.47	12.17	10.48	8.34	5.71	3.16	0.68
550–560	15	15.22	15.04	14.49	13.58	12.27	10.57	8.43	5.77	3.20	0.68
560–570	15	15.33	15.14	14.60	13.67	12.36	10.64	8.48	5.79	3.20	0.65
570–580	15	15.48	15.30	14.74	13.81	12.48	10.75	8.57	5.86	3.23	0.65
580–600	16	3.11	3.07	2.96	2.78	2.51	2.17	1.73	1.19	0.66	0.13
600–620	16	3.08	3.04	2.93	2.75	2.49	2.15	1.72	1.19	0.67	0.13
620–640	16	3.09	3.06	2.95	2.77	2.52	2.18	1.76	1.23	0.70	0.15
640–660	16	3.02	2.99	2.88	2.71	2.47	2.15	1.74	1.23	0.72	0.16
660–680	16	3.06	3.02	2.92	2.75	2.50	2.18	1.78	1.27	0.75	0.17
680–700	16	2.99	2.96	2.86	2.70	2.46	2.15	1.75	1.26	0.76	0.17

[a] The authors are grateful to Dr. Sasha Madronich for generously providing these calculations.

[b] This column lists the power of 10 by which all entries should be multiplied. For example, at $\theta = 0°$ the total actinic flux in the wavelength interval from 306 to 308 nm is 1.42×10^{14} photons cm^{-2} s^{-1}.

TABLE 3.12 Percentage Increase in Actinic Fluxes at the Earth's Surface for a 5% Decrease in Total Column Ozone Calculated by Madronich (1998)[a]

Wavelength interval (nm)	Solar zenith angle (deg)									
	0	10	20	30	40	50	60	70	78	86
290–292	65.2	66.4	70.4	78.0	90.9	110.6	106.7	96.3	94.8	93.8
292–294	47.5	48.4	51.1	56.2	64.9	78.7	85.0	71.2	69.1	68.1
294–296	35.5	36.1	38.0	41.6	47.7	57.5	67.5	55.4	52.2	51.1
296–298	26.0	26.5	28.0	30.4	34.6	41.5	50.9	45.4	39.7	38.2
298–300	19.6	19.9	20.8	22.7	25.7	30.7	38.3	39.8	31.0	29.5
300–302	14.7	14.9	15.6	17.0	19.2	22.8	28.6	34.0	26.7	23.2
302–304	11.1	11.3	11.8	12.8	14.4	17.1	21.5	27.6	23.9	18.8
304–306	8.4	8.5	8.9	9.7	10.9	12.8	16.1	21.5	22.2	15.8
306–308	6.4	6.8	6.8	7.3	8.2	9.7	12.2	16.5	19.7	13.9
308–310	4.8	4.9	5.1	5.5	6.2	7.3	9.2	12.5	16.3	12.9
310–312	3.7	3.8	3.9	4.2	4.8	5.6	7.0	9.6	13.1	12.4
312–314	2.8	2.9	3.0	3.2	3.6	4.2	5.3	7.3	10.2	11.7
314–316	4.4	2.2	2.3	2.4	2.7	3.2	4.0	5.5	7.8	10.4
316–318	1.6	1.6	1.7	1.9	2.1	2.4	3.0	4.2	6.0	8.9
318–320	1.2	1.2	1.3	1.4	1.5	1.8	2.2	3.1	4.4	7.1
320–325	0.7	0.7	0.8	0.8	0.9	1.1	1.3	1.8	2.7	4.6
325–330	0.3	0.4	0.4	0.4	0.4	0.5	0.6	0.9	1.3	2.3

[a] We are grateful to Dr. Sasha Madronich for these calculations.

values for these parameters in carrying out photolysis calculations for particular locations. This is especially true for unusual situations such as high particle and/or surface-level ozone concentrations or unusual geography such as mountains, which shield the light at large solar zenith angles (e.g., Castro *et al*., 1997).

g. Effects of Clouds on $F(\lambda)$

All the calculated actinic fluxes discussed so far refer to a cloudless sky. The effects of clouds are complex, in that they reduce the direct radiation at the earth's surface from the sun but, at the same time, can increase the total actinic flux directly above the cloud due to scattering from the top surface of the cloud. Madronich (1987) has treated the case of large uniform clouds of various optical depths which, however, are sufficiently large that the cloud completely diffuses both the reflected and the transmitted light. The actinic flux above the cloud then becomes a combination of the incident light (a combination of direct sunlight and

TABLE 3.13 Percentage Change of Calculated Actinic Flux at the Earth's Surface Using Best Estimate Albedos as a Function of Solar Zenith Angle and Selected Wavelengths When Model Aerosol Concentrations Are Either Zero or Doubled[a]

Wavelength (nm)	Actinic flux change (%)									
	0°[b]	10°	20°	30°	40°	50°	60°	70°	78°	86°
340–345										
No aerosol	+8.2	+8.4	+8.8	+9.5	+10.7	+12.7	+16.1	+22.3	+26.5	+17.6
Double	−6.1	−6.3	−6.6	−7.3	−8.3	−10.1	−12.8	−16.1	−16.4	−12.5
400–405										
No aerosol	+5.8	+6.0	+6.4	+7.1	+8.3	+10.7	+15.3	+6.2	+46.8	+35.7
Double	−4.0	−4.1	−4.5	−5.3	−6.6	−8.8	−12.6	−19.4	−24.9	−15.9
540–550										
No aerosol	+0.9	+1.0	+1.2	+1.8	+2.9	+5.1	+10.4	+25.4	+67.1	+261
Double	−0.8	−0.9	−1.4	−2.2	−3.7	−6.4	−11.6	−21.4	−33.6	−27.4

[a] From Peterson (1976) and Demerjian *et al*. (1980); although these are based on actinic fluxes different from those in Table 3.7, the relative changes calculated here should be similar to those that would be derived using the model from which the data in Table 3.7 were derived; the changes in the particle concentration are relative to the base case shown in Table 3.7.
[b] Solar zenith angle.

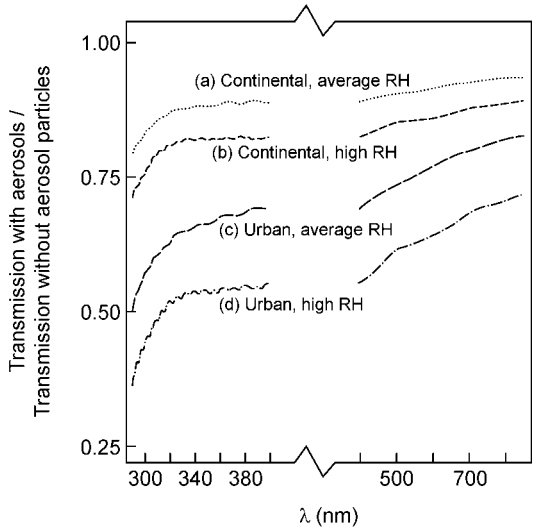

FIGURE 3.25 Calculated ratio of transmission of UV and visible light to the earth's surface in the presence of aerosol particles compared to that with no aerosol particles for typical continental aerosol particles at (a) average summer RH and (b) high summer RH and for urban aerosol particles with (c) average RH and (d) high RH. (Adapted from Erlick and Frederick, 1998.)

downward-directed diffuse light), the light that has undergone diffuse reflection at the top of the cloud, and the light that has passed through the cloud, undergone reflection at the surface, and then been transmitted back upward through the cloud.

Table 3.14 shows the results of some of Madronich's calculations of the actinic flux enhancements for two cases of a collimated direct beam of light striking the top of a cloud, first under typical summer conditions at a solar zenith angle of 20° for the case of a 5% surface albedo and second, for typical winter conditions with a solar zenith angle of 70° and a surface albedo of 80%, which would be characteristic of snow, for example.

TABLE 3.14 Calculated Enhancements or Depressions of Actinic Fluxes above and below Perfectly Light-Diffusing Clouds of Different Optical Depths[a]

Conditions	Cloud optical depth	Above cloud	Below cloud
Summer[b]	0.0 (clear sky; no cloud)	1.09	1.09
	8	1.65	1.35
	128	2.70	0.19
Winter[c]	0.0 (clear sky; no cloud)	1.55	1.55
	8	1.59	0.81
	128	1.65	0.27

[a] From Madronich, 1987.

[b] Calculated for "typical" summer conditions of a solar zenith angle of 20° and a surface albedo of 5% with an incident light beam that is collimated.

[c] Calculated for "typical" winter conditions of a solar zenith angle of 70° and a surface reflectivity of 80% for a collimated incident light beam.

The cloudless case shown first for a small solar zenith angle and typical summertime conditions shows an enhancement due to reflections from the surface. The cloud with an optical depth of 8 corresponds to a total of 67% transmission of the light through the cloud, but essentially all of it is diffused by the cloud and is therefore not directly transmitted light. The cloud with an optical depth of 128 only transmits a total of 9% of the light, essentially all of which is again diffuse.

Under the typical summertime conditions, the thinner cloud shows an increase of 65% in the actinic flux above the cloud whereas the thicker cloud shows an increase of almost a factor of three, the maximum theoretically possible. This is due to scattering of diffuse light from the top of the cloud, as well as from the ground. As expected, below the thicker cloud, the total actinic flux is reduced, in this calculation, to 19% of the clear-sky value. However, for the thinner cloud of optical density 8, the actinic flux below the cloud is actually calculated to be *greater* than for the cloudless case. This occurs in the case of a small solar zenith angle and direct (rather than diffuse) incident light because the direct incident light is diffused as it traverses the cloud; as discussed earlier for the case of the actinic flux above a Lambertian surface, conversion of a direct to diffuse source leads to an enhancement in the actinic flux.

Similar trends are predicted for the winter case chosen, except that the unexpected below-cloud enhancement discussed is not seen.

Interestingly, in the air inside the cloud itself, particularly near the top of the cloud, there can be significant enhancements of the actinic flux due to this scattering phenomenon. The enhancements expected depend on a variety of factors, including the solar zenith angle, the amount of direct vs diffuse incident light, surface albedo, cloud optical depth, etc. Madronich (1987) suggests for a "typical" summer average that the enhancement factors vary linearly from 1.7 near the top of the cloud, to 1.0 (i.e., no enhancement) in the middle of the cloud, to 0.4 (i.e., a reduction in actinic flux) at the bottom of the cloud.

This behavior has been borne out experimentally. Figure 3.26, for example, shows some vertical measurements of the actinic flux below, in, and above a cloud (Vilà-Guerau de Arellano *et al.*, 1994). The dotted line shows the calculated actinic flux in the absence of clouds for these particular conditions. At the cloud

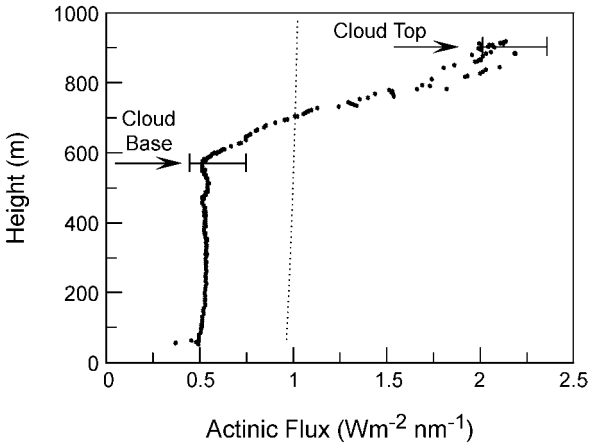

FIGURE 3.26 Vertical measurements of actinic fluxes below, in, and above a cloud. The dotted line shows calculated clear-sky values (from Vilà-Guerau de Arellano *et al*., 1994).

FIGURE 3.27 Dr. Wolfgang Junkermann prepares for a flight to measure actinic fluxes in Germany. The radiometer can be seen mounted by the wheel. Typical data are shown in Figure 3.28. (The authors are grateful to Dr. Junkermann for providing this photograph.)

base, the measured flux is 0.56 W m^{-2} nm^{-1}, compared to a calculated value for a cloudless sky of 0.93 W m^{-2} nm^{-1}. At the top of the cloud, the flux increased significantly to 2.1 W m^{-2} nm^{-1}. Inside the cloud itself, the flux increased linearly.

In short, while the flux under a cloud is generally less than the clear-sky value, inside and above the cloud it can be significantly larger, leading to enhanced rates of photolysis of photochemically active species. For example, the photolysis of O_3 to form electronically excited $O(^1D)$, followed by the reaction of the latter with water vapor, is a major source of OH in the troposphere. As a result, actinometric measurements are often made by measuring the rate of production of $O(^1D)$ directly, known as $J(O^1D)$, or, alternatively, using a light detector calibrated for this photolysis process. Junkermann (1994), for example, has used a hang glider (Fig. 3.27) equipped with a photoelectric detector to fly spiral flight paths from the top of a mountain to the valley floor in Germany while measuring vertical profiles of the light intensity coming into a 2π radiometer as described earlier (Fig. 3.20). Two such hemispherical detectors are used, one of which is downward facing and one of which is upward facing; the sum of the two gives the spherically integrated actinic flux, which is the parameter of interest for measuring total photolysis rates in the atmosphere. To relate this measurement of light intensity to $J(O^1D)$, a combination of optical filters and appropriate detectors is used (Junkermann *et al*., 1989).

Figure 3.28 gives a typical measurement of the upward component of $J(O^1D)$ as well as the total value during one flight made at a solar zenith angle of 62° (Junkerman *et al*., 1994). The values of $J(O^1D)$ are clearly reduced below the cloud, increase linearly inside the cloud, and are more than double the below-cloud values above the cloud top. As expected, the OH concentrations above the cloud are higher as well. For example, Mauldin *et al*. (1997) report OH concentrations of $(8–15) \times 10^6$ OH cm^{-3} above clouds compared to $(3–5) \times 10^6$ OH cm^{-3} in cloud-free regions. Similarly, Volz-Thomas *et al*. (1996) measured values of $J(NO_2)$ that were about twice as high above clouds compared to cloud-free days.

The intensity of all wavelengths is not affected equally by clouds. For example, Bordewijk *et al*. (1995) reported that the relationship between total solar radiation and UV in the 285- to 345-nm region measured at ground level is nonlinear, with relatively higher amounts of UV reaching the surface. Indeed, they suggest that even when the total solar radiation is decreased by 20% due to clouds, the UV intensity can be unchanged. Seckmeyer *et al*. (1996) also reported a wavelength dependence for radiation reaching the earth's surface through clouds. It has been shown that this dependence is not due to the properties of water in the clouds but rather to longer effective path lengths due to scattering (e.g., Kylling *et al*., 1997; Mayer *et al*., 1998). The increased path then gives a wavelength dependence through Rayleigh scattering and the enhanced light absorption by O_3 and particles. The backscattered light from clouds (which can be measured by satellites) not only has been reported to be wavelength dependent but also differs for high-level clouds compared to low- or mid-level clouds (e.g., see Wen and Frederick (1995) and Chapter 14.C).

One final interesting aspect of clouds and actinic fluxes is that inside the cloud droplets themselves, an

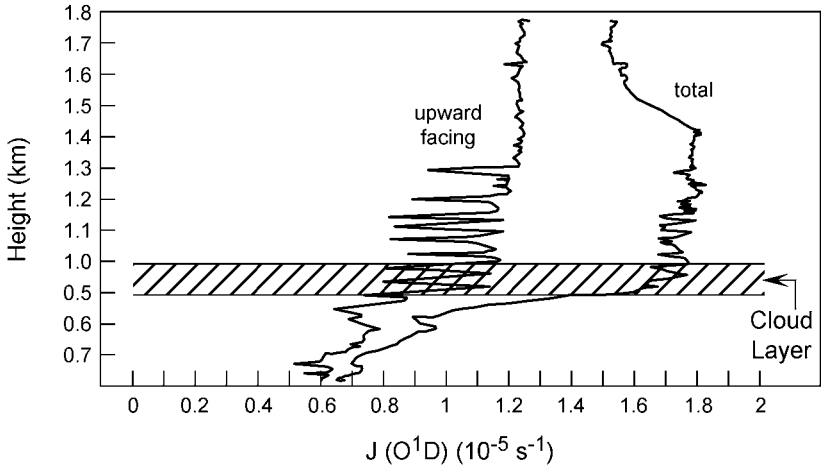

FIGURE 3.28 Vertical measurement of $J(O^1D)$ using an upward-facing detector and the total $J(O^1D)$ measured using both upward- and downward-facing detectors (from Junkermann, 1994).

increased actinic flux is expected compared to the surrounding air. As discussed in detail by Madronich (1987), there are several different effects that must be taken into account when a light beam strikes a water droplet in air. Initially, of course, some of the light will be reflected from the surface and not enter the drop itself. The portion of the incident beam that enters the droplet is subject to absorption, depending on the droplet composition and the wavelength of light, which also effectively reduces the actinic flux. However, counterbalancing these effects is the possibility of multiple internal reflections occurring at the inner droplet surface, which redirects the light beam back into the droplet. In addition, refraction of the light beam at the air–water interface as it enters the drop leads to an increased path length through the drop itself, in effect increasing the probability of light absorption (Beer–Lambert law).

The net enhancement factor for a droplet consisting of pure water can be as much as 1.6 (Madronich, 1987). Calculations by Ruggaber *et al.* (1997) suggest that the actinic flux inside cloud drops with a typical size distribution and dissolved particulate matter is more than a factor of two greater than in the cloud interstitial air. This effect of enhanced actinic flux inside droplets may be quite important for aqueous-phase photochemistry in fogs and clouds.

h. Comparison of Calculated Actinic Fluxes to Experimentally Measured Values

As described earlier, measurements of actinic fluxes are made using chemical actinometry, particularly the photolysis of NO_2 or O_3, or using flat-plate or 2π radiometers. Intercomparisons of such measurements have been made by a number of investigators, as well as comparison with calculated photolysis rates using published actinic fluxes such as those in Table 3.7. In general, there is good agreement between results obtained with different radiometers and calculated values, with the largest uncertainties generally being at shorter wavelengths (< 310 nm) and larger solar zenith angles (e.g., see Seckmeyer *et al.*, 1995; Kato *et al.*, 1997; and Halthore *et al.*, 1997).

Figure 3.29, for example, shows measurements of the photolysis rate of O_3, $J(O_3)$, made at the Mauna Loa Observatory on two different days, compared to model calculations of the photolysis rate constant (Shetter *et al.*, 1996). The two model calculations use different assumptions regarding the quantum yield for O_3 photolysis in the absorption "tail" beyond 310 nm (see Chapter 4.B). The measurements are in excellent agreement for the second day but somewhat smaller than the model calculations on the first.

Similarly, Fig. 3.30 shows measurements of $J(NO_2)$ at an altitude of 7–7.5 km as a function of solar zenith angle compared to a multidirectional model calculation (Volz-Thomas *et al.*, 1996). The agreement in this case is generally good. However, this is not always the case. For example, Fig. 3.31 shows some measurements of $J(NO_2)$ as a function of solar zenith angle made by different groups at different locations and using different techniques (Kraus and Hofzumahaus, 1998).

The reasons for discrepancies between various measurements and between the measured and model calculated values are not clear. Lantz *et al.* (1996) suggest that one factor that will affect instantaneous photolysis rates is cloud cover and that under some circumstances, the instantaneous photolysis rates may exceed

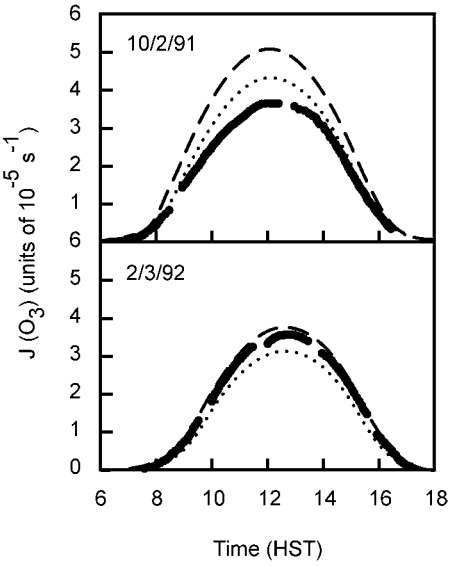

FIGURE 3.29 Measured rates of O_3 photolysis, $J(O_3)$, shown as heavy solid line, at Mauna Loa Observatory on two days (October 2, 1991, and February 3, 1992) compared to model calculations using two different assumptions (shown by the lighter dotted and dashed lines, respectively) for the quantum yield for O_3 photolysis at $\lambda > 310$ nm. (Adapted from Shetter *et al*., 1996.)

the clear-sky values. However, the average photolysis rate will not exceed the clear-sky value. This remains an area of active investigation.

i. Actinic Fluxes in the Stratosphere

Tables 3.15, 3.16, and 3.17 give Madronich's calculated actinic fluxes for altitudes of 15, 25, and 40 km, respectively. The reduction in actinic flux as the light travels through the atmosphere is very evident. Thus, at 40 km but not at 15 km, there is substantial light

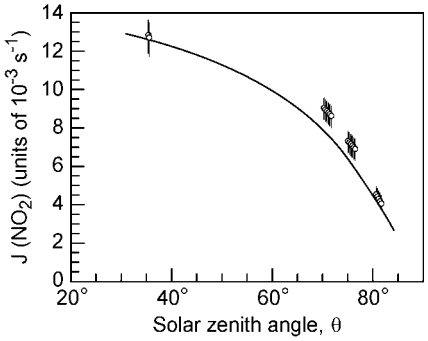

FIGURE 3.30 Values of $J(NO_2)$ at 7- to 7.5-km altitude as a function of solar zenith angle (θ) measured using 2π radiometers (circles) compared to a model calculated photolysis rate (solid line). (Adapted from Volz-Thomas *et al*., 1996.)

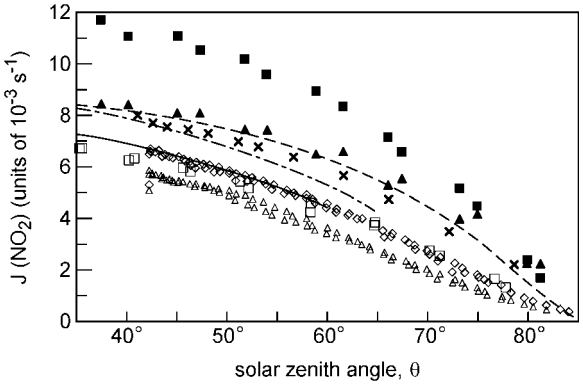

FIGURE 3.31 Some values of $J(NO_2)$ measured using different techniques as a function of solar zenith angle: (△ ◇) Kraus and Hofzumahaus (1998); (×) Madronich *et al*. (1983); (□) Brauers and Hofzumahaus (1992); (▲) Shetter *et al*. (1992); (■) Lantz *et al*. (1996); short dashed line is from Parrish *et al*. (1983); –·– is from Dickerson *et al*. (1982) and solid line is from Müller and Schurath (1986). (Adapted from Kraus and Hofzumahaus, 1998.)

intensity at 200 nm. As discussed in Chapter 12, this is why chlorofluorocarbons, which absorb light in the 200-nm region, do not photodissociate until they reach the mid to upper stratosphere.

Figure 3.32 shows some calculated actinic fluxes in the stratosphere at 20-, 30-, 40-, and 50-km altitude at a solar zenith angle of 30° (DeMore *et al*., 1997) as well as at ground level. The surface albedo was assumed to be 0.3 and the aerosol concentrations typical of "moderate volcanic conditions."

The "window" in the stratosphere around 200 nm (where CFCs absorb) between the O_2 and O_3 absorptions (Fig. 3.13) is clearly evident in the actinic fluxes shown in Fig. 3.32. Figure 3.32 also clearly illustrates the tropospheric actinic cutoff of approximately 290 nm.

3. Procedure for Calculating Photolysis Rates

As discussed in Section 3.C.2a, the rate of loss of a molecule A from the troposphere by photolysis is given by Eq. (CC):

$$d[\mathrm{A}]/dt = -k_\mathrm{p}[\mathrm{A}], \qquad \text{(CC)}$$

where k_p is the photolysis rate constant (s^{-1}) given by Eq. (OO):

$$k_\mathrm{p} = \int_\lambda \phi(\lambda)\sigma(\lambda)F(\lambda)\,d\lambda. \qquad \text{(OO)}$$

The primary quantum yield $\phi(\lambda)$ represents the fraction of excited molecules that undergo photochemistry

TABLE 3.15 Actinic Flux Values $F(\lambda)$ at an Altitude of 15 km above the Earth's Surface as a Function of Wavelength Interval and Solar Zenith Angle within Specified Wavelength Intervals for Best Estimate Surface Albedo Calculated by Madronich (1998)[a]

Wavelength interval (nm)	Exponent[b]	Solar zenith angle (deg)									
		0	10	20	30	40	50	60	70	78	86
		Actinic fluxes (photons cm^{-2} s^{-1})									
290–292	14	0.00	0.00	0.00	0.00	0.00	0.00	0.00	0.00	0.00	0.00
292–294	14	0.00	0.00	0.00	0.00	0.00	0.00	0.00	0.00	0.00	0.00
294–296	14	0.02	0.02	0.01	0.01	0.00	0.00	0.00	0.00	0.00	0.00
296–298	14	0.06	0.06	0.05	0.03	0.02	0.01	0.00	0.00	0.00	0.00
298–300	14	0.13	0.12	0.11	0.08	0.05	0.03	0.01	0.00	0.00	0.00
300–302	14	0.23	0.23	0.20	0.17	0.12	0.07	0.03	0.00	0.00	0.00
302–304	14	0.50	0.49	0.45	0.39	0.30	0.20	0.10	0.02	0.00	0.00
304–306	14	0.82	0.80	0.75	0.67	0.55	0.40	0.23	0.07	0.01	0.00
306–308	14	1.16	1.14	1.09	0.99	0.85	0.65	0.42	0.17	0.03	0.00
308–310	14	1.44	1.43	1.37	1.27	1.12	0.91	0.64	0.31	0.08	0.00
310–312	14	2.07	2.05	1.98	1.87	1.69	1.43	1.06	0.59	0.20	0.01
312–314	14	2.46	2.44	2.38	2.26	2.08	1.82	1.43	0.89	0.37	0.03
314–316	14	2.69	2.67	2.62	2.52	2.35	2.10	1.72	1.16	0.56	0.05
316–318	14	3.23	3.21	3.16	3.05	2.88	2.62	2.21	1.58	0.85	0.11
318–320	14	3.24	3.22	3.18	3.09	2.95	2.72	2.35	1.77	1.05	0.18
320–325	14	9.81	9.77	9.67	9.47	9.13	8.57	7.64	6.08	4.03	1.01
325–330	14	13.78	13.75	13.65	13.45	13.08	12.46	11.39	9.52	6.90	2.37
330–335	14	14.32	14.29	14.21	14.04	13.72	13.17	12.20	10.46	7.94	3.21
335–340	14	13.45	13.44	13.38	13.25	13.00	12.55	11.73	10.24	8.04	3.64
340–345	14	14.19	14.18	14.13	14.01	13.77	13.34	12.54	11.06	8.83	4.23
345–350	14	13.95	13.94	13.89	13.79	13.58	13.18	12.45	11.05	8.93	4.45
350–355	14	15.63	15.62	15.58	15.47	15.26	14.85	14.08	12.59	10.29	5.32
355–360	14	13.70	13.69	13.66	13.58	13.41	13.08	12.43	11.19	9.23	4.93
360–365	14	14.91	14.91	14.88	14.80	14.63	14.29	13.63	12.33	10.27	5.64
365–370	15	1.82	1.82	1.82	1.81	1.79	1.75	1.67	1.52	1.28	0.72
370–375	15	1.59	1.58	1.58	1.58	1.56	1.53	1.47	1.34	1.13	0.65
375–380	15	1.78	1.78	1.78	1.77	1.76	1.72	1.66	1.52	1.29	0.76
380–385	15	1.48	1.48	1.48	1.47	1.46	1.44	1.38	1.27	1.09	0.66
385–390	15	1.60	1.60	1.60	1.60	1.59	1.56	1.51	1.39	1.20	0.74
390–395	15	1.58	1.58	1.58	1.58	1.57	1.55	1.50	1.39	1.20	0.76
395–400	15	1.90	1.90	1.90	1.90	1.89	1.86	1.81	1.68	1.47	0.94
400–405	15	2.63	2.63	2.63	2.62	2.61	2.57	2.49	2.33	2.04	1.32
405–410	15	2.52	2.52	2.52	2.52	2.51	2.48	2.41	2.25	1.98	1.31
410–415	15	2.60	2.60	2.60	2.60	2.59	2.56	2.49	2.34	2.07	1.38
415–420	15	2.62	2.62	2.62	2.62	2.61	2.58	2.51	2.37	2.10	1.43
420–430	15	5.09	5.09	5.09	5.09	5.07	5.02	4.90	4.63	4.14	2.86
430–440	15	5.15	5.15	5.16	5.16	5.14	5.10	4.99	4.74	4.27	3.02
440–450	15	6.00	6.00	6.01	6.01	6.00	5.96	5.84	5.56	5.04	3.64
450–460	15	6.50	6.50	6.50	6.49	6.47	6.42	6.29	5.99	5.45	3.99
460–470	15	6.51	6.51	6.51	6.51	6.49	6.44	6.32	6.04	5.51	4.09
470–480	15	6.56	6.56	6.56	6.55	6.54	6.49	6.38	6.10	5.59	4.19
480–490	15	6.35	6.35	6.35	6.35	6.34	6.29	6.19	5.93	5.44	4.09
490–500	15	6.51	6.50	6.50	6.50	6.49	6.45	6.34	6.09	5.60	4.24
500–510	15	6.52	6.52	6.51	6.50	6.47	6.41	6.29	6.01	5.50	4.12
510–520	15	6.34	6.34	6.33	6.32	6.29	6.24	6.12	5.86	5.38	4.05
520–530	15	6.52	6.52	6.51	6.50	6.47	6.41	6.29	6.01	5.51	4.10
530–540	15	6.68	6.71	6.67	6.65	6.62	6.55	6.42	6.13	5.59	4.10
540–550	15	6.63	6.63	6.62	6.60	6.57	6.50	6.37	6.08	5.54	4.05
550–560	15	6.73	6.73	6.71	6.69	6.64	6.57	6.42	6.12	5.56	4.03
560–570	15	6.75	6.74	6.73	6.70	6.65	6.57	6.41	6.08	5.49	3.87
570–580	15	6.80	6.80	6.78	6.75	6.70	6.62	6.46	6.12	5.51	3.84
580–600	16	1.36	1.36	1.36	1.35	1.34	1.33	1.30	1.23	1.11	0.79
600–620	16	1.36	1.36	1.35	1.35	1.34	1.32	1.29	1.22	1.11	0.79
620–640	16	1.36	1.36	1.36	1.35	1.34	1.33	1.30	1.24	1.14	0.86
640–660	16	1.35	1.34	1.34	1.33	1.32	1.31	1.28	1.23	1.15	0.90
660–680	16	1.38	1.38	1.37	1.37	1.35	1.34	1.31	1.26	1.18	0.96
680–700	16	1.35	1.35	1.34	1.34	1.33	1.31	1.29	1.25	1.18	0.99

[a] The authors are grateful to Dr. Sasha Madronich for generously providing these calculations.

[b] This column lists the power of 10 by which all entries should be multiplied. For example, at $\theta = 0°$ the total actinic flux in the wavelength interval from 306 to 308 nm is 1.16×10^{14} photons cm^{-2} s^{-1}.

TABLE 3.16 Actinic Flux Values $F(\lambda)$ at an Altitude of 25 km above the Earth's Surface as a Function of Wavelength Interval and Solar Zenith Angle within Specified Wavelength Intervals for Best Estimate Surface Albedo Calculated by Madronich (1998)[a]

Wavelength interval (nm)	Exponent[b]	Solar zenith angle (deg)									
		0	10	20	30	40	50	60	70	78	86
		Actinic fluxes (photons cm^{-2} s^{-1})									
290–292	14	0.06	0.05	0.05	0.03	0.02	0.01	0.00	0.00	0.00	0.00
292–294	14	0.11	0.11	0.09	0.07	0.05	0.03	0.01	0.00	0.00	0.00
294–296	14	0.21	0.20	0.18	0.15	0.11	0.07	0.03	0.00	0.00	0.00
296–298	14	0.34	0.33	0.31	0.27	0.21	0.14	0.07	0.02	0.00	0.00
298–300	14	0.46	0.45	0.43	0.38	0.32	0.24	0.14	0.05	0.01	0.00
300–302	14	0.58	0.57	0.55	0.50	0.44	0.35	0.23	0.10	0.02	0.00
302–304	14	0.94	0.93	0.90	0.84	0.75	0.63	0.46	0.24	0.07	0.00
304–306	14	1.22	1.21	1.18	1.12	1.02	0.89	0.69	0.42	0.16	0.01
306–308	14	1.48	1.46	1.43	1.37	1.27	1.13	0.93	0.62	0.29	0.02
308–310	14	1.63	1.62	1.59	1.53	1.44	1.31	1.11	0.81	0.45	0.04
310–312	14	2.17	2.16	2.12	2.06	1.96	1.81	1.57	1.21	0.74	0.12
312–314	14	2.47	2.46	2.42	2.36	2.26	2.11	1.87	1.50	1.01	0.23
314–316	14	2.62	2.61	2.58	2.53	2.43	2.29	2.07	1.71	1.23	0.38
316–318	14	3.10	3.09	3.06	3.00	2.91	2.76	2.52	2.13	1.61	0.61
318–320	14	3.09	3.08	3.06	3.01	2.92	2.79	2.58	2.23	1.74	0.78
320–325	14	9.35	9.33	9.27	9.15	8.95	8.61	8.06	7.13	5.84	3.20
325–330	14	13.21	13.19	13.13	13.01	12.78	12.40	11.75	10.62	9.04	5.82
330–335	14	13.79	13.78	13.73	13.63	13.43	13.09	12.49	11.42	9.93	6.90
335–340	14	13.03	13.02	12.98	12.90	12.75	12.47	11.96	11.04	9.73	7.13
340–345	14	13.79	13.78	13.75	13.68	13.54	13.26	12.76	11.84	10.52	7.89
345–350	14	13.59	13.58	13.56	13.50	13.37	13.12	12.66	11.79	10.52	8.01
350–355	14	15.27	15.26	15.24	15.18	15.05	14.80	14.31	13.37	12.00	9.25
355–360	14	13.41	13.41	13.39	13.35	13.25	13.04	12.63	11.85	10.68	8.32
360–365	14	14.63	14.62	14.61	14.57	14.47	14.27	13.85	13.03	11.78	9.26
365–370	15	1.79	1.79	1.79	1.78	1.77	1.75	1.70	1.60	1.46	1.15
370–375	15	1.56	1.56	1.56	1.56	1.55	1.53	1.49	1.41	1.28	1.02
375–380	15	1.75	1.75	1.75	1.75	1.74	1.72	1.68	1.59	1.46	1.17
380–385	15	1.46	1.46	1.46	1.46	1.45	1.44	1.40	1.33	1.22	0.99
385–390	15	1.59	1.59	1.59	1.58	1.58	1.56	1.53	1.46	1.34	1.09
390–395	15	1.57	1.57	1.57	1.57	1.56	1.55	1.52	1.45	1.34	1.09
395–400	15	1.88	1.88	1.89	1.89	1.88	1.87	1.83	1.75	1.62	1.33
400–405	15	2.61	2.61	2.61	2.61	2.60	2.58	2.53	2.42	2.24	1.86
405–410	15	2.50	2.51	2.51	2.51	2.50	2.48	2.44	2.34	2.17	1.80
410–415	15	2.59	2.59	2.59	2.59	2.58	2.57	2.52	2.42	2.26	1.88
415–420	15	2.61	2.61	2.61	2.61	2.60	2.59	2.55	2.45	2.29	1.92
420–430	15	5.06	5.06	5.07	5.07	5.06	5.04	4.97	4.79	4.48	3.78
430–440	15	5.13	5.13	5.14	5.14	5.14	5.12	5.06	4.89	4.59	3.90
440–450	15	5.98	5.99	5.99	6.00	6.00	5.98	5.91	5.73	5.40	4.62
450–460	15	6.48	6.48	6.48	6.48	6.47	6.44	6.36	6.16	5.81	4.98
460–470	15	6.50	6.50	6.50	6.50	6.49	6.47	6.39	6.20	5.85	5.04
470–480	15	6.54	6.54	6.55	6.55	6.54	6.52	6.45	6.26	5.93	5.11
480–490	15	6.34	6.34	6.35	6.35	6.35	6.32	6.26	6.08	5.76	4.97
490–500	15	6.50	6.50	6.50	6.50	6.50	6.48	6.42	6.25	5.92	5.11
500–510	15	6.51	6.51	6.51	6.50	6.48	6.44	6.36	6.17	5.83	4.99
510–520	15	6.34	6.33	6.33	6.32	6.31	6.27	6.19	6.01	5.69	4.87
520–530	15	6.52	6.52	6.51	6.50	6.48	6.45	6.37	6.18	5.84	4.97
530–540	15	6.68	6.70	6.67	6.66	6.64	6.60	6.51	6.32	5.96	5.03
540–550	15	6.63	6.63	6.62	6.61	6.59	6.55	6.46	6.27	5.91	4.97
550–560	15	6.73	6.73	6.72	6.70	6.67	6.62	6.52	6.31	5.94	4.97
560–570	15	6.75	6.75	6.73	6.72	6.68	6.63	6.52	6.31	5.91	4.87
570–580	15	6.81	6.80	6.79	6.77	6.74	6.68	6.58	6.35	5.95	4.87
580–600	16	1.36	1.36	1.36	1.36	1.35	1.34	1.32	1.27	1.20	0.99
600–620	16	1.36	1.36	1.35	1.35	1.34	1.33	1.31	1.26	1.19	0.98
620–640	16	1.36	1.36	1.36	1.35	1.35	1.33	1.32	1.28	1.21	1.02
640–660	16	1.35	1.34	1.34	1.34	1.33	1.32	1.30	1.26	1.20	1.03
660–680	16	1.38	1.38	1.37	1.37	1.36	1.34	1.32	1.28	1.22	1.07
680–700	16	1.35	1.35	1.34	1.34	1.33	1.31	1.30	1.26	1.21	1.07

[a] The authors are grateful to Dr. Sasha Madronich for generously providing these calculations.

[b] This column lists the power of 10 by which all entries should be multiplied. For example, at $\theta = 0°$ the total actinic flux in the wavelength interval from 306 to 308 nm is 1.48×10^{14} photons cm^{-2} s^{-1}.

TABLE 3.17 Actinic Fluc Values $F(\lambda)$ at an Altitude of 40 km above the Earth's Surface as a Function of Wavelength Interval and Solar Zenith Angle within Specified Wavelength Intervals for Best Estimate Surface Albedo Calculated by Madronich (1998)[a]

Wavelength interval (nm)	Exponent[b]	Solar zenith angle (deg)									
		0	10	20	30	40	50	60	70	78	86
		Actinic fluxes (photons cm^{-2} s^{-1})									
202–205	14	0.03	0.02	0.02	0.02	0.02	0.02	0.02	0.02	0.01	0.00
205–210	14	0.06	0.06	0.06	0.06	0.06	0.06	0.05	0.04	0.03	0.01
210–215	14	0.14	0.14	0.14	0.14	0.13	0.12	0.11	0.09	0.06	0.01
215–220	14	0.15	0.15	0.15	0.14	0.13	0.12	0.10	0.07	0.04	0.00
220–225	14	0.17	0.16	0.16	0.15	0.14	0.12	0.09	0.05	0.02	0.00
225–230	14	0.11	0.11	0.11	0.10	0.09	0.07	0.05	0.02	0.00	0.00
230–235	14	0.08	0.08	0.08	0.07	0.06	0.04	0.02	0.01	0.00	0.00
235–240	14	0.06	0.05	0.05	0.04	0.03	0.02	0.01	0.00	0.00	0.00
240–245	14	0.05	0.04	0.04	0.03	0.02	0.01	0.01	0.00	0.00	0.00
245–250	14	0.03	0.03	0.02	0.02	0.01	0.01	0.00	0.00	0.00	0.00
250–255	14	0.03	0.02	0.02	0.02	0.01	0.01	0.00	0.00	0.00	0.00
255–260	14	0.05	0.05	0.05	0.04	0.02	0.01	0.00	0.00	0.00	0.00
260–265	14	0.09	0.09	0.08	0.06	0.04	0.02	0.01	0.00	0.00	0.00
265–270	14	0.23	0.22	0.20	0.17	0.13	0.08	0.03	0.01	0.00	0.00
270–275	14	0.31	0.30	0.28	0.24	0.19	0.13	0.07	0.02	0.00	0.00
275–280	14	0.44	0.43	0.41	0.37	0.31	0.24	0.14	0.05	0.01	0.00
280–285	14	0.86	0.85	0.82	0.77	0.69	0.58	0.42	0.22	0.06	0.00
285–290	14	1.57	1.56	1.52	1.47	1.37	1.24	1.02	0.69	0.32	0.01
290–292	14	1.36	1.36	1.34	1.30	1.25	1.16	1.03	0.79	0.47	0.05
292–294	14	1.29	1.29	1.27	1.25	1.21	1.14	1.04	0.85	0.57	0.10
294–296	14	1.39	1.38	1.37	1.35	1.32	1.26	1.17	1.00	0.73	0.19
296–298	14	1.44	1.43	1.42	1.41	1.38	1.33	1.26	1.12	0.88	0.31
298–300	14	1.38	1.37	1.37	1.35	1.33	1.30	1.24	1.13	0.94	0.43
300–302	14	1.32	1.31	1.31	1.30	1.28	1.26	1.21	1.13	0.98	0.53
302–304	14	1.72	1.72	1.72	1.71	1.69	1.66	1.61	1.52	1.36	0.85
304–306	14	1.89	1.89	1.88	1.87	1.85	1.82	1.78	1.70	1.56	1.08
306–308	14	2.00	2.00	1.99	1.98	1.95	1.92	1.88	1.80	1.68	1.25
308–310	14	1.99	1.99	1.98	1.96	1.94	1.90	1.86	1.78	1.67	1.33
310–312	14	2.46	2.45	2.44	2.42	2.38	2.34	2.27	2.17	2.05	1.70
312–314	14	2.64	2.63	2.62	2.59	2.55	2.49	2.41	2.30	2.16	1.84
314–316	14	2.70	2.69	2.68	2.65	2.61	2.54	2.45	2.32	2.17	1.87
316–318	14	3.12	3.11	3.09	3.06	3.01	2.93	2.82	2.66	2.46	2.14
318–320	14	3.06	3.06	3.04	3.01	2.96	2.88	2.77	2.59	2.39	2.07
320–325	14	9.18	9.16	9.12	9.04	8.90	8.68	8.33	7.77	7.10	6.09
325–330	14	12.97	12.96	12.91	12.82	12.65	12.36	11.88	11.09	10.09	8.59
330–335	14	13.59	13.58	13.54	13.45	13.30	13.03	12.55	11.74	10.69	9.09
335–340	14	12.87	12.86	12.83	12.77	12.64	12.41	11.99	11.25	10.26	8.73
340–345	14	13.65	13.64	13.62	13.56	13.44	13.21	12.79	12.03	11.01	9.38
345–350	14	13.47	13.46	13.44	13.39	13.28	13.08	12.68	11.96	10.97	9.38
350–355	14	15.14	15.14	15.12	15.08	14.97	14.75	14.33	13.55	12.46	10.68
355–360	14	13.31	13.31	13.30	13.27	13.18	13.01	12.66	12.00	11.06	9.50
360–365	14	14.53	14.53	14.52	14.49	14.41	14.23	13.88	13.18	12.18	10.49
365–370	15	1.78	1.78	1.78	1.77	1.77	1.75	1.70	1.62	1.50	1.30
370–375	15	1.55	1.55	1.55	1.55	1.54	1.53	1.49	1.42	1.32	1.14
375–380	15	1.75	1.75	1.75	1.74	1.74	1.72	1.68	1.61	1.50	1.30
380–385	15	1.45	1.45	1.45	1.45	1.45	1.44	1.41	1.35	1.26	1.09
385–390	15	1.58	1.58	1.58	1.58	1.58	1.56	1.53	1.47	1.37	1.20
390–395	15	1.56	1.56	1.56	1.56	1.56	1.55	1.52	1.46	1.37	1.20
395–400	15	1.88	1.88	1.88	1.88	1.88	1.87	1.84	1.77	1.66	1.45
400–405	15	2.60	2.60	2.60	2.60	2.59	2.58	2.54	2.44	2.29	2.01
405–410	15	2.50	2.50	2.50	2.50	2.50	2.48	2.44	2.36	2.22	1.95
410–415	15	2.58	2.58	2.58	2.58	2.58	2.57	2.53	2.44	2.30	2.03
415–420	15	2.60	2.60	2.60	2.60	2.60	2.59	2.55	2.47	2.33	2.06
420–430	15	5.05	5.05	5.06	5.06	5.06	5.04	4.98	4.83	4.56	4.04

(continues)

TABLE 3.17 *(continued)*

Wavelength interval (nm)	Exponent[b]	Solar zenith angle (deg)									
		0	10	20	30	40	50	60	70	78	86
430–440	15	5.13	5.13	5.13	5.14	5.14	5.12	5.07	4.92	4.67	4.15
440–450	15	5.98	5.98	5.99	6.00	6.00	5.99	5.93	5.77	5.49	4.89
450–460	15	6.47	6.47	6.48	6.48	6.47	6.45	6.38	6.20	5.90	5.27
460–470	15	6.49	6.49	6.49	6.50	6.49	6.47	6.41	6.24	5.95	5.33
470–480	15	6.54	6.54	6.54	6.55	6.54	6.53	6.47	6.31	6.02	5.41
480–490	15	6.34	6.34	6.34	6.35	6.35	6.33	6.28	6.13	5.86	5.28
490–500	15	6.50	6.49	6.50	6.50	6.50	6.49	6.44	6.30	6.03	5.44
500–510	15	6.51	6.51	6.50	6.50	6.48	6.46	6.39	6.23	5.96	5.38
510–520	15	6.33	6.33	6.33	6.32	6.31	6.28	6.22	6.08	5.82	5.26
520–530	15	6.52	6.52	6.51	6.51	6.49	6.47	6.40	6.26	6.00	5.43
530–540	15	6.68	6.71	6.67	6.66	6.65	6.62	6.56	6.41	6.15	5.57
540–550	15	6.63	6.63	6.63	6.62	6.60	6.58	6.51	6.37	6.11	5.55
550–560	15	6.73	6.73	6.72	6.71	6.69	6.65	6.58	6.43	6.16	5.60
560–570	15	6.76	6.75	6.74	6.73	6.71	6.67	6.59	6.44	6.18	5.62
570–580	15	6.82	6.81	6.80	6.79	6.76	6.73	6.65	6.50	6.24	5.68
580–600	16	1.36	1.36	1.36	1.36	1.35	1.35	1.33	1.30	1.25	1.14
600–620	16	1.36	1.36	1.36	1.35	1.35	1.34	1.32	1.29	1.24	1.13
620–640	16	1.36	1.36	1.36	1.35	1.35	1.34	1.33	1.30	1.25	1.14
640–660	16	1.35	1.34	1.34	1.34	1.33	1.32	1.30	1.27	1.23	1.12
660–680	16	1.38	1.38	1.37	1.37	1.36	1.35	1.33	1.29	1.25	1.14
680–700	16	1.35	1.35	1.34	1.34	1.33	1.32	1.30	1.27	1.22	1.12

[a] The authors are grateful to Dr. Sasha Madronich for generously providing these calculations.
[b] This column lists the power of 10 by which all entries should be multiplied. For example, at $\theta = 0°$ the total actinic flux in the wavelength interval from 306 to 308 nm is 2.0×10^{14} photons cm^{-2} s^{-1}.

(as opposed to a photophysical process such as fluorescence or energy transfer). For example, once NO_2 has absorbed light and is in an electronically excited state, it can either dissociate or energy transfer to other molecules in air, most commonly N_2 or O_2, and return to the ground state:

$$NO_2 + h\nu \rightarrow NO_2^* \quad (6)$$

$$NO_2^* \rightarrow NO + O(^3P) \quad (7)$$

$$NO_2^* + M\ (N_2, O_2) \rightarrow NO_2 + M. \quad (8)$$

Only reaction (7) leads to the removal of NO_2 via photochemistry and hence the quantum yield for reaction (7) is needed to calculate the photolysis rate. Data on both primary quantum yields and absorption cross section $\phi(\lambda)$, characteristic of each molecule, are found in Chapter 4.

It must again be stressed that the absorption cross sections, $\sigma(\lambda)$, used to calculate photolysis rates are to the base e, not base 10, even though the latter is what has often been measured and reported in the literature in the past.

The actinic flux $F(\lambda)$, describing the intensity of light available to the molecule for absorption, depends on many factors, including geographical location, time, season, presence or absence of clouds, and the total amount of O_3 and particles in the air which scatter light as it passes through the atmosphere. At the earth's surface, however, the actinic flux estimates and associated data of Madronich (1998) in Table 3.7 are commonly used to estimate rates and lifetimes of species with respect to photolysis under cloudless conditions.

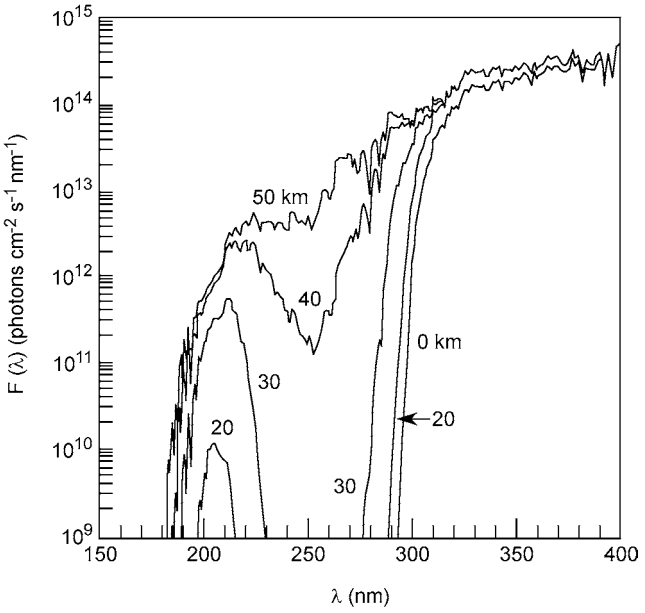

FIGURE 3.32 Calculated actinic fluxes as a function of altitude for a solar zenith angle of 30° and a surface albedo of 0.3. (From DeMore *et al*., 1997.)

Because the actinic flux data are reported as averages over certain wavelength intervals, rather than integrating over Eq. (OO) in a continuous manner, in practice one calculates the sum of the product $\phi(\lambda)\sigma(\lambda)F(\lambda)$ over discrete wavelength intervals $\Delta\lambda$. The intervals are chosen to match the available flux data; for example, in Table 3.7, actinic fluxes are reported as averages over 2-nm intervals from 290 to 320 nm, which is important for the O_3 absorption, 5-nm intervals from 320 to 420 nm, 10-nm intervals from 420 to 580 nm, and 20-nm intervals from 580 to 700 nm. Since the primary quantum yield, $\phi(\lambda)$, and the absorption cross section, $\sigma(\lambda)$, are not normally reported over identical intervals, representative averages of these parameters over the same intervals for which the actinic flux data are reported must be calculated from the literature data.

In the most commonly used form, then, Eq. (OO) becomes:

$$k_{\mathrm{p}}(\mathrm{s}^{-1}) = \sum_{\lambda=290\ \mathrm{nm}}^{\lambda_i} \phi_{\mathrm{av}}(\lambda)\sigma_{\mathrm{av}}(\lambda)F_{\mathrm{av}}(\lambda), \quad \text{(PP)}$$

where $\phi_{\mathrm{av}}(\lambda)$ is the primary quantum yield for the photolysis of the molecules averaged over the wavelength interval $\Delta\lambda$, centered at λ, $\sigma_{\mathrm{av}}(\lambda)$ is the absorption cross section, *base e*, averaged over the wavelength interval $\Delta\lambda$, centered at λ, and $F_{\mathrm{av}}(\lambda)$ is the actinic flux in photons $\mathrm{cm}^{-2}\ \mathrm{s}^{-1}$ summed over the wavelength interval $\Delta\lambda$, centered at λ, at a solar zenith angle θ (Table 3.7) corrected for season (Table 3.8). If desired, corrections for surface elevation, altitude, etc. can be included. Note that the values in the tables are the *total* actinic fluxes over the wavelength intervals given. They are *not* per nm.

The sum (or integral if Eq. (OO) is used) is carried out from the lower limit of wavelengths in the troposphere, 290 nm, to some wavelength λ_i at which either the primary quantum yield or the absorption cross section becomes negligible.

Experimentally, while the determination of absorption cross sections is fairly straightforward, measuring primary quantum yields is not, due to interference from rapid secondary reactions. As a result, in cases where quantum yield data are not available, calculations of *maximum* rates of photolysis are often carried out in which it is assumed that $\phi(\lambda) = 1.0$. It should be emphasized in such cases that this represents only a maximum rate constant for photolysis; the true rate constant may be much smaller, even zero, if photophysical fates of the excited molecule such as fluorescence or quenching predominate.

TABLE 3.18 Absorption Cross Sections, $\sigma(\lambda)$, and Primary Quantum Yields, $\phi(\lambda)$, for Reactions (9a) and (9b) for CH_3CHO at Room Temperature and 1 atm in Air[a]

Wavelength, λ (nm)	Absorption cross section, σ (10^{-20} cm^2 molecule^{-1} s^{-1})	Quantum yield (9a)	Quantum yield (9b)
290	4.89	0.53	0.01
292	4.68		
294	4.33		
295	4.27	0.48	0.0
296	4.24		
298	4.41		
300	4.16	0.43	
302	3.86		
304	3.48		
305	3.42	0.37	
306	3.42		
308	3.33		
310	2.93		
312	2.53		
314	2.44		
315	2.20	0.17	
316	2.04		
318	1.98		
320	1.72	0.10	
325	1.14	0.04	
330	0.688	0.0	

[a] Atkinson *et al*. (1997).

4. Example: Photolysis of Acetaldehyde at the Earth's Surface

To illustrate the application of Eqs. (OO) and (PP), let us calculate the rate of photolysis of acetaldehyde. Aldehydes such as CH_3CHO play an important role in tropospheric chemistry because they photodissociate to produce free radicals. In the case of acetaldehyde, there are four possible sets of products:

$$\mathrm{CH_3CHO} + h\nu \rightarrow \mathrm{CH_3} + \mathrm{HCO}, \quad \text{(9a)}$$

$$\rightarrow \mathrm{CH_4} + \mathrm{CO}, \quad \text{(9b)}$$

$$\rightarrow \mathrm{H} + \mathrm{CH_3CO}, \quad \text{(9c)}$$

$$\rightarrow \mathrm{H_2} + \mathrm{CH_2CO}. \quad \text{(9d)}$$

For the purposes of illustration, the rate of photolysis will be calculated for conditions of a cloudless day at the earth's surface at 30°N latitude six hours after noon on July 1.

From Eq. (PP), we need the primary quantum yields for each of the processes (9a)–(9d), the absorption cross sections, *base e*, and the actinic flux values, $F(\lambda)$. Table 3.18 gives IUPAC recommendations (Atkinson *et al*., 1997) for the absorption cross sections and primary quantum yields for CH_3CHO. Primary quantum

TABLE 3.19 Calculated Photolysis Rate Constants for CH_3CHO Photolysis at 30°N Latitude Six Hours after Noon on July 1

Wavelength interval, $\Delta\lambda$ (nm)	Actinic flux, $F_{av}(\lambda)$ (10^{14} photons $cm^{-2}\ s^{-1}$)	Absorption cross section, $\sigma_{av}(\lambda)$ ($10^{-20}\ cm^2$ $molecule^{-1}$)	Quantum yield for reactions (9a) and (9b)		$\phi_{av}^{9a}\sigma_{av}DF_{av}$ ($10^{-6}\ s^{-1}$)[a]	$\phi_{av}^{9b}\sigma_{av}DF_{av}$ ($10^{-6}\ s^{-1}$)[a]
			$\phi_{av}^{9a}(\lambda)$	$\phi_{av}^{9b}(\lambda)$		
290–292	0	4.78	0.52	0.01	0	0
292–294	0	4.51	0.50	0	0	0
294–296	0	4.27	0.48	0	0	0
296–298	0	4.33	0.46	0	0	0
298–300	0	4.29	0.44	0	0	0
300–302	0	4.01	0.42	0	0	0
302–304	0	3.67	0.40	0	0	0
304–306	0	3.42	0.37	0	0	0
306–308	0	3.38	0.33	0	0	0
308–310	0.01	3.13	0.27	0	0.008	0
310–312	0.02	2.73	0.25	0	0.013	0
312–314	0.04	2.49	0.21	0	0.020	0
314–316	0.06	2.20	0.17	0	0.022	0
316–318	0.10	2.01	0.14	0	0.027	0
318–320	0.13	1.85	0.11	0	0.026	0
320–325	0.52	1.43	0.07	0	0.050	0
325–330	0.96	0.914	0.02	0	0.017	0
			Totals[a]: $\Sigma\phi_{av}^{9a}\sigma_{av}DF_{av} = 0.183 \times 10^{-6}\ s^{-1} = k_p^{9a}$		$\Sigma\phi_{av}^{9b}\sigma_{av}DF_{av} = 0\ s^{-1} = k_p^{9b}$	

[a] D = earth–sun correction distance of 0.966.

yields for (9c) and (9d) are not given because they are sufficiently small that they can be ignored. Hence we only need to consider reactions (9a) and (9b).

As is typical for such data, values at *specific* wavelengths are given, rather than averages over the wavelength *intervals* for which the actinic flux data are provided in Table 3.7. Hence it is necessary to use the data in Table 3.18 to obtain averages over the appropriate wavelength intervals. One can plot the data in Table 3.18 as a function of wavelength and integrate over each interval to obtain the appropriate average. Indeed, the absorption cross sections are given every nm by Atkinson *et al*. (1997). In the case of slowly varying functions, a reasonable approximation can be obtained by using a simple numerical average of the values at each end of the wavelength interval. The averages over the appropriate intervals obtained in this manner are shown in Table 3.19.

To use the actinic flux data in Table 3.7, we need to know the solar zenith angle at 30°N latitude six hours after noon on July 1. We can obtain this from Table 3.9. Since the values are symmetrical about noon, we use the data for 0600 on July 1 at 30°N latitude, which from Table 3.9 corresponds to a solar zenith angle of 78.7°. To obtain the actinic fluxes corresponding to this solar zenith angle, one returns to Table 3.7 and interpolates between the 78° and 86° values given in the last two columns. For simplicity in presenting these calculations, we use the values given for 78°. A correction for the earth–sun distance must also be made using the data of Table 3.8. For July 1, this correction factor is 0.966; i.e., the actinic flux values in Table 3.7 must be multiplied by D = 0.966.

Table 3.19 summarizes these corrected values of $F(\lambda)$ for the wavelength region of interest for CH_3CHO.

Once the actinic fluxes, quantum yields, and absorption cross sections have been summarized as in Table 3.19, the individual products $\phi_{av}(\lambda)\sigma_{av}(\lambda)F(\lambda)$ for each wavelength interval can be calculated and summed to give k_p. Note that the individual reaction channels (9a) and (9b) are calculated separately and then added to get the total photolysis rate constant for the photolysis of acetaldehyde. However, the rate constants for the individual channels are also useful in that (9a) produces free radicals that will participate directly in the NO to NO_2 conversion and hence in the formation of O_3, etc., while (9b) produces relatively unreactive stable products.

In this case, the photolysis rate constant for reaction (9b) is zero because the quantum yield drops off rapidly to zero above 290 nm, and at this large solar zenith

angle, the actinic flux is negligible at wavelengths below 300 nm. Hence only reaction (9a), leading to free radicals, contributes to the photolysis of CH_3CHO under these conditions. Adding up the individual contributions at each wavelength interval, one obtains $k_p^{tot} = k_p^{9a} = 1.83 \times 10^{-7}$ s^{-1}. Hence the rate of loss of acetaldehyde by photolysis is given by:

$$\frac{d[CH_3CHO]}{dt} = -k_p[CH_3CHO],$$

where $k_p = 1.83 \times 10^{-7}$ s^{-1}, and in this particular case, the loss proceeds entirely via one channel, (9a).

As described in Chapter 5, the *natural lifetime* for acetaldehyde with respect to photolysis under these conditions can be calculated from k_p for the overall reaction. The natural lifetime, τ, is defined as the time for the concentration of CH_3CHO to fall to $1/e$ of its initial value, where e is the base of natural logarithms. The natural lifetime of acetaldehyde under these conditions is therefore given by $\tau = 1/k_p = 5.5 \times 10^6$ s = 63 days. Of course, these conditions do not exist for 63 days, so the lifetime is hypothetical. However, it does provide a sort of "back-of the envelope" method of assessing the relative rapidity of loss of the compound by photolysis compared to other processes, such as reaction with OH.

D. PROBLEMS

For the following problems, where necessary use absorption cross sections and quantum yield data found in the relevant sections of Chapter 4.

1. Following the procedure outlined in Section 3.C.1a, calculate the solar zenith angle for your city or town at the following times: (a) noon on January 1; (b) 8:00 a.m. on March 15 ("Beware the ides of March..."); (c) noon on June 21; (d) 3:30 p.m. on September 1; (e) 9:00 a.m. on December 21. The latitudes and longitudes for various locations can be found, for example, in the *Rand McNally International Atlas*.

2. Following the procedure in Section 3.C.2c, calculate the earth–sun correction factors for the actinic flux on the following dates: (a) January 1; (b) February 25; (c) April 15; (d) June 8; (e) September 1; (f) November 15. You can check some of these answers against Table 3.8.

3. Calculate the photolysis rate constant, k_p, for the photolysis of Cl_2 at solar zenith angles of (a) 10, (b) 30, (c) 50, (d) 70, and (e) 86°, respectively, at the surface of the earth on January 1.

4. Calculate the photolysis rate constants, k_p, for each of the two photolysis paths as well as the overall photolysis rate constant for the photolysis of $ClONO_2$ at solar zenith angles of (a) 0, (b) 40, and (c) 78°, respectively, at the surface of the earth on February 25 (see Problem 2 for the earth–sun correction factor). Assume the quantum yield for production of $Cl + NO_3$ is 0.65 and that for $ClO + NO_2$ is 0.35 from 290 to 320 nm and that for $Cl + NO_3$ is 1.0 from 320 nm to longer wavelengths.

5. Calculate the photolysis rate constant, k_p, for the photolysis of methyl nitrate (CH_3ONO_2) at solar zenith angles of (a) 10, (b) 30, (c) 50, (d) 70, and (e) 86°, respectively, at the surface of the earth on June 8 (see Problem 2 for the earth–sun correction factor).

6. Choose one of the following molecules: (a) $CH_3CH_2ONO_2$, (b) 2-propyl nitrate, (c) PAN, (d) $ClONO_2$, (e) $BrONO_2$, (f) HOCl, (g) HOBr, (h) H_2O_2, (i) CH_3OOH, (j) N_2O_5, (k) HNO_3, (l) HO_2NO_2, (m) CH_3I. Calculate the photolysis rate constant at 11:00 a.m. true solar time at 30°N on March 1 at the earth's surface. Assume 298 K unless data are not given for that temperature, in which case use the closest temperature for which data are given. Use the data given for the "best estimate" surface albedo. If there are missing parameters, e.g., quantum yields, state clearly the assumptions you are making. If the solar zenith angle is within a degree of those for which data are given, you may use the flux values given without interpolation.

7. For the molecules given in Problem 6, calculate the photolysis rate constant at the earth's surface at 50°N on April 1 at a time 1.5 h before the sun crosses the meridian. Assume 298 K unless data are not given for that temperature, in which case use the closest temperature for which data are given. Use the data given for the "best estimate" surface albedo. If there are missing parameters, e.g., quantum yields, state clearly the assumptions you are making. If the solar zenith angle is within a degree of those for which data are given, you may use the flux values given without interpolation.

8. Use the data in Tables 3.7, 3.15, 3.16, and 3.17 to calculate the ratio of the actinic flux for "best estimate" albedo at 40, 25, and 15 km to that at 0 km for the wavelength intervals 300–302, 400–405, and 500–510 nm, respectively. Comment on the reason for the differences between the three wavelength regions.

9. Use the data in Tables 3.7 and 3.11 to calculate the ratio of the actinic flux at the earth's surface for an 80% surface albedo compared to the "best estimate" albedo at solar zenith angles of 0 and 78° for the following wavelength regions: 298–300, 318–320, and 400–405 nm. Comment on the expected effects on photochemistry in the boundary layer.

10. Comment on why the percentage increase in actinic flux at the surface for a 5% decrease in O_3 is greater at larger solar zenith angles (Table 3.12).

11. The surface albedo can have a large effect on the total light available for photolysis in the troposphere. Calculate the factor by which the photolysis of H_2O_2 would increase at a solar zenith angle of 60° on December 1 over snow with a surface albedo of 80% compared to a normal "best estimate" surface albedo.

References

Angle, R. P., M. Brennand, and H. S. Sandhu, "Surface Albedo Measurements at 53°N Latitude," *Atmos. Environ., 26A,* 1545–1547 (1992).

Atkinson, R., D. L. Baulch, R. A. Cox, R. F. Hampson, J. A. Kerr, M. J. Rossie, and J. Troe, "Evaluated Kinetic and Photochemical Data for Atmospheric Chemistry. Supplement V. IUPAC Subcommittee on Gas Kinetic Data Evaluation for Atmospheric Chemistry," *J. Phys. Chem. Ref. Data, 26,* 521–1011 (1997).

Bordewijk, J. A., H. Slaper, H. A. J. M. Reinen, and E. Schlamann, "Total Solar Radiation and the Influence of Clouds and Aerosols on the Biologically Effective UV," *Geophys. Res. Lett., 22,* 2151–2154 (1995).

Brauers, T., and A. Hofzumahaus, "Latitudinal Variation of Measured NO_2 Photolysis Frequencies over the Atlantic Ocean between 50°N and 30°S," *J. Atmos. Chem., 15,* 269–282 (1992).

Calvert, J. G., and J. N. Pitts, Jr., *Photochemistry*, Wiley, New York, 1966.

Castro, T., L. G. Ruiz-Suarez, J. C. Ruiz-Suarez, M. J. Molina, and M. Montero, "Sensitivity Analysis of a UV Radiation Transfer Model and Experimental Photolysis Rates of NO_2 in the Atmosphere of Mexico City," *Atmos. Environ., 31,* 609–620 (1997).

Crosley, D. R., "Rotational and Translational Effects in Collisions of Electronically Excited Diatomic Hydrides," *J. Phys. Chem., 93,* 6273–6282 (1989).

Dave, J. V., *Development of Programs for Computing Characteristics of Ultraviolet Radiation,* Final Report under Contract NAS 5-21680, NASA Report CR-139134, National Aeronautics and Space Administration, Goddard Space Flight Center, Greenbelt, MD, NTIS No. N75-10746/6SL, 1972.

Davis, H. F., B. Kim, H. S. Johnston, and Y. T. Lee, "Dissociation Energy and Photochemistry of NO_3," *J. Phys. Chem., 97,* 2172–2180 (1993).

Demerjian, K. L., K. L. Schere, and J. T. Peterson, "Theoretical Estimates of Actinic (Spherically Integrated) Flux and Photolytic Rate Constants of Atmospheric Species in the Lower Troposphere," *Adv. Environ. Sci. Technol., 10,* 369–459 (1980).

DeMore, W. B., S. P. Sander, D. M. Golden, R. F. Hampson, M. J. Kurylo, C. J. Howard, A. R. Ravishankara, C. E. Kolb, and M. J. Molina, "Chemical Kinetics and Photochemical Data for Use in Stratospheric Modeling," in JPL Publication 97-4, Jet Propulsion Laboratory, Pasadena, CA, January 15, 1997.

Dickerson, R. R., D. H. Stedman, and A. C. Delany, "Direct Measurements of Ozone and Nitrogen Dioxide Photolysis Rates in the Troposphere," *J. Geophys. Res., 87,* 4933–4946 (1982).

Dickerson, R. R., S. Kondragunta, G. Stenchikov, K. L. Civerolo, B. G. Doddridge, and B. N. Holben, "The Impact of Aerosols on Solar Ultraviolet Radiation and Photochemical Smog," *Science, 278,* 827–830 (1997).

Eck, T. F., P. K. Bhartia, P. H. Hwang, and L. L. Stowe, "Reflectivity of Earth's Surface and Clouds in Ultraviolet from Satellite Observations," *J. Geophys. Res., 92,* 4287–4296 (1987).

Erlick, C., and J. E. Frederick, "Effects of Aerosols on the Wavelength Dependence of Atmospheric Transmission in the Ultraviolet and Visible. 2. Continental and Urban Aerosols in Clear Skies," *J. Geophys. Res., 103,* 23275–23285 (1998).

Frederick, J. E., A. E. Koob, A. D. Alberts, and E. C. Weatherhead, "Empirical Studies of Tropospheric Transmission in the Ultraviolet: Broadband Measurements," *J. Appl. Meteorol., 32,* 1883–1892 (1993).

Friedman, H., in *Physics of the Upper Atmosphere* (J. A. Ratcliffe, Ed.), Academic Press, New York, 1960.

Gilbert, A., and J. Baggott, *Essentials of Molecular Photochemistry*, CRC Press, Boca Raton, FL, 1991.

Goody, R. M., and Y. L. Yung, *Atmospheric Radiation—Theoretical Basis*, Oxford Univ. Press, New York, 1989.

Halthore, R. N., S. E. Schwartz, J. J. Michalsky, G. P. Anderson, R. A. Ferrare, B. N. Holben, and H. M. Ten Brink, "Comparison of Model Estimated and Measured Direct-Normal Solar Irradiance," *J. Geophys. Res., 102,* 29991–30002 (1997).

Herman, J. R., and E. A. Celarier, "Earth Surface Reflectivity Climatology at 340–380 nm from TOMS Data," *J. Geophys. Res., 102,* 28003–28011 (1997).

Herzberg, G. *Molecular Spectra and Molecular Structure, I. Spectra of Diatomic Molecules*, 1950; *II. Infrared and Raman Spectra of Polyatomic Molecules*, 1945; *III. Electronic Spectra and Electronic Structure of Polyatomic Molecules*, Van Nostrand, Princeton, NJ, 1967.

Howard, J. N., J. I. F. King, and P. R. Gast, "Thermal Radiation," *Handbook of Geophysics*, Chap. 16. Macmillan, New York (1960).

Huber, K., and G. Herzberg, *Molecular Spectra and Molecular Structure. IV. Constants of Diatomic Molecules*, Van Nostrand, Princeton, NJ, 1979.

Ishiwata, T., I. Fujiwara, Y. Naruge, K. Obi, and I. Tanaka, "Study of NO_3 by Laser-Induced Fluorescence," *J. Phys. Chem., 87,* 1349–1352 (1983).

Jacobson, M. Z., "Studying the Effects of Aerosols on Vertical Photolysis Rate Coefficient and Temperature Profiles over an Urban Airshed," *J. Geophys. Res., 103,* 10593–10604 (1998).

Johnston, H. S., H. F. Davis, and Y. T. Lee, "NO_3 Photolysis Product Channels: Quantum Yields from Observed Energy Thresholds," *J. Phys. Chem., 100,* 4713–4723 (1996).

Junkermann, W. "Measurements of the $J(O^1D)$ Actinic Flux Within and Above Stratiform Clouds and Above Snow Surfaces", *Geophys. Res. Lett. 21,* 793–796 (1994).

Junkermann, W., U. Platt, and A. Volz-Thomas, "A Photoelectric Detector for the Measurement of Photolysis Frequencies of Ozone and Other Atmospheric Molecules," *J. Atmos. Chem., 8,* 203–227 (1989).

Kato, S., T. P. Ackerman, E. E. Clothiaux, J. H. Mather, G. G. Mace, M. L. Wesely, F. Murcray, and J. Michalsky, "Uncertainties in Modeled and Measured Clear-Sky Surface Shortwave Irradiances," *J. Geophys. Res., 102,* 25881–25898 (1997).

Kelley, P., R. R. Dickerson, W. T. Luke, and G. L. Kok, "Rate of NO_2 Photolysis from the Surface to 7.6 km Altitude in Clear-Sky and Clouds," *Geophys. Res. Lett., 22,* 2621–2624 (1995).

Kraus, A., and A. Hofzumahaus, "Field Measurements of Atmospheric Photolysis Frequencies for O_3, NO_2, HCHO, CH_3CHO, H_2O_2, and HONO by UV Spectroradiometry," *J. Atmos. Chem., 31,* 161–180 (1998).

Krotkov, N. A., P. K. Bhartia, J. R. Herman, V. Fioletov, and J. Kerr, "Satellite Estimation of Spectral Surface UV Irradiance in the Presence of Tropospheric Aerosols. 1. Cloud-Free Case," *J. Geophys. Res., 103,* 8779–8793 (1998).

Kylling, A., A. Albold, and G. Seckmeyer, "Transmittance of a Cloud Is Wavelength-Dependent in the UV-Range: Physical Interpretation," *Geophys. Res. Lett., 24,* 397–400 (1997).

Lantz, K. O., R. E. Shetter, C. A. Cantrell, S. J. Flocke, J. G. Calvert, and S. Madronich, "Theoretical, Actinometric, and Radiometric Determinations of the Photolysis Rate Coefficient of NO_2 during the Mauna Loa Observatory Photochemistry Experiment 2," *J. Geophys. Res., 101,* 14613–14629 (1996).

Lean, J., "Variations in the Sun's Radiative Output," *Rev. Geophys., 29,* 505–535 (1991).

Leighton, P. A., *Photochemistry of Air Pollution,* Academic Press, New York, 1961.

Lenoble, J., *Atmospheric Radiative Transfer*, A. Deepak Publishing, Hampton, VA, 1993.

Liou, K.-N., *An Introduction to Atmospheric Radiation*, Academic Press, New York, 1980.

Madronich, S. "Photodissociation in the Atmosphere. 1. Actinic Flux and the Effects of Ground Reflections and Clouds," *J. Geophys. Res., 92,* 9740–9752 (1987).

Madronich, S., "The Atmosphere and UV-B Radiation at Ground Level," in *Environmental UV Photobiology* (A. R. Young, Ed.), pp. 1–39, Plenum, New York, 1993.

Madronich, S., personal communication (1998). We are most grateful to Dr. Madronich for providing the results of his calculations for use by the atmospheric chemistry community.

Madronich, S., D. R. Hastie, B. A. Ridley, and H. I. Schiff, "Measurement of the Photodissociation Coefficient of NO_2 in the Atmosphere. I. Method and Surface Measurements," *J. Atmos. Chem., 1,* 3–25 (1983).

Mauldin, R. L., III, S. Madronich, S. J. Flocke, and F. L. Eisele, "New Insights on OH: Measurements around and in Clouds," *Geophys. Res. Lett., 24,* 3033–3036 (1997).

Mayer, B., A. Kylling, S. Madronich, and G. Seckmeyer, "Enhanced Absorption of UV Radiation Due to Multiple Scattering in Clouds: Experimental Evidence and Theoretical Explanation," *J. Geophys. Res., 103,* 31241–31254 (1998).

McDermid, I. S., and J. B. Laudenslager, "Radiative Lifetimes and Quenching Rate Coefficients for Directly Excited Rotational Levels of OH($A^2\Sigma^+, v' = 0$), *J. Chem. Phys., 76,* 1824–1831 (1982).

McLinden, C. A., J. C. McConnell, E. Griffoen, C. T. McElroy, and L. Pfister, "Estimating the Wavelength-Dependent Ocean Albedo under Clear-Sky Conditions Using NASA ER 2 Spectroradiometer Measurements," *J. Geophys. Res., 102,* 18801–18811 (1997).

Molina, L. T., and M. J. Molina, "Absolute Absorption Cross Sections of Ozone in the 185- to 350-nm Wavelength Range," *J. Geophys. Res., 91,* 14501–14508 (1986).

Müller, R., and U. Schurath, "Entwicklung eines, Gerätes zur kontinuierlichen Messung der Photodissoziations-Geschwindigkeit von Aldehyden in der Atmosphäre durch Nachweis des erzeugten CO," Gesellschaft für Strahlen-und Umweltforschung mbH München, Abschlussbericht Vorhaben KBF 53 (1986).

Neckel, H., and D. Labs, "The Solar Radiation between 3300 and 12500 Å," *Solar Phys., 90,* 205–258 (1984).

Nelson, H. H., L. Pasternack, and J. R. McDonald, "Laser-Induced Excitation and Emission Spectra of NO_3," *J. Phys. Chem., 87,* 1286–1288 (1983).

Okabe, H. *Photochemistry of Small Molecules*, Wiley, New York, 1978.

Orlando, J. J., G. S. Tyndall, G. K. Moortgat, and J. G. Calvert, "Quantum Yields for NO_3 Photolysis between 570 and 635 nm," *J. Phys. Chem., 97,* 10996–11000 (1993).

Parrish, D. D., P. C. Murphy, D. L. Albritton, and F. C. Fehsenfeld, "The Measurement of the Photodissociation Rate of NO_2 in the Atmosphere," *Atmos. Environ., 17,* 1365–1379 (1983).

Peterson, J. T., "Calculated Actinic Fluxes (290–700 nm) for Air Pollution Photochemistry Applications," U.S. Environmental Protection Agency Report No. EPA-600/4-76-025, June 1976.

Ruggaber, A., R. Dlugi, A. Bott, R. Forkel, H. Herrmann, and H.-W. Jacobi, "Modelling of Radiation Quantities and Photolysis Frequencies in the Aqueous Phase in the Troposphere," *Atmos. Environ., 31,* 3137–3150 (1997).

Schwander, H., P. Koepke, and A. Ruggaber, "Uncertainties in Modeled UV Irradiances Due to Limited Accuracy and Availability of Input Data," *J. Geophys. Res., 102,* 9419–9429 (1997).

Seckmeyer, G., B. Mayer, G. Bernhard, R. L. McKenzie, P. V. Johnston, M. Kotkamp, C. R. Booth, T. Lucas, T. Mestechkina, C. R. Roy, H. P. Gies, and D. Tomlinson, "Geographical Differences in the UV Measured by Intercompared Spectroradiometers," *Geophys. Res. Lett., 22,* 1889–1892 (1995).

Seckmeyer, G., R. Erb, and A. Albold, "Transmittance of a Cloud is Wavelength-Dependent in the UV-Range," *Geophys. Res. Lett., 23,* 2753–2755 (1996).

Shetter, R. E., A. H. McDaniel, C. A. Cantrell, S. Madronich, and J. G. Calvert, "Actinometer and Eppley Radiometer Measurements of the NO_2 Photolysis Rate Coefficient during the Mauna Loa Observatory Photochemistry Experiment," *J. Geophys. Res., 97,* 10349–10359 (1992).

Shetter, R. E., C. A. Cantrell, K. O. Lantz, S. J. Flocke, J. J. Orlando, G. S. Tyndall, T. M. Gilpin, C. A. Fischer, S. Madronich, and J. G. Calvert, "Actinometric and Radiometric Measurement and Modeling of the Photolysis Rate Coefficient of Ozone to $O(^1D)$ during Mauna Loa Observatory Photochemistry Experiment. 2," *J. Geophys. Res., 101,* 14631–14641 (1996).

Spencer, J. W., "Fourier Series Representation of the Position of the Sun," *Search, 2,* 172 (1971).

Stamnes, K., S.-C. Tsay, W. Wiscombe, and K. Jayaweera, "Numerically Stable Algorithm for Discrete-Ordinate-Method Radiative Transfer in Multiple Scattering and Emitting Layered Media," *Appl. Opt., 27,* 2502–2509 (1988).

Turro, N. J., *Modern Molecular Photochemistry*, Benjamin/Cummings, Menlo Park, CA, 1978.

Vilà-Guerau de Arellano, J., P. G. Duynkerke, and M. van Weele, "Tethered-Balloon Measurements of Actinic Flux in a Cloud-Capped Marine Boundary Layer," *J. Geophys. Res., 99,* 3699–3705 (1994).

Volz-Thomas, A., A. Lerner, H.-W. Pätz, M. Schultz, D. S. McKenna, R. Schmitt, S. Madronich, and E. P. Röth, "Airborne Measurements of the Photolysis Frequency of NO_2," *J. Geophys. Res., 101,* 18613–18627 (1996).

Wayne, R. P., *Principles and Applications of Photochemistry*, Oxford University Press, Oxford, 1988.

Wen, G., and J. E. Frederick, "The Effects of Horizontally Extended Clouds on Backscattered Ultraviolet Sunlight," *J. Geophys. Res., 100,* 16387–16393 (1995).